UNIVERSIDADE TÉCNICA DE LISBOA
INSTITUTO SUPERIOR TÉCNICO

POLITECHNIKA WARSZAWSKA
WYDZIAŁ ELEKTRONIKI I TECHNIK INFORMACYJNYCH

MIMO GEOMETRICALLY BASED CHANNEL MODEL

Hubert Kokoszkiewicz

Dissertation submitted for obtaining the degree of magister inżynier telekomunikacji (Master of Science in Telecommunication Engineering)

Supervisors: Doctor Luís Manuel de Jesus Sousa Correia, IST
Dr inż. Jerzy Kołakowski, PW

Jury

President: Doctor Maria Paula Queluz, IST
Members: Doctor Luís Manuel de Jesus Sousa Correia, IST
Doctor Carlos Fernandes, IST

September 2005

Acknowledgements

First of all, I wish to thank Prof. Luis Correia, because without his help, finishing this marathon would not have been possible. His advice gave me a new point of view, and sometimes my world was rotated by 180 degrees. However, everything led me to a clearly defined purpose. Every weekly meeting left a mark on my telecommunication and document editing knowledge. He was always a source of interesting facts about Portugal, which is especially enjoyable for a foreigner. The invitation to Monsaraz was an opportunity to experience a feast for my body and soul.

Thanks for Dr. Jerzy Kołakowski for giving me the necessary telecommunication background to write this work. He always offered me a warm reception and always had time to offer advice and his knowledge.

With the help of Martijn Kuipers, the creation of this work was simpler. Open-minded discussions during weekly meetings and occasionally chats in a café have had a significant impact on my progress in this work. His advice regarding the implementation of the simulator was very helpful. A big hug for checking my English, which has proven to be a never ending story for him.

To Politechnika Warszawska, that has given me opportunity to participate in Socrates-Erasmus exchange and for years of supporting during my studies.

I would like to express my gratitude to all members of GROW. I received a lot of help and motivation from them.

Thanks to „Fundacja Wspierania Rozwoju Radiokomunikacji i Technik Multimedialnych" for financial support during the scholarship in Lisbon.

To my parents that I can always count on them, because they are with me wherever I am.

Great thanks for Marta, who was always supporting and motivating me despite our long-time separation.

Abstract

The main aim of this work is the investigation of a system with multi antenna for both sides of the radio link, i.e., a MIMO system. The advantages of the system have been checked for different scenarios, a micro-, a pico- and a macro-cell have been considered. Spectral capacity was chosen as criteria on for comparison of scenarios. The analysis has been made with reference to UMTS, and all necessary parameters were taken from its specifications of one.

The radio channel has been modelled by the Geometrically Based Single Bounced (GBSB) model, which is a member of the geometrical model group. A simulator was developed, which implements the GBSB model in the three mentioned scenarios. The implementation of the simulator takes into consideration that both receiver and transmitter have a set of antennas, so that the simulator generates real MIMO radio channel.

A MIMO system for three scenarios was investigated changing the parameters of both receiver and transmitter. The influence of various numbers of antennas for both sides of the radio link was checked. A different spacing between antennas was also considered. The impact of various mutual positions of the Mobile Terminal (MT) and Base Station (BS) has been analyzed as well.

When comparing capacities for various numbers of antennas with reference to different scenarios, the best results are obtained for the micro-cell. The macro-cell scenario has the smallest capacities. The capacity reached in the macro-cell scenario is smaller than the one for the micro-cell by 38% in extreme cases. The railway station scenario achieves results comparable with the micro-cell. For all scenarios, the more the antennas are separated the greater the capacity is obtained. However, a spacing of λ gives enough separation between antennas. The change of the mutual position of the MT and the BS has the greatest impact on the capacity of the micro-cell scenario. The capacity for the worst case is smaller than the one for best case by 21%.

Keywords:

MIMO, UMTS, Capacity, Channel Modelling

Streszczenie

Celem niniejszej pracy jest zbadanie właściwości systemu radiowego z wieloantenowym odbiornikiem oraz nadajnikiem, powszechnie zwanym systemem typu MIMO. Właściwości tego systemu sprawdzono w trzech różnych środowiskach: micro-cell, macro-cell i pico-cell. Jako kryterium porównawcze dla powyższych środowisk wybrano pojemność spektralną. Analizę przeprowadzono w odniesieniu do UMTS-u, w związku, z czym wszystkie niezbędne do symulacji parametry zdefiniowano poprzez specyfikację systemu.

Kanał radiowy opisano za pomocą przez Geometrically Based Single Bounce (GBSB) model, który zalicza się do grupy modeli geometrycznych.. Model GBSB zaimplementowano w symulatorze, który jest dedykowany dla trzech wyżej wymienionych scenariuszy. W implementacji symulatora uwzględniono fakt, że zarówno nadajnik, jak i odbiornik, wyposażone są w wieloelementowe zestawy antenowe, co pozwala w wyniku działania otrzymać rzeczywisty kanał radiowy dla systemu MIMO.

Symulacje przeprowadzono względem trzech różnych parametrów systemu MIMO: liczby anten dla dwóch stron łącza radiowego, separacji między antenami oraz względem wzajemnego położenia nadajnika i odbiornika.

Przyjmując jako kryterium porównawcze pojemność kanału najlepsze wyniki uzyskano dla micro-celli. Natomiast macro-cella charakteryzuje się pojemnościami o najmniejszych wartościach. W najbardziej krytycznych przypadkach, pojemności uzyskiwane w macro-celli są mniejsze od pojemności z micro-celli o 38%. Z kolei wyniki dla pico-celli są porównywalne z rezultatami uzyskanymi dla micro-celli. Dla wszystkich scenariuszy, cechą wspólną jest fakt, że im anteny nadajnika lub odbiornika są bardziej odseparowane tym uzyskiwane pojemności są większe. Zmiana wzajemnego położenia MT oraz BS oddziałuje najbardziej w micro-celli. Pojemność dla najgorszego zorientowania anten nadajnika i odbiornika jest o 21% mniejsza niż dla najlepszego wzajemnego ustawienia anten.

Słowa kluczowe:

MIMO, UMTS, Pojemność kanału radiowego, Modelowanie kanału radiowego

Table of Contents

List of Figures

List of Tables

List of Acronyms

AoA	Angle of Arrival
AoD	Angle of Departure
AWGN	Additive White Gaussian Noise
BS	Base Station
CDMA	Code Division Multiple Access
CIR	Channel Impulse Response
COST	European CO-operation in the field of Scientific and Technical Research
CSI	Channel State Information
DL	Downlink
DPCCH	Dedicated Physical Control Channel
DUM	Discrete Uniform Model
EDGE	Enhanced Data Rates for GSM Evolution
FDD	Frequency Division Duplexing
FDMA	Frequency Division Multiple Access
FTW	Froschungszentrum Telekommunikation Wien
GBSB	Geometrically Based Single Bounce
GPRS	General Packet Radio Service
GSM	Global System for Mobile Communication
GWSSUS	Gaussian Wide Sense Stationary Uncorrelated Scattering
HSCSD	High Speed Circuit Swiched Data
IEEE	Institute of Electrical and Electronics Engineers
IST	Instituto Superior Técnico

LoS	Line of Sight
MC-CDMA	Multi-Carrier Code Division Multiplexing Access
MIMO	Multiple-Input Multiple-Output
MT	Mobile Terminal
MU	Multi User
MUI	Multi User Interference
NLoS	Non Line of Sight
OVSF	Orthogonal Variable Spreading Factor
PDF	Probability Density Function
PDP	Power Delay Profile
QPSK	Quadrature Phase Shift Keying
RMS	Root Mean Square
Rx	Receiver
SISO	Single-Input Single-Output
STBC	Space Time Block Coding
STC	Space Time Coding
SVD	Singular Value Decomposition
TD-CDMA	Time Division – Code Division Multiple Access
TDD	Time Division Duplexing
TDMA	Time Division Multiple Access
ToA	Time of Arrival
Tx	Transmitter
UL	Uplink
UMTS	Universal Mobile Telecommunications System
USD	Uniform Sectored Distribution

W-CDMA	Wideband – Code Division Multiple Access
WLAN	Wireless Local Area Network

List of Symbols

a	Radius of the circular antenna array
AF	Antenna factor
B_C	Coherence Bandwidth
b_{ell}	Minor axis of the ellipse
c	Speed of light
C	Capacity of a radio channel
$\overline{C}$	Average of the sum of MIMO subchannel capacities
$conv$	Convolution
$corr$	Correlation between singals
$\boldsymbol{cov}$	Covariance matrix
$\boldsymbol{C_R}$	The coupling matrix for the set of receiving antennas
$\boldsymbol{C_T}$	The coupling matrix for the set of transmitting antennas
d	Spacing between antennas in the antenna array
d_0	Distance between the MT and the BS
d_1	Distance between a receiving antenna and a scatterer
d_2	Distance between a scatterer and a transmitting antenna
d_c	Cluster density
dim	A dimension of a scenario for the simulator
d_m	Distance between antennas in a MIMO set
E_b	Energy per one bit
E_{Rx}	Amplitude of received multipath component
E_{Tx}	Energy sent by each transmit antenna in MIMO system

f	Radio frequency
f_{ell}	Focal length of the ellipse
f_m	Maximum Doppler shift
G	Radiation pattern of an antenna array
$\boldsymbol{g}$	Matrix containing Channel Impulse Response
$\boldsymbol{G}$	Fourier transform of $\boldsymbol{g}$.
G_0	Radiation pattern of a radiator
G_p	Processing gain
G_{Rx}	Radiation pattern of a receiving antenna
G_{Tx}	Radiation pattern of a transmitting antenna
$\boldsymbol{h}$	Normalised matrix containing Channel Impulse Response
$\boldsymbol{H}$	Fourier transform of $\boldsymbol{h}$.
h_{eff}	Effective length of the receiving antenna
h_k	Amplitude of the channel impulse response
$\boldsymbol{H_n}$	Normalised channel transfer matrix related with $\boldsymbol{T}$
i_{BS}	Inter-cell to intra-cell interferences ratio at the BS
I_{inter}	Power of the inter-cell interference
I_{intra}	Power of the intra-cell interference
i_{MT}	Inter-cell to intra-cell BS interference ratio received by the MT
$\boldsymbol{I_n}$	n-dimensional identity matrix
I_n	Feeding amplitude of n^{th} antenna in the antenna array
k	Wave number
$\overline{L}_{pj}$	Average attenuation between the BS and j^{th} user
$\boldsymbol{N}$	Vector containing power of noise received by each antenna
N_0	Power of thermal noise

n_a	Number of antennas in the antenna array
N_{cl}	Number of clusters
N_{DL}	Number of connections per cell
n_{min}	The lowest value among n_R and n_T
n_R	Number of output antennas for a MIMO system
N_{Rx}	Noise sensitivity of the Rx
$\overline{n_{sc}}$	Average number of scatterers per cluster for the simulator
N_{sc}	Fixed number of scatterers for different radio channel models
N_{sp}	Noise spectral density
n_T	Number of input antennas for a MIMO system
N_{UL}	Number of users per cell
$\boldsymbol{P}$	Distribution of the power on the transmitting side
$\overline{P}$	Mean power gain
P_k	Power of the channel impulse response
P_{Rx}	Power of the received signal
$\overline{P}_{Rx}$	Average power received by each output antenna
P_{Tx}	Total transmitt power, regerdless the number of the input antennas
$p_{\tau,\varphi}$	Probability density function for the GBSB model
q	Normalising factor for $\boldsymbol{H_n}$
R	Radius of the circle where the scatterers are deployed
$\boldsymbol{R}$	Correlation matrix
R_A	Feedpoint impedance of an antenna
R_{bj}	Bit rate for j^{th} user
R_c	WCDMA chip rate
R_{max}	Maximum radius of a region

$\boldsymbol{S}$	Matrix describing the transformation of input data
$\boldsymbol{s_{dev}}$	Position of the device on the 2D plane
SIR_{DL}	Signal to Interference and noise Ratio for the downlink
SIR_{UL}	Signal to Interference and noise Ratio for the uplink
$\boldsymbol{T}$	Non-normalised channel transfer matrix
T_C	Coherence Time
$\boldsymbol{U}$	Unitary matrix containing the singular vectors of the matrix $\boldsymbol{H}$ after SVD
v	Velocity
V	Voltage of the signal detected by the receiving antenna
$\boldsymbol{V}$	Unitary matrix containing the singular vectors of the matrix $\boldsymbol{H}$ after SVD
$v_{i,b}$	Superposition of the steering vectors
v_j	Activity factor for the j^{th} user
w_{str}	Street width
$\boldsymbol{x}$	Vector containing the radiated symbols for particular input antennas in particular instance of time
$\boldsymbol{X}$	The complex amplitude of x.
x_{Rx}	x-coordinate of a receiving antenna
x_{sc}	x-coordinate of a scatterer
x_{Tx}	x-coordinate of a transmitting antenna
$\boldsymbol{y}$	Vector containing received symbols
$\boldsymbol{Y}$	The complex amplitude of y.
y_{Rx}	y-coordinate of a receiving antenna
y_{sc}	y-coordinate of a scatterer
y_{Tx}	y-coordinate of a transmitting antenna

$\overline{\alpha}$	Average orthogonality factor in the cell
α_n	Angular position of n^{th} element on the *x*-*y* plane
α_{SIR}	Orthogonality factor
β_{SIR}	Interference reduction factor
Γ	Complex reflection coefficient of a scatterer
$\overline{\eta_{DL}}$	Average load for the downlink
η_{DL}	Load for the downlink
η_{UL}	Load for the uplink
θ	Angle of departure
θ_{aa}	Angle of radiation pattern
λ	Wavelength
λ_e	Eigenvalue
ρ	Signal to noise ratio
$\boldsymbol{\Sigma}$	Matrix containing singular values of the matrix $\boldsymbol{H}$
Σ	Singular value
σ_θ	Angular spread of the AoD
σ_τ	RMS time delay spread
σ_φ	Angular spread of the AoA
τ	Delay
$\bar{\tau}$	Mean Excess Delay
$\overline{\tau^2}$	Mean Square Excess Delay
τ_k	k^{th} instant
τ_{max}	Maximum delay
φ	Angle of arrival
φ_0	Angle of arrival of the LoS component

Φ_0	Phase shift between consecutive radiators in the antenna array
φ_{aa}	Angle of radiation pattern
φ_{BW}	Range of change of angle of arrival
φ_n	Phase of the n^{th} element in the antenna array
Φ_n	Phase feeding of n^{th} radiator
φ_{Rx}	Phase of received multipath component
φ_{Rx}	Phase of received signal
φ_{sc}	Phase of the complex reflection coefficient of a scatterer
Ψ	Phase coefficient of antenna array
ω_D	Angular velocity of scatterer

List of Software

Dev C++	Bloodshed Software, GNU General Public License
Matlab	MathWorks
Microsoft Word	Microsoft Corporation
Microsoft Excel	Microsoft Corporation

1

Introduction

This chapter presents motivations of this thesis, its aims, its ranges and original contributions. An outline of the work is also presented.

1.1 Motivations

Nowadays wireless systems are developing in a high pace. During the last two decades, a huge progress in mobile telecommunications has been observed. This is related with a few domains of communications.

New generations of wireless systems bring an increase of transmission rates, coming form demands of the telecommunication market. Subscribers want to have a new wide diversity of services, e.g., high quality images and videos which causes that high bit rates are necessary to satisfy users' demands. Taking the limited resources of bandwidth frequency into consideration, new solutions must be invented in order to give high transmit rates regarding the mentioned limitation. New systems stratify the demand of high spectral efficiency. When the development of radio systems is analysed, one can notice that the need of high throughputs is always among the main motivations.

Cellular systems have been reshaped with an amazing rate. The first generation of the mobile cellular systems using an analogue technology served only a voice service and a data transmission with very low rate. These systems were absent of compatibility among different similar systems. Single systems operated on small regions, e.g., Nordic Mobile Telephone (NMT) in some European countries, Advanced Mobile Phone Service (AMPS) in the U.S.A., and others were established for different regions. Some fragments of the globe were covered by different operators, but a displacement around the world with an MT (Mobile Terminal) providing any service was impossible, because service providers used distinct systems.

The second generation of the mobile cellular systems takes advantage from digital technologies, e.g., digital signal processing and voice coding. New solutions gave a growth of capabilities and the range of provided services was augmented. One of the advantages of second generation systems is the capability to work among networks provided by different operators. The system was also developed with reference to a need of high bit rates. Besides the voice service, new ones are offered to subscribers, e.g., short text message and packet date transmission. The Global System for Mobile Communication (GSM) is well-recognized among second generation systems [GSMW05], [MoPa92]. Despite GSM gives bit rates higher than the previous systems, it was not enough to the satisfy demands of subscribers. So, some improvements had to be done. A solution based on a circuit-switching is High Speed Circuit Switched Data (HSCSD) which gives date rates up to 64 kb/s. The next one uses a packet data transmission, General Packet

Radio Service (GPRS). GPRS is dedicated mainly for using an MT as an access to Internet. It is not used to serve voice calls. The packet transmission for GSM can operate with rates up to 171 kb/s, which implies a significant load to the system, because resources are strongly used. Enhanced Data Rates for GSM Evolution (EDGE) uses a complex scheme of a modulation to increase data rate. EDGE allows an MT transmits data with rate up to 384 kb/s.

Next to GSM, IS-95 using Code Division Multiple Access (CDMA) represents also cellular systems of second generation, which is also standard worldwide [CDGO05]. Bit rates available for first releases were not enough to satisfy demands of the telecommunication market. IS-95 was replaced by cdma2000 and this last one was enhanced to Multi-Carrier Code Division Multiple Access (MC-CDMA).

The Universal Mobile Telecommunication System (UMTS) is a successor of second generation systems. UMTS is representative of third generation mobile cellular systems and provides a common interface joining some universal standards. This gives the ability to serve new services with high data rate. In favourable conditions related with the cell coverage and mobility of scenario, UMTS is supposed to give data rates up 2 Mbit/s in a 5MHz bandwidth.

Among Wireless Local Area Networks (WLANs), a demand of high bit rates is observed as well. On the telecommunication market, two main technologies can be distinguished. One of them is related with IEEE 802.11 standards [IEEE05]. Nowadays, IEEE 802.11b is very popular. This WLAN standard provides data rates up to 11 Mb/s using a frequency 2.4 GHz. The next one is IEEE 802.11g which one gives data rates up to 54 Mb/s. The increase of the throughput was possible, because Orthogonal Frequency Division Multiplexing (OFDM) is used. OFDM uses a large number of subcarriers for simultaneously transmission of the same signal.

Another representative of WLANs is High Performance Radio Local Area Network (HIPERLAN). The second version of HIPERLAN works at the 5 GHz band in a 20 MHz channel bandwidth, providing bit rates are similar to IEEE 802.11g, so HIPERLAN/2 gives 54 Mb/s. A high bit rate is possible by using more complex modulation schemes: 16QAM and 64QAM.

Multi-Input Multi-Output (MIMO) systems can bring a solution for the need of high bit rates for mobile cellular systems, WLANs and others. The above presented ways of increasing of

throughput are compatible with the MIMO approach. The mentioned solutions base on complex upgrade of devices, while the MIMO approach uses the multipath phenomena in the radio channel and a spatial gain of the channel. This causes that the Shannon border of capacity for the Gaussian radio channel can be crossed.

A MIMO system consists of a few input and output antennas, but MIMO can not be treated as an antenna array where all antenna elements are treated as a single system. In the MIMO case, each antenna is a single element that must be considered separately. All pairs of input and output antennas establish links between the receive and transmit sides. If the links are independent, a gain of radio channel can be observed and achieved results are a few times greater than ones for Single-Input Single-Output (SISO) systems. The independence of the links between input and output sides is related with their Channel Impulse Responses (CIRs). If CIRs are not correlated, it means that they are independent and the radio channel can be treated as non correlated. For the non correlated radio channel case, a few independent subchannels can be established. Each subchannel can be used to transmit an independent piece of information. The number of subchannels is constrained by the number of output antennas, but input ones also have some influence on the achieved capacity.

The state of the correlation of the radio channel is related with the environment of propagation. A decorrelation of the radio channels can only exist in an environment, where a multipath component phenomenon takes place. The potential gain of a MIMO system depends in fact on how strong the phenomenon is. Environments with a large distribution of obstacles give a high decorrelation of the radio channel.

A MIMO system transmits different pieces of information using the same bandwidth and at the same time. So, the question how to recognise a single information can be put forward. Each piece of information is transmitted by a different link. Every link is influenced by the environment. If the impact of the environment is different for each link, so a few independent radio links are established, despite using the same radio resources. This approach is very similar to the idea of code in CDMA, but MIMO is based on spatial identification, which strongly depends on the multipath propagation environment.

The gain of a MIMO system is related with some parameters as distance between antennas. An increase of the distance gives greater decorrelation among links, because antennas are placed at

more distant point in the environment. So, the influence of single obstructions is different on particular links.

The gain of a MIMO system should be checked in different conditions of propagation with dissimilar distributions of the scatterers. So, in this work the application of MIMO in different scenarios is analysed. Three scenarios will be considered: micro-, pico- and macro-cells.

1.2 Structure of the dissertation

The structure of this work consists of six chapters, followed by a set of annexes.

In Chapter 2, aspects related with the system and channel model are described. This work is written with reference to UMTS, so some issues of this system are presented. The air interface of UMTS and interferences are described. Also some problems related with the capacity are addressed. In the chapter, a review of radio channel models can be found, among them the Geometrically Based Single Bounce (GBSB) model. The GBSB model after some improvements simulates the radio channel in the simulator. The model is considered in three scenarios, so descriptions of the used scenarios can be found in the chapter. At the end of Chapter 2, linear and circular antenna arrays are described.

Chapter 3 is focused on MIMO systems aspects. The systems are described with reference to signal correlation. The main advantages of a MIMO system are presented as well. In the chapter, considerations related with the capacity of MMO systems can be found. The GBSB model adopted for a MIMO system is derived in the chapter.

All issues related with the implementation of the model in the simulator can be found in Chapter 4. The chapter is divided into two parts. The first one describes all aspects of the simulator with reference to SISO systems. Input and output parameters are presented and a structure of the code is shown. Also, a way of assessing the simulator is described in the chapter. In the second part, all problems with enhancement of the simulator in order to simulate the MIMO radio channel are presented. The structure of this part is similar to first one, but remarks are related with MIMO aspects.

In Chapter 5, details about simulations are presented. First, the chosen scenarios are carefully described. Information about the city street, rail station and highway scenario can be found at

the beginning of the chapter. In the following parts of the chapter, results of the simulations are presented. The simulations regard different number of antennas, various mutual positions of the BS and the MT, and various spacing between antennas.

Chapter 6 contains conclusions from carried out simulations related with the three considered scenarios. Some clues related with performing more simulations can also be found in the chapter.

Annexes consist of supplement to all chapters. In the annexes, not presented in previous parts of the work, graphs can be found. Some considerations necessary to explain achieved results are put in the annexes.

2

System and channel model

In this chapter, some information related with radio interface of UMTS can be found. The system is also presented with reference to capacity and interferences. A review of radio channel models can be found in the chapter as well. The GBSB model is described in detail. In the end, some aspects related with linear and circular antenna arrays are presented.

2.1 UMTS – system aspects

2.1.1 Aspects of air interface

In Universal Mobile Telecommunications System (UMTS), one can distinguish two transmission modes between the Mobile Terminal (MT) and the Base Station (BS), which are related with the use of the frequency spectrum. Frequency bands are divided into complementary and non-complementary regions. Additionally, fragments of the spectrum are reserved for satellite communication, but this is out of interest for this work. The bandwidths for UMTS are shown in Figure 2.1.

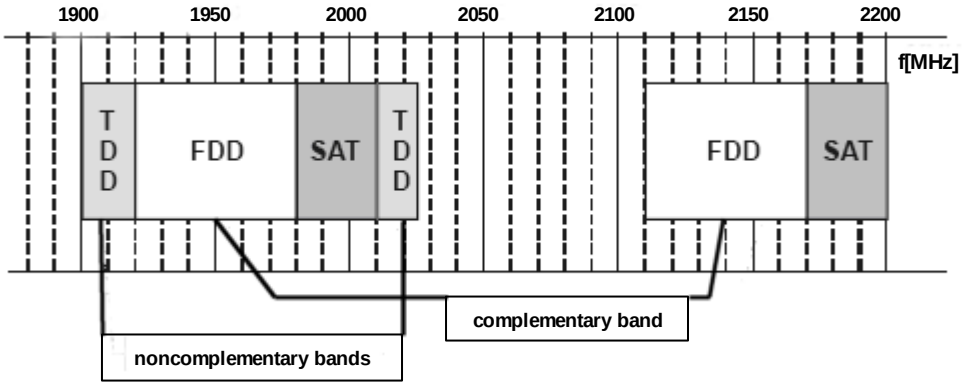

Figure 2.1 – UMTS bandwidth [KoCi04].

The non-complementary bandwidths are connected with Time Division Duplex (TDD), which are allocated at [1900-1920] MHz and [2010-2025] MHz. In these parts of the spectrum, Time Division-Code Division Multiple Access (TD-CDMA) is used [KoCi04].

TDD is a transmission method that uses only one frequency channel for transmitting and receiving, separating them by different time slots. This means that both the MT and the BS radiate power using the same frequency carrier, but in different periods of time.

In Figure 2.2 one can see time slots for three users. Users number 1 and number 2 use only one slot for the downlink (DL) and one slot for the uplink (UL), but user number 3 needs a bigger throughput for the download, therefore, the system allocates more time slots for the download.

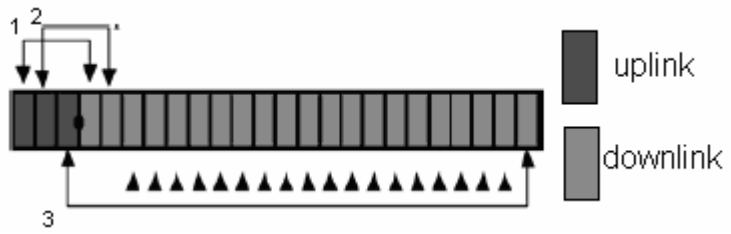

Figure 2.2 – Slots in TDD [KoCi04].

Generally speaking, there are the same propagation conditions in both directions. But it must be taken into consideration that the coherence time, the period that a radio channel can be treated like constant (later, it will be described more carefully), can be shorter than the time duplex interval, in which case the channel characteristics are dissimilar for the two directions of the radio link.

Frequency Division Duplex (FDD) is used in the complementary part of the bandwidth, which is allocated at [1920-1980] MHz (UL) and [2110, 2170] MHz (DL). Different from the method for TDD, Wideband-CDMA (W-CDMA) [KoCi04] is used. In FDD there are 12 radio channels, while in TDD there are 7.

The application of FDD means occupation of two identical bandwidths, which is very useful for voice transmission. For typical speech, both the UL and the DL are busy with the same ratio. In data or multimedia transmission, there exists a clear asymmetry in the UL and DL occupation. A link toward the subscriber can be used more intensive. Sometimes there is a tenfold difference in throughput of information. Concluding, TDD is best suitable for data and multimedia transmission, because in this technique link asymmetry is available. The number of time slots for the DL and UL depend on the need of the subscriber. System resources can be allocated in a dynamic way.

FDD is a transmission in which the two sides of the radio link use a different bandwidth to transmit. The distance in the radio spectrum between the MT and the BS is constant and equals 190 MHz for each cell. Due to this, there are different conditions for signal propagation for the DL and the UL. Thus, one must consider these links separately. Parameters for FDD and TDD are presented in Table 2.1.

There are three kinds of channels related with UMTS [KoCi04]:

- Physical channel – realise the transmission using the radio resources. They are defined by the radio channel (central frequency and bandwidth) and the scrambling codes.
- Transport channel – determine the way of the transmission:
  - Common – this type of channel is used to send information to all MTs within a cell.
  - Dedicated – carry information between the MT and the BS. It is possible to control the throughput and the power of the transmitter.
- Logical channel – determine the type of information.

Table 2.1 – Parameters of FDD and TDD in UMTS [KoCi04].

Duplex Method	FDD	TDD
Multi-access technique	FDMA, CDMA	TDMA, CDMA
Distance between adjacent channels [MHz]	5	5/1.6
Radio channel throughput [Mchip/s]	3.84	3.84/1.28
Spreading	4…512	1…16
Frame duration [ms]	10	
Amount time slots per frame	15	
Changing throughput to subscriber	Length of code	Amount of time slots and length of code
Protecting coding	Convolution codes and turbo-codes	
Interleave [ms]	10, 20, 40, 80	
Modulation	QPSK	
Detection in receiver	Coherent with pilot	Coherent with training sequence
Power control [Hz]	1500	100…800

2.1.2 Interference and capacity

A link from the MT to the BS determines the quality of the overall communication [KoCi04]. Power control of transmitters is a very important factor influencing the capacity of the entire system. In a system with code spreading, it is essential that the BS receives the signals from every user with the same power level.

According to [3GGP00], the signal to interference and noise ratio for the UL and the DL are respectively given by:

$$SIR_{UL} = \frac{G_p P_{Rx}}{(I - \beta_{SIR}) I_{intra} + I_{inter} + N_0} \quad (2.1)$$

$$SIR_{DL} = \frac{G_P P_{Rx}}{\alpha_{SIR} I_{intra} + I_{inter} + N_0} \quad (2.2)$$

where:

- G_p: spreading gain – ratio bandwidth after spreading to bandwidth before spreading
- $P_{Rx[W]}$: power of the received signal
- $N_{0[W]}$: power of the thermal noise
- $I_{intra[W]}$: power of the interference generated inside the own cell
- $I_{inter[W]}$: power of the interference from other cells
- α_{SIR}: orthogonality factor
- β_{SIR}: interference reduction factor

The orthogonality factor α_{SIR} describes the influence of the multipath propagation on the characteristics of the DL for the radio interface (with code division). When α_{SIR} equals 0, it means perfect detection conditions and intra-cell interference does not exist. The opposite situation takes place when α_{SIR} equals 1.Typical values of orthogonality factor are [3GGP00]:

- 0.4 for macro-cells
- 0.06 for micro-cells

The expression for the power of the interference from other cells, inter-cell interference, accumulates the influences of radio signal transmitted by users from adjacent cells. Additionally, another cellular operator can be a source of interference.

The capacity of a mobile cellular system determines the maximum number of users per cell. In UMTS, capacity is bounded mainly by the DL, because the transmit power of BS is limited. It is also related with aspects like spreading codes, user's behaviour (meaning, e.g., throughput or velocity of terminal) and many others. In UMTS, there are three main factors, which directly describe capacity:

- air interface traffic load
- the maximum BS transmission power
- number of OVSF codes

The influence of the number of OVSF codes on the overall system capacity is important in some situations, e.g., when almost all MTs are located near the BS and demand a low rate data transfer, see Table 2.2.

Table 2.2 – Maximum bit rate for Dedicated Physical Control Channel (DPCCH) [KoCi04].

Number of OVSF Codes	Bit rate for DPDCH [kbit/s]
256	15
128	30
64	60
32	120
16	240
8	480
4	960

The capacity of the system is also dependent on load factors, which define load both in the UL and the DL, respectively given by:

$$\eta_{\mathrm{UL}} = (1 + i_{BS}) \sum_{j=1}^{N_{UL}} \left(1 + \frac{\frac{R_c}{R_{bj}}}{\left(\frac{E_b}{N_{sp}} \right)_j \nu_j} \right)^{-1} \tag{2.3}$$

$$\eta_{\mathrm{DL}} = \left(\left(1 - \overline{\alpha} \right) + i_{MT} \right) \sum_{j=1}^{N_{DL}} \nu_j \frac{\left(\frac{E_b}{N_{sp}} \right)_j}{\frac{R_c}{R_{bj}}} \tag{2.4}$$

where:

- N_{UL}: number of users per cell
- N_{DL}: number of connections per cell = N_{UL} × (1 + soft handover overhead)
- ν_j: activity factor of user j at the physical layer, usually 0.67 for speech and 1 for data
- E_b: signal energy per bit
- N_{sp}: noise spectral density (including thermal noise and interference)
- R_c: WCDMA chip rate (3.84 Mchip/s)
- R_{bj}: bit rate of user j
- i_{BS}: inter-cell to intra-cell interferences ratio as seen by the BS receiver

- i_{MT}: inter-cell to intra-cell BS power received by the MT, typically 0.65 for macrocell and 0.2 for microcell
- $\overline{\alpha}$: average ortogonality factor in the cell, from range [0,1], typically values are 0.6 for vehicular and 0.9 for pedestrian [Reis04]

The capacity of the system is also bounded by the maximum power of the BS:

$$P_{\max} = \frac{N_0 R_c}{1-\overline{\eta_{\mathrm{DL}}}} \sum_{j=1}^{N_{UL}} \frac{\left(\frac{E_b}{N_0}\right)}{\frac{R_c}{R_{bj}}} \overline{L_{pj}} \tag{2.5}$$

where:

- $\overline{L_{pj}}$: average attenuation between the BS and user *j*
- $\overline{\eta_{DL\ [\mathrm{bit/s}]}}$: average throughput for downlink

One can see that the capacity increases with the processing gain or decreases with E_b/N_0. But a drop of E_b/N_0 is always related with a decrease of quality of service. Taking under consideration the fact that the specific profile of human conversation makes it possible to introduce an activity factor, applying this coefficient causes the capacity of the system to improve [KoCi04].

The dynamic exchange between the capacity and the quality exists in each code spreading system. When the number of users in the cell decreases, it causes E_b/N_0 to increase. Moreover, a lower number of subscribers in the cell causes a drop of power of the intra-interferences. This means an improve of quality makes it possible to transmit data with higher throughput. A similar relationship exists between capacity and coverage.

2.2 Channel models

2.2.1 General aspects

Considerations about the models of a radio channel and the aspects of propagation are very important to create a simulator of radio channel. The use of such a tool is necessary in conditions where it is impossible to do measurements, e.g., in an inaccessible terrain, where the

simulation is the sole way to achieve very valuable information about the profile of the radio channel. The results from simulations can be used in the design or to make improvements in the area of radio planning, sensible deployment of BSs, and many others. Only a well examined channel model provides the opportunity to make improvements. It is also possible to make estimations of the capacity and the coverage of the system, which is really important for operators.

Three kinds of propagations model can be distinguished:

- empirical (statistical) model
- deterministic model
- mixed, based on the empirical and deterministic model

Before discussing channel models, it is necessary to introduce the propagation aspects. There are three main mechanisms considered during the analysis of propagation [Kosi04]:

- reflection – takes place if the dimension of the obstruction is significantly bigger than the wave length.
- diffraction – appears when waves meet objects with sharp edges. The wave is bent by the edge of an obstruction.
- scattering – is present if the dimension of the obstruction is smaller than the wave length, e.g., plants, rain, rough surfaces.

The radio channel can be described using time dispersion parameters like [Kosi04]:

- Mean Excess Delay

$$\bar{\tau}_{[s]} = \frac{\sum_k h_k^2 \tau_k}{\sum_k h_k^2} = \frac{\sum_k P_k \tau_k}{\sum_k P_k} \tag{2.6}$$

- RMS Delay Spread

$$\sigma_{\tau[s]} = \sqrt{\overline{\tau^2} - \left(\bar{\tau}\right)^2} \tag{2.7}$$

where:

$$\overline{\tau^2}_{[s^2]} = \frac{\sum_k h_k^2 \tau_k^2}{\sum_k h_k^2} = \frac{\sum_k P_k \tau_k^2}{\sum_k P_k} \tag{2.8}$$

- $h_{k[V]}$: amplitude the Channel Impulse Response (CIR) at instant τ_k

- $P_{k[W]}$: a power of the CIR at instant τ_k

The radio channel can also be defined by a coherence bandwidth and a coherence time. The coherence bandwidth is a range of frequencies over which the radio channel is flat. It means that all spectral components pass the channel with the same gain and with a linear phase shift. The coherence bandwidth can be also defined in another way. It is possible to define the coherence bandwidth as the range of frequencies over which the frequency correlation is above 0.9, which gives [Kosi04]:

$$B_{C[Hz]} = \frac{1}{50\sigma_\tau} \tag{2.9}$$

In the typical mobile radio channel, the coherence bandwidth is significantly narrower than the frequency spacing in FDD. It means that the UL and the DL bandwidth should be considered separately [MaCo04].

The coherence bandwidth does not describe the varying nature of the channel caused by motion of a transmitter or a receiver, which is taken into consideration by the coherence time. The coherence time is the duration over which the CIR is essentially invariant, and it can be defined as [Kosi04]:

$$T_{C[s]} \propto \frac{1}{f_m} \tag{2.10}$$

where:

- $f_{m[Hz]}$: a maximum Doppler shift frequency:

$$f_m = \frac{v}{\lambda} \tag{2.11}$$

- $v_{[m/s]}$: velocity of the MT or the BS
- $\lambda_{[m]}$: wavelength

If a correlation above 0.5 is assumed, the coherence time has the following form:

$$T_{C[s]} = \frac{9}{16\pi f_m} \tag{2.12}$$

If the symbol period of the baseband signal is greater than the coherence time, the signal is changing during its transmission. The coherence time definition implies that two signals,

arriving with a time separation greater than the coherence time, are affected differently by the radio channel.

In most causes, especially when the velocity of the MT is low, the coherence time is longer than the time interval in TDD [MaCo04]. Thus, it is possible to use the same model for both ways of transmission.

2.2.2 Models

Empirical models are defined by statistical distributions, which are the result of the analysis of many measurement sessions. These models are very flexible and do not demand the tricky knowledge about an environment, but their accuracy is not very high.

In the deterministic models, the knowledge of the environments is needed. This approach uses a database of terrains and buildings within the desirable environment. Also electromagnetic techniques are exploited. Deterministic models estimate the propagation of radio waves analytically, relying on mathematical formulas. Two techniques are known: solving electromagnetic formulas, and ray tracing. The former is highly complicated, and the latter needs a huge computer power.

In a deterministic view, accuracy depends only on the accuracy of reproduction of the environment. So, it is possible to obtain an accurate channel model. But a disadvantage of this approach is that it demands huge amounts of geometry information about localisations of obstructions and a large computational effort.

Combined models, which mix the two models presented above, can achieve good accuracy, but do not demand such huge computational efforts, like the deterministic ones. These models are some kind of compromise between accuracy and complexity. As it is presented in [MaCo04], arriving signals can result from geometric contributors – just like in the deterministic model, but some properties of the contributors (e.g., localisation, physical characteristics) can be modelled statistically.

Some systems with omni-directional antennas working in a statistical model are described by a signal strength, a power delay profile (PDP), and a Doppler spectrum. An example of a model which has a path loss with distance as an output parameter is the COST 231 Okumura-Hata model [DaCoT99]. Each environment specification is described by different equations. The model provides fast calculations and is not complex. But the calculation's precision is not very high, and depends on the structure of the terrain.

The Ikegami model is an example of a deterministic model [DaCoT99]. The Ikegami model provides a deterministic prediction of field strength in some destinations points. To apply this method, a database including information about buildings, heights, shapes and localisations, is necessary. The model relies on ray tracing, and uses geometrical optics to model reflections of optical rays.

Space-time models provide spatial information and parameters like Angle of Arrival (AoA) and Time of Arrival (ToA), and are very important to analyze smart antennas and beamformers of space-time systems. In systems with multiple antennas, information about direction is very important and models that provide these types of data are required. Below, examples of the mentioned models are presented:

- Lee's Model
- Discrete Uniform Model
- Gaussian Wide Sense Stationary Uncorrelated Scattering Model
- Uniform Sectored Distribution Model
- Geometrically Based Single Bounce Channel Model

Lee's model was one of the first models, which considered spatial modelling [Lee73]. The Lee model assumes that reflection contributors are evenly deployed in a circle. At the centre of the circle is an MT, see Figure 2.3.

Scatters are distributed around the MT, and a receiver installed on the MT can only detect NLoS components. The drawn reflectors represent overall behaviour of blockers enclosed by the circle [Marq01].

Based on definitions of R and d_0 from Figure 2.3, one can derive a form describing the AoA (2.13) [Marq01].

$$\varphi_i = \frac{R}{d_0} sin\left(\frac{2\pi}{N_{sc}} i\right) \tag{2.13}$$

where:

- $i = 1,..., N_{sc}$
- N_{sc}: number of scatterers (all are uniformly distributed on circle)
- $d_{0[m]}$: distance between the MT and the BS
- $R_{[m]}$: radius of the circle, where the scatterers are deployed

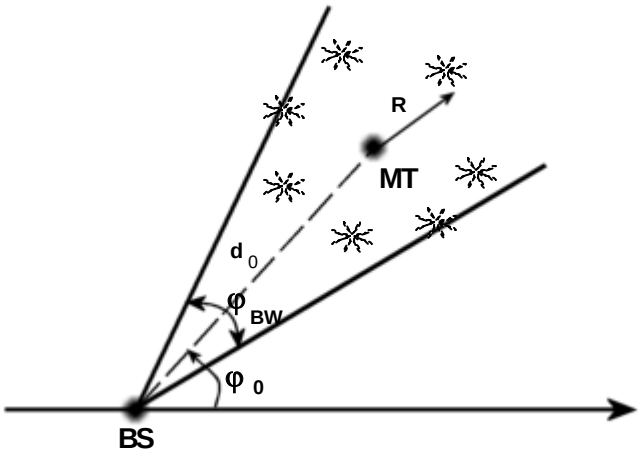

Figure 2.3 – Lee's model.

The signal correlations between two array elements, with assumptions that the complex magnitude has zero mean and unitary variance, has the form [Marq01]:

$$corr(d,\varphi_0) = \frac{1}{N}\sum_{i=0}^{N-1} exp\left[-j\frac{2\pi d}{\lambda} cos(\varphi_0 + \varphi_i)\right] \tag{2.14}$$

where:

- $d_{[m]}$: spacing between antennas in an antenna array

In its original form, this model was used to determine the correlation, but it was expanded to consider small-scale fading caused by the Doppler shift, by imposing an angular velocity on the ring of scatterers. The angular velocity of the scatterers, corresponding to the maximum Doppler shift, is equal to [ErCa98]:

$$\omega_D = \frac{V}{R} \tag{2.15}$$

where:

- $v_{[m/s]}$: velocity of the MT

In case of effective's scatterers on ellipse lines, the concentration of scatterers is focused on two areas: one finds them in ellipses connected with minimum delay, and with maximum delay. And in between them, the concentrations are low. This kind of distribution is called "U-shape".

The Discrete Uniform Model (DUM) is useful to predict the correlation function between any of two elements of an antenna array [ErCa98]. DUM is similar to the earlier presented Lee model. The model assumes N_{sc} uniformly distributed scatterers in space, within a narrow beamwidth, as shown in Figure 2.4. As one can see, the beamwitdh is centred relative to the LoS component.

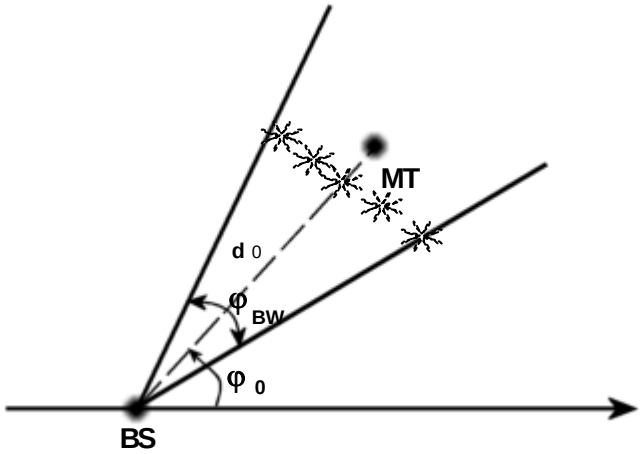

Figure 2.4 – Discrete Uniformly Distribution model.

The formula describing the AoA is given by [ErCa98]:

$$\varphi_i = \frac{1}{N-1}\varphi_{BW} i \tag{2.16}$$

where:

- $i = -\frac{N_{sc}-1}{2},\ldots,\frac{N_{sc}+1}{2}$

Correlation between two antenna elements can be described by:

$$corr(d,\varphi_0) = \frac{1}{N_{sc}} \sum_{i=-\frac{N_{sc}-1}{2}}^{\frac{N_{sc}+1}{2}} \exp\left[-j2\pi d \cdot \cos(\varphi_0 + \varphi_i)\right] \tag{2.17}$$

According to [ErCa98], the AoA distribution in the rural and suburban environments has a Gaussian continuous distribution, and the characteristic of the AoA in the urban environments

tends to be discrete. Therefore, to describe the correlation function between two antenna arrays one should use the discrete version of the AoA distribution.

Using this model, it is possible to determine the array correlation matrix, but it does not enable to calculate such parameters like delay spread, and Doppler spread, which require simulations.

The Gaussian Wide Sense Stationary Uncorrelated Scattering (GWSSUS) model is an example of a statistical model. This model assumes that scatterers are grouped into clusters in space. The received signal is a result of scatterers, which are grouped in N_{cl} clusters [Marq01]. The difference between delays, which are correlated with particular contributors, is not larger than the period of the signal, so the channel can be considered as wideband. There is no correlation between clusters. It is possible to model a frequency-selective fading channel, by including multiple clusters. The vector of the received signal can be described as [ErCa98]:

$$y(t) = \sum_{i=1}^{N_{cl}} v_{i,b} conv(t - \tau_k) \tag{2.18}$$

where:

- N_{cl}: number of clusters
- *conv(t)*: the convolution of the modulation pulse shape with the receiver filter impulse response
- $v_{i,b}$: superposition of the steering vectors during the i^{th} data burst within the k^{th} cluster

$$v_{i,b} = \sum_{j=1}^{N_{sc,k}} E_{Rx\,i,j} e^{j\phi_{Rx\,i,j}} G_{Rx}\left(\varphi_{0,j} - \varphi_{i,j}\right) \tag{2.19}$$

- $N_{sc,k}$: number of scatterers within k^{th} cluster
- $E_{Rx\,i,j}$[V] amplitude of i^{th} component reflected from j^{th} cluster
- $\Phi_{Rx\,i,j}$[rad]: phase of i^{th} component reflected from j^{th} cluster
- $\varphi_{i,j}$[rad]:AoA of i^{th} component reflected from j^{th} cluster
- $\varphi_{0,j}$[rad]:mean value of AoA from j^{th} cluster
- $G_{Rx}(\varphi)$: array response vector in the direction of φ

In the case that every cluster consists of a sufficient large number of the scatterers $v_{i,b}$ can be assumed according to a Gaussian distribution. This model assumes that time delays τ_k can be considered constant over several burst, phases $\Phi_{Rx\,i,j}$ vary more significantly, and vectors $v_{i,b}$ are zero mean complex Gaussian distributed wide sense stationary random processes (stationary

during several data bursts in this case) [Marq01]. In case there is no LoS, the mean value will be zero due to the uniformly distributed phase form range [0,2π[. When LoS is present, the mean value corresponds to the array response vector [ErCa98]:

$$E\{v_{i,b}\} \propto G_{Rx}(\varphi_{0,j})$$

The expression for the covariance matrix for the j^{th} cluster has the form [Marq01]:

$$\mathbf{cov}_i = E\{v_{i,b} v_{i,b}{}^H\} = \sum_{j=1}^{N_{sc,k}} \left|E_{Rx,i,j}\right|^2 E\{G_{Rx}(\varphi_{0,i} - \varphi_{i,j}) G_{Rx}(\varphi_{0,i} - \varphi_{i,j})^H\} \tag{2.20}$$

The Gaussian Wide Sense Stationary Uncorrelated Scattering model provides a fairly general result for the form of the covariance matrix [ErCa98]. This model requires some additional information of the propagation environment, because it does not give any indication about the amount and localisation of scatterers.

The concept of Uniform Sectored Distribution Model (USD), based on [MaHu03], is presented in Figure 2.5. This model assumes that all scatterers are uniformly distributed within some region, which is bounded by some angular and radial range. Every scatterer has a coefficient, which magnitude and phase are selected random from the distribution of U[0,1] for magnitude, and of U[0,2π] for phase. When the number of scatterers reaches infinity, the received signal will be similar to Raleigh faded with uniform phase [MaHu03]. This model is convenient to consider aspects connected with the effects of angle spread on spatial diversity techniques [ErCa98].

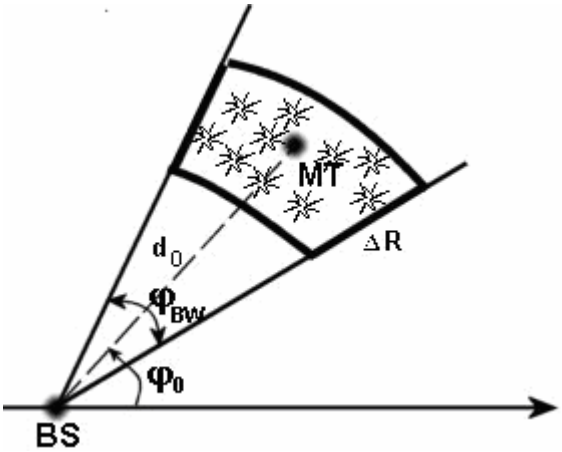

Figure 2.5 – USD model.

In Geometrically Based Single Bounce (GBSB) [LiRa99] channel models, the ToA and the AoA are derived with reference to the position of the transmit antenna, the position of receive antenna and a distribution of scatterers. Trigonometric relations are used to determine the mentioned parameters, but the distribution of scatterers is drawn. Also the specification of scatterers is random, because the magnitude and the phase have random values. Every scatterer generates one multipath component, which arriving at the receiver has a unique magnitude and phase. Also the delay time is random. The scatterer has no dimension, and therefore the scatterers do not overshadow each other. So the GBSB Model is a combination of deterministic and statistical features.

2.2.3 Scenarios

Usually three main typical scenarios are taken into account: a pico-, a micro- and a macro-cell. The location of the BS and the MT with reference to the deployment of scatterers is the main feature that distinguishes the scenarios [MaCo04]. The radius of the cell is also a factor which is helpful to sort the mentioned scenarios. According to the definition of Prasad [Pras98], the pico-cell has radius smaller than 200 m, the micro-cell has radius within [0.2, 1] km, and the macro-cell is larger than 1 km.

The area of the pico-cell is bounded by a circle, with the BS at its centre. The location of the MT is not defined, and depends on the actual position of the user. The LoS component exists in the considered scenario. A density of scatterers, Figure 2.6, is specific to each individual environment.

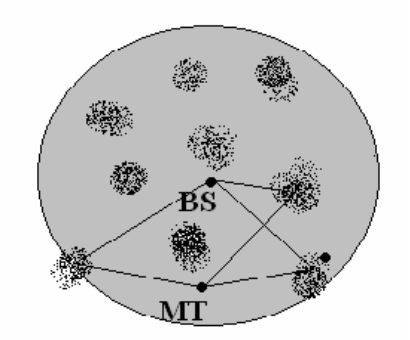

Figure 2.6 – Pico-cell scattering model.

The pico-cell is usually located inside buildings (e.g., hall of shopping centers). Dimensions of the place, where the pico-cell is established, mainly influences the radius of circle.

In micro-cells, the scattering takes place in the surroundings of both the BS and the MT, and also in the region between them [MaCo04]. The micro-cell scenario usually occurs when both the BS and the MT are located bellow rooftops, e.g., a street in the urban area. Scatterers are deployed, with the same density, around the BS, the MT, and in the zone between them.

When modelling a street-type environment the considered region should be bounded by the street width. The zone of multipath propagation has the shape of an ellipse, Figure 2.7, whose foci are the BS and the MT. The minor axis of the ellipse is determined by the width of the street.

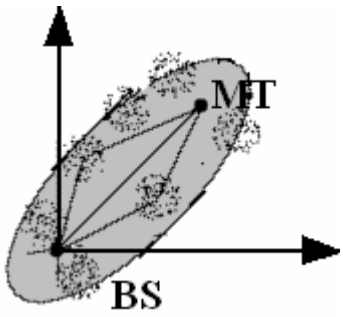

Figure 2.7 – Micro-cell scattering model.

Additionally, not only single bounces should be taken into account. Therefore, an effective street width is introduced, which is weighed by an effective street width ratio. Some parameters for the micro-cell model are presented in Table 2.3.

In the macro-cell scenario, the height of the BS antenna is larger than the height of the MT antenna, from which it follows that the scattering contributions are located in the area near to the location of the MT [MaCo04].

In the macro-cell case, the region of influence has the shape of circle, Figure 2.8. The scattering contributions in the vicinity of the BS will be disregarded.

The dimension of the circle is stipulated by a distribution of scatterers. The scatterers, placed on an external circle, produce the multipath components with the longest time delay. An assumption of a planar model is still correct, as long as the distance between the MT and the BS is large comparing to the difference between antenna heights.

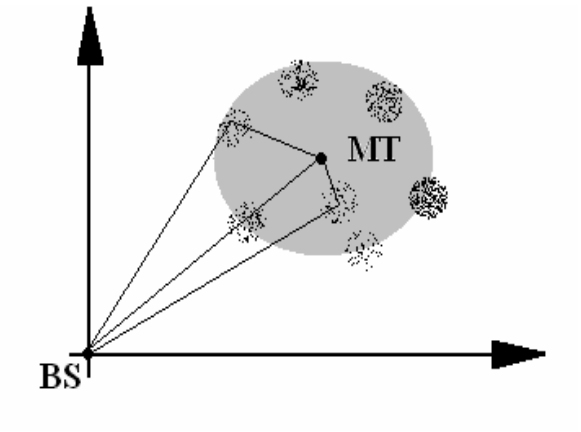

Figure 2.8 – Macro-cell scattering model.

Table 2.3 – Parameter list for the micro-, pico-, macro-cell model [MaCo04].

	Pico-cell	**Micro-cell**	**Macro-cell**
Region of influence:			
Region shape	Circle	Ellipse	Circle
Cluster distribution	Uniform within region		
Scattering circle radius	Measurement dependent		
Street width	Street dependent		
Effective street width ratio	Measurement dependent		
Cluster:			
Distribution of scatterers within clusters	Gaussian		
Cluster dimension (standard deviation)	Measurement dependent		
Cluster density	Measurement dependent		
Number scatterers per cluster	Poisson, Measurement dependent		
Average number scatterers per cluster	Measurement dependent		
Scatterers:			
Reflection coefficient magnitude distribution	Uniform [0, 1]		
Reflection coefficient phase distribution	Uniform [0, 2π[		
LoS path:	Yes	Yes	No

The next important difference between the macro- and the micro-cell is the fact that in the former there is no LoS component. The density of scattering contributors is essentially larger around the MT. So the LoS component is obstructed by the surrounding scatterers. Some parameters of the macro-cell scenario are presented in Table 2.3.

2.2.4 Geometrically Based Single Bounce Model

In the following part of this dissertation, the GBSB model [LiRa99] is presented in detail. This model is chosen to the implemented in a radio channel simulator.

In the GBSB model, the propagation environment is composed of scatterers, which are placed by statistical distributions, which are characteristic of specific conditions. More details about the deployment of scatterers can be taken from a description of the considered scenario, Table 2.3. Every scatterer is a source of one multipath component. A signal radiated from the transmitter and picked up at the receiver goes through the position of the corresponding scatterer, Figure 2.9. The scatterer is described by a random complex coefficient (2.21), which determines the influence on the multipath component. The magnitude of the coefficient, as well as the phase are random values,

$$\Gamma = |\Gamma| e^{j\Phi_{sc}} \tag{2.21}$$

where:

- $|\Gamma|$: the magnitude of the reflection coefficient, which has a uniform distribution in range [0,1]
- $\Phi_{sc\,[rad]}$: the phase of the reflection coefficient, which has a uniform distribution in range $[0,2\pi]$

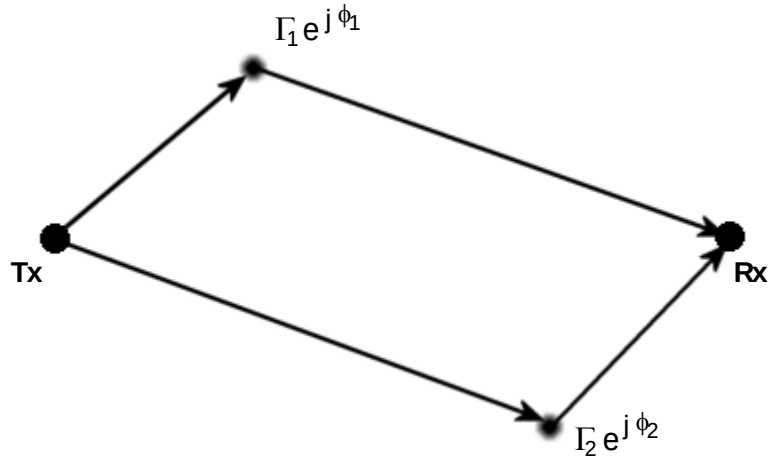

Figure 2.9 – Scatterers in the GBSB model.

After bouncing of the scatterer, the multipath component changes its magnitude and phase. The magnitude of the multipath is divided by the magnitude of the corresponding scatterer and the phase of the scatterer adds to the phase of the multipath component.

During some research by Saleh and Valenzuela [SaVa87], [LKTB02], Vainikainen [AMSM02], and Bonek [MoBo99] a specific phenomenon was observed, i.e., the scatterers are grouped into clusters. In the area of a cluster there is dense deployment of reflectors. The time of arrival of the multipath component depends on the location and shape of the clusters. Looking at the number of groups of multipath, it is possible to approximate the number of clusters in the environment. The distribution of clusters is characteristic for a considered scenario, Table 2.3.

The phenomenon of grouping the scatterers into clusters is the main difference between the GBSB model [LiRa99]and IST-TUL model [Marq01]. The IST-TUL model was developed by the Group For Research On Wireless of the Instituto Superior Técnico (IST).

The GBSB assumes that both the receiver (Rx) and the transmitter (Tx) are in the same plane that is parallel to the ground. Additionally, it is assumed, that all scatters are also located in this plane. Thus, it is natural that all multipath components also belong to this plane.

The model does not include rough surface scattering, diffraction, multiple bounce multipath and other mechanisms of propagation [LiRa99]. These assumptions make the analysis simpler, but the real zone of propagation is not modelled in a perfect way.

When both the Rx and Tx antenna are omni-directional, a complex envelope model for the multipath CIR is given by [LiRa99]:

$$\boldsymbol{h}(t) = \sum_{i=0}^{L-1} E_{Rx,i}\,\delta(t-\tau_i) = \sum_{i=0}^{L-1} \left|E_{Rx,i}\right| e^{j\Phi_{Rx,i}}\,\delta(t-\tau_i) \tag{2.22}$$

where:

- $\Phi_{Rx,i}$: phase of the i^{th} component
- τ_i: delay of the i^{th} component

It is possible to derive the probability density function based on geometrical consideration, for the case of elliptical deployment of the scatterers. This PDF has the form [Marq01]:

$$p_{\tau,\varphi}(\tau,\varphi)=\begin{cases}\dfrac{\left(d_0{}^2-\tau^2c^2\right)\left(d_0{}^2c+\tau^2c^3-2\tau c^2 d_0\cos(\varphi-\varphi_0)\right)}{\pi\tau_{\max}c\sqrt{\tau_{\max}^2c^2-d_0{}^2}\left(d_0\cos(\varphi-\varphi_0)-\tau c\right)^3}, & \dfrac{d_0}{c}<\tau\le\tau_{\max}\\ 0 & ,\text{elsewhere}\end{cases} \tag{2.23}$$

where:

- τ_{max}: observation time window
- d_0, φ_0: geometry parameters defined on Figure 2.10

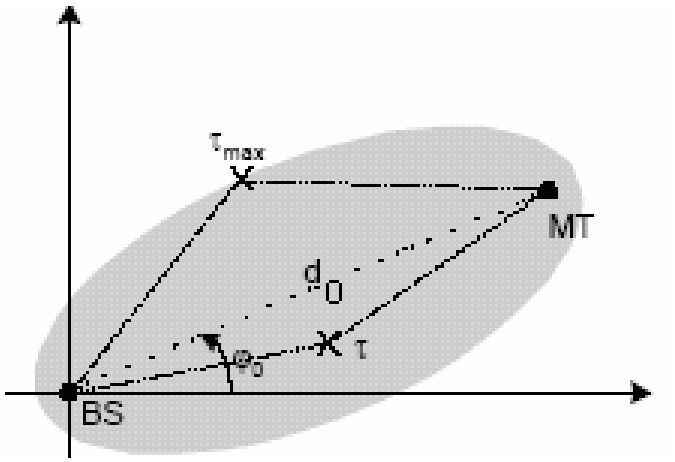

Figure 2.10 – Geometry for GBSBEM [Marq01].

To derive the joint density function for the AoA and the ToA, for the case of circular deployment of the scatterers, it is necessary to take advantage of the Jacobian Transformation, which makes it possible to achieve the PDF in an easy way. The resulting PDF is

$$p_{\tau,\varphi}(\tau,\varphi)=\frac{\left(d_0{}^2-\tau^2c^2\right)\left(d_0{}^2c+\tau^2c^3-2\tau c^2 d_0\cos(\varphi-\varphi_0)\right)}{4\pi R_{\max}^2\left(d_0\cos(\varphi-\varphi_0)-\tau c\right)^3} \tag{2.24}$$

where:

- R_{max}, φ_0: geometry parameter defined in Figure 2.11

The validity area for the BS and the MT cases are, respectively:

$$\frac{d_0{}^2-2d_0\tau c\cos(\varphi-\varphi_0)+\tau^2c^2}{\tau c-d_0\cos(\varphi-\varphi_0)}\le 2R_{\max}\wedge\tau>\frac{d_0}{c}$$

and (2.25)

$$\frac{d_0{}^2-\tau^2c^2}{d_0\cos(\varphi-\varphi_0)-\tau c}\le 2R_{\max}\wedge\tau>\frac{d_0}{c}$$

Out of the validity area the PDF is equal to zero.

The presented model is based on geometrical assumptions, so all output parameters are calculated in a geometrical way. All variables, which are needed to obtain the parameters, are presented in Figure 2.12.

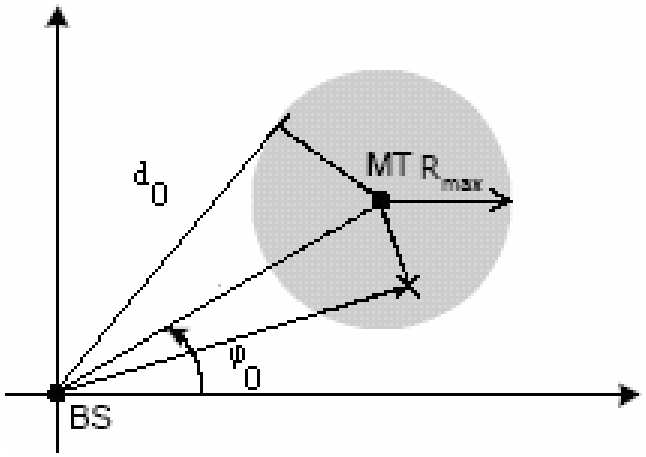

Figure 2.11 – Geometry for GBSBCM [Marq01].

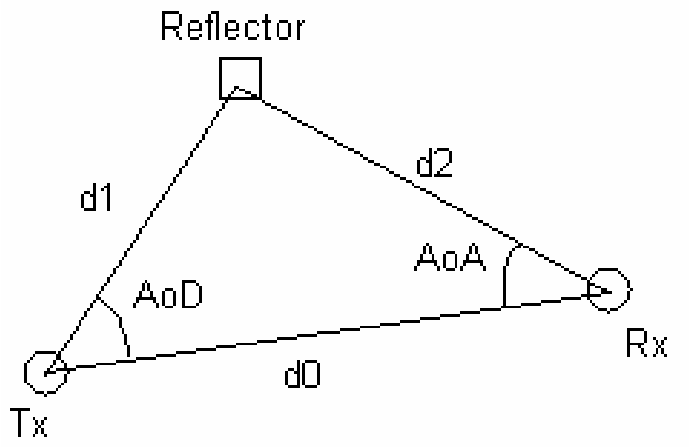

Figure 2.12 – Definition of some output parameters.

The AoA (φ) and AoD (θ) are obtained using the cosine formula:

$$\varphi_{[\mathrm{deg}]} = \arccos\left(\frac{d_0^2 + d_2^2 - d_1^2}{2 d_0 d_2}\right) \tag{2.26}$$

$$\theta_{[\mathrm{deg}]} = \arccos\left(\frac{d_0^2 + d_1^2 - d_2^2}{2 d_0 d_1}\right) \tag{2.27}$$

where distances d_0, d_1, d_2 are calculated from:

$$d_{0[m]} = \sqrt{(x_{Rx} - x_{Tx})^2 + (y_{Rx} - y_{Tx})^2} \tag{2.28}$$

$$d_{1[m]} = \sqrt{(x_{sc} - x_{Tx})^2 + (y_{sc} - y_{Tx})^2} \tag{2.29}$$

$$d_{2[m]} = \sqrt{(x_{Rx} - x_{sc})^2 + (y_{Rx} - y_{sc})^2} \tag{2.30}$$

where:

- (x_{Rx}, y_{Rx}): position of the Rx antenna
- (x_{Tx}, y_{Tx}) – position of the Tx antenna
- (x_{Ref}, y_{Ref}) – position of a reflector

The attenuation in free space and the reflection by scatterers must be taken into consideration to calculate the amplitude of a multipath component. The amplitude of the electric field detected at the Rx, is defined by:

$$E_{Rx[\mathrm{V/m}]} = \frac{\sqrt{30 \cdot P_{Tx} \cdot G_{Tx}(\theta)}}{d_1 + d_2} \cdot \Gamma \tag{2.31}$$

In case of the LoS component:

$$E_{Rx[\mathrm{V/m}]} = \frac{\sqrt{30 \cdot P_{Tx} \cdot G_{Tx}(0)}}{d_0} \tag{2.32}$$

where:

- $P_{Tx[\mathrm{W}]}$: the power of the Tx
- Γ: the reflection coefficient of the reflector
- G_{Tx}: radiation pattern of Tx antenna
- G_{Rx}: radiation pattern of Rx antenna

The signal detected by the antenna is described by equation [Orfa02]:

$$V = E_{Rx} \cdot h_{eff} \tag{2.33}$$

where:

- $h_{eff\,[\mathrm{m}]}$: effective lenght of antenna:

$$h_{eff} = \frac{\lambda}{\pi}\sqrt{\frac{R_A G_{Rx}(\varphi)}{120\pi}} \tag{2.34}$$

- $R_{A[\Omega]}$: feedpoint impedance of the antenna

Phase is another parameter obtained from simulation. The phase is related with the distance covered by the corresponding multipath component and complex reflection coefficient. The signal propagating from the Tx to the Rx covers the distance, which may not be equal to an integer multiple of the wave length. In case the signal reflects from a scatterer, an additional phase shift Φ_{sc} exists. An equation for the phase shift has the form:

$$\Phi_{Rx[^0]} = mod360\left(\left(\frac{d_1}{\lambda} - \left\lfloor \frac{d_1}{\lambda} \right\rfloor + \frac{d_2}{\lambda} - \left\lfloor \frac{d_2}{\lambda} \right\rfloor\right) \cdot 360 - \Phi_{sc}\right) \tag{2.35}$$

In case of the LoS component:

$$\Phi_{Rx[^0]} = \left(\frac{d_0}{\lambda} - \left\lfloor \frac{d_0}{\lambda} \right\rfloor\right) \cdot 360 \tag{2.36}$$

where:

- *mod360*(…): operation of modulo 360
- $\Phi_{sc[^0]}$: the reflector phase shift

The ToA describes the time delay of component, which is connected only with the distance of propagation:

$$\tau_{[s]} = \frac{d_1}{c} + \frac{d_2}{c} \tag{2.37}$$

and for the LoS component:

$$\tau_{[s]} = \frac{d_0}{c} \tag{2.38}$$

2.3 Antenna arrays – general aspects

In the channel simulator, both the Rx and the Tx can have singular radiators, multiple antennas, or antenna arrays. Some aspects connected with a linear and circular arrays, are presented in the next parts of the work.

There are two approaches for systems using several antennas; the antenna arrays and the multiple antennas are distinguished. The former takes into consideration the mutual coupling between the antennas, all antennas in the set influence one another, thus, all antennas can be treated like one abstract antenna with one radiation pattern. Looking at the transmit side of a

radio system it is worth noticing that each of the antennas transmits the same piece of information. The shape of the radiation pattern depends on some factors, the impact of each factor being described below. The latter approach does not consider the condition about the mutual coupling between antennas. Each of the antennas is treated separately, and the radiation pattern of the whole structure is the sum of radiation patterns of all antennas. In this case, the distance between antennas is larger, so they do not influence one another. In a real system, the small coupling between antennas exists, but in this work it will be neglected. This way of looking to a set of antennas is addressed for the MIMO system. So, each of the input antennas can transmit different information.

A uniform linear array consists of radiators, which are distributed uniformly along a line, with constant spacing *d*, Figure 2.13.

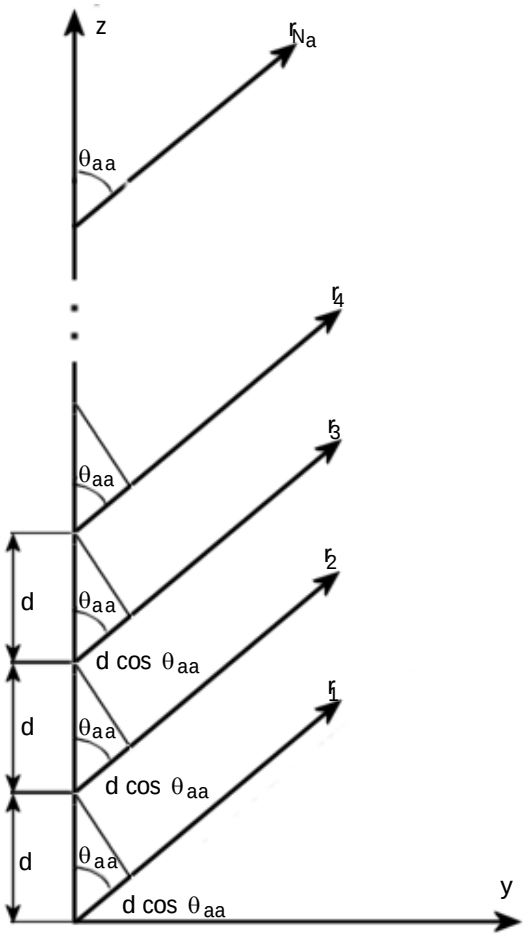

Figure 2.13 – Uniform linear array.

In the simplest array, all radiators are fed with the same amplitude and phase. The radiation pattern for the antenna array can be obtained as multiplication of a single antenna radiation

pattern and the Antenna Factor (AF). For the linear antenna array, the AF has the form of [VCGC03]:

$$AF = \sum_{n=1}^{N_a} e^{j\psi(n-1)} \tag{2.39}$$

where:

- N_a: number of antennas in array
- $\psi_{[rad]}$: phase coefficient given by:

$$\psi = kd\cos\theta + \psi_0 \tag{2.40}$$

- $\psi_{0[rad]}$: phase shift between radiators
- k: wave number

$$k = \frac{2\pi}{\lambda}$$

- d: spacing between antennas

(2.41)

The AF can be written in reduced form:

$$AF = \frac{\sin\left(\frac{N_a}{2}\psi\right)}{\sin\left(\frac{1}{2}\psi\right)} \tag{2.42}$$

The final radiation pattern for antenna array can be written as:

$$G(\theta_{aa}, \varphi_{aa}) = AF \cdot G_0(\theta_{aa}, \varphi_{aa}) \tag{2.43}$$

- $G_0(\theta_{aa},\varphi_{aa})$: radiation pattern of singular antenna

In a circular array, all radiators are distributed in the shape of a circle, Figure 2.14. The AF for the circular antenna array is of the form [VCGC03]:

$$AF(\theta_{aa}, \varphi_{aa}) = \sum_{n=1}^{N_a} I_n e^{j[ka\sin\theta\cos(\phi_{aa}-\alpha_n)+\Phi_n]} \tag{2.44}$$

where:

- $a_{[rad]}$: radius of circle
- I_n: feedings amplitude of n^{th} radiator – relative to the center of circle
- Φ_n: feedings phase of n^{th} radiator – relative to the center of circle
- $\alpha_n = 2\pi\frac{n}{N_a}$: the angular position of n^{th} element on the *x*-*y* plane

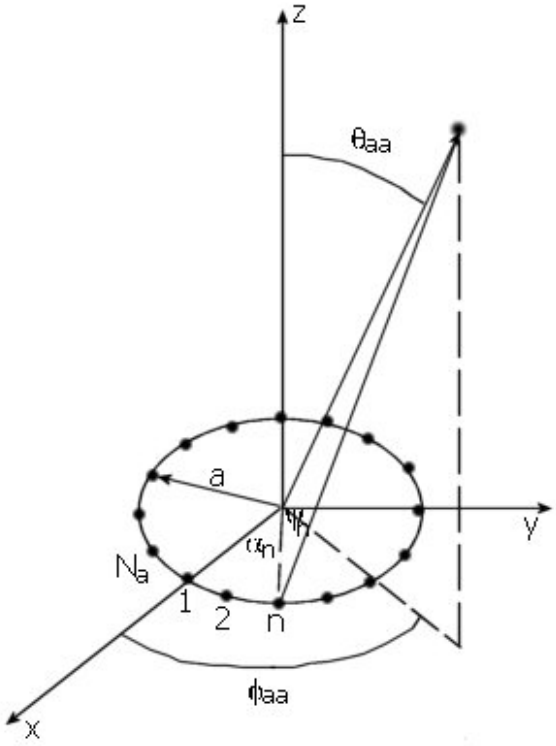

Figure 2.14 – Circular array [VCGC03].

3

MIMO Systems

This chapter includes a general description of MIMO systems. Considerations about correlation in the radio channel are placed here as well. The capacity of MIMO systems is presented. The GBSB model adopted for MIMO case is presented as well.

3.1 General aspects

Multiple-Input Multiple-Output (MIMO) exploits several antennas on the transmit and receive side of a radio system. MIMO takes advantage of the multipath propagation, which is characteristic for almost all radio systems. The phenomena on causes that the level of received signals depends on time, frequency and space. MIMO is treated as the next generation of adaptive smart antenna arrays. But in these two techniques there is a tremendous difference in approach to multipath propagation. The antenna array is based on selecting one of all the multipath components, whereas MIMO uses all arriving rays to achieve a better performance.

A diversity reception, which is well known in various radio applications, improves only BER statistics and reduces the probability of total outage. However, a system comprised of several antennas at the input and several antennas at the output not only improves of BER performance, but also causes an increase of channel capacity.

A scheme of ($n_R \times n_T$) MIMO array is depicted in Figure 3.1, is composed of n_T transmit antennas and n_R receive antennas [FoGa98]. The vector,

$$\boldsymbol{x}(k) = [x_1(k), x_1(k), ..., x_{n_T}(k)] \tag{3.1}$$

contains radiated symbols at time k from particular input antennas, which can transmit independent bit streams. The vector:

$$\boldsymbol{y}(k) = [y_1(k), y_1(k), ..., y_{n_R}(k)] \tag{3.2}$$

is composed of received symbols at time k. A relation between transmitted and received signal is shown in

$$\boldsymbol{y}(k) = \boldsymbol{h}(k) * \boldsymbol{x}(k) + \boldsymbol{N}(k) \tag{3.3}$$

where:

- $\boldsymbol{h}$: a matrix containing CIRs h_{ij} (CIR between the signals from j^{th} transmitter and i^{th} receiver)
- i: index of the receivers, $\{1, n_R\}$
- j: index of the transmitters, $\{1, n_T\}$
- (*): an operator of a convolution of digital signals
- $\boldsymbol{N(k)}$: a vector containing power of noise received by each antenna at k instance of time

In case of full decorrelation between all entries from matrix $\boldsymbol{h}$, it can be said that there are n_R parallel independent radio subchannels. The subchannels use the same frequency bandwidth and the same moment of time. This approach is very similar to the idea of code in CDMA, but MIMO is based on spatial identification, which strongly depends on the specifics of a multipath propagation environment. This situation is quite possible in a radio channel which has a dense distribution of scatterers. Reflectors generate the multipath components, which increase the decorrelation.

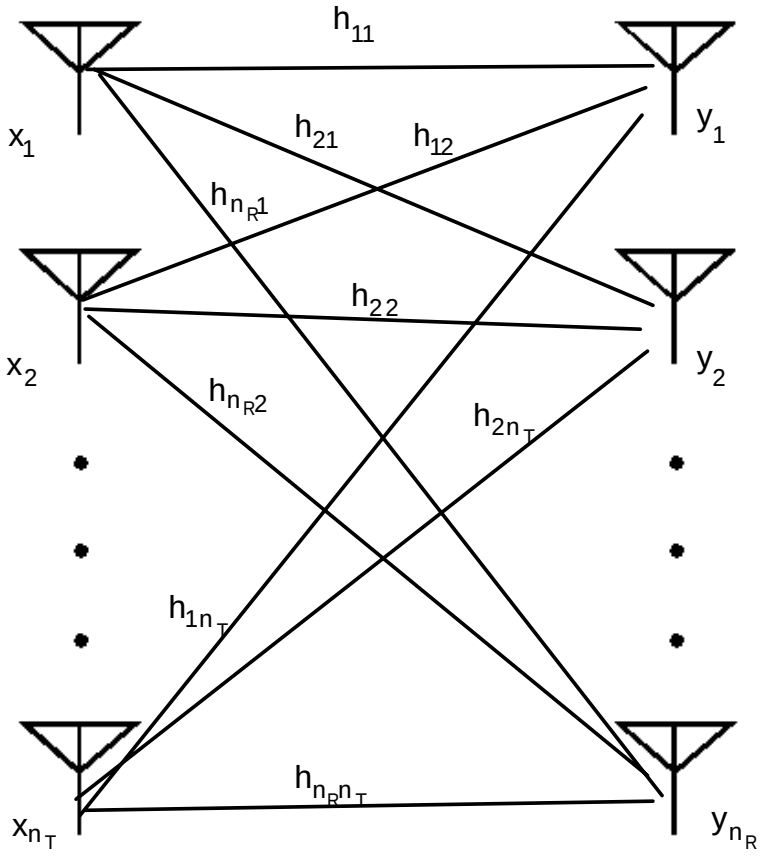

Figure 3.1 – Scheme of a MIMO system.

3.2 Signal correlation

MIMO is a system composed of several input and output antennas as is depicted in Figure 3.1. Depending on the application each, input antenna can be used to radiate a signal originated from different modulation schemes and carrying an independent data stream. The transmit signals are kept in (3.1), whereas receive signals are kept in (3.2) and both sides of the radio link are related by (3.3).

The input and output sides are connected by the CIR matrix ***g*** [FoGa98], the fixed linear matrix with Additive White Gaussian Noise (AWGN). Although fixed, the channel will often be taken to be random. The matrix has n_T columns and n_R rows and collects the CIRs between all pairs of the input and output antennas. The Fourier transform of ***g*** is denoted as ***G***. If a narrowband channel is assumed, ***G*** is treated as constant over the band of interest. The channel impulse response matrix ***g*** has also a normalised form ***h***, which is more convenient to use, (3.4). The elements of ***h*** matrix are normalised so that the average gain for the radio channel is equal to unity.

$$\boldsymbol{h} = \sqrt{\frac{P_{Tx}}{\overline{P}_{Rx}}}\boldsymbol{g} \tag{3.4}$$

where:

- $P_{Tx[\mathrm{W}]}$: the total transmit power, regardless the number of the input antennas
- $\overline{P}_{Rx\ [\mathrm{W}]}$: the average power received by each output antenna

The layout of the matrix ***h*** is

$$\boldsymbol{h} = \begin{bmatrix} h_{11} & h_{12} & \dots & h_{1n_T} \\ h_{21} & \dots & & \\ \dots & & \dots & \\ h_{n_R 1} & & & h_{n_R n_T} \end{bmatrix} \tag{3.5}$$

where:

- h_{ij}: a CIR between signal from the j^{th} transmit antenna to the i^{th} receive antenna

The same normalisation can be done on matrix ***G***, and as result matrix ***H*** is obtained

$$\boldsymbol{H} = \sqrt{\frac{P_{Tx}}{\overline{P}}}\boldsymbol{G} \tag{3.6}$$

After using the Fourier transform, the equations of the system have the form

$$\boldsymbol{Y} = \boldsymbol{HX} + \boldsymbol{N} \tag{3.7}$$

where:

- $\boldsymbol{X}_{[\mathrm{V}]}$: the complex amplitude of the x
- $\boldsymbol{Y}_{[\mathrm{V}]}$: the complex amplitude of the y

The above presented matrix ***H*** does not take into consideration mutual coupling between antennas. The antennas on each of side of a radio link are located very close, thus, radiators

influence on each other. On the input side, the independent data is fed to the individual antennas, but ,because of the close spacing, the radiated data streams become correlated. On the output side, the data streams receive by each antenna are also correlated. Considering the mutual coupling, the equations of the system have the following form [UtBi05]:

$$\boldsymbol{Y} = \boldsymbol{C_R H C_T X} + \boldsymbol{N} \tag{3.8}$$

- $\boldsymbol{C_R}$: is the coupling matrix for the receiving antenna array
- $\boldsymbol{C_R}$: is the coupling matrix for the transmitting antenna array

It is worth noticing that since a vector is the main unit of data, it is conveniently to use matrix operations to resolve a set of equations. If the matrix $\boldsymbol{H}$ is nonsingular, it is possible to find the unequivocal solution of the system. Singular Value Decomposition (SVD) is a way of checking if the system is solvable [Ande00]. After using SVD, the matrix $\boldsymbol{H}$ can be presented as

$$\boldsymbol{H} = \boldsymbol{U\,\Sigma\,V^H} \tag{3.9}$$

where:

- $\boldsymbol{U}$: unitary matrix containing the singular vectors of the matrix $\boldsymbol{H}$ after SVD
- $\boldsymbol{V}$: unitary matrix containing singular vectors of the matrix $\boldsymbol{H}$ after SVD
- a square unitary $\boldsymbol{W}$ is unitary if $\boldsymbol{W^H = W^{-1}}$
- $\boldsymbol{\Sigma}=diag[\sigma_1, \sigma_2, \ldots, \sigma_{min(nT,nR)}]$: are the singular values of the matrix $\boldsymbol{H}$
- $[]^H$: Hermitian operation

The form of $\boldsymbol{H}$ after SVD is helpful in the detection process, consisting of solving a system of the following equation.

$$\boldsymbol{Y} = \boldsymbol{U\Sigma\Sigma^H X} + \boldsymbol{N} \tag{3.10}$$

Additional matrix variables (3.11) and (3.12) are introduced which simplifies the form of (3.10).

$$\boldsymbol{Y'} = \boldsymbol{U^{-1}Y} \tag{3.11}$$

$$\boldsymbol{X'} = \boldsymbol{V^H X} \tag{3.12}$$

A simpler version of (3.10) is given by

$$\boldsymbol{Y'} = \boldsymbol{\Sigma X'} + \boldsymbol{N'} \tag{3.13}$$

where:

- $\boldsymbol{N' = U^{-1} N}$

Equation (3.13) can be interpreted like *r* parallel independent subchannels between transmit and receive sides. The number of parallels subchannels depends on the rank of the matrix ***H***, which is determined by a number of non-zero singular values. Additionally, the number of subchannels is constrained by the value of n_T or n_R. The interpretation of (3.13) is presented in Figure 3.2. The singular values $\{\sigma_1, \sigma_R\}$ are related with the values $\{\lambda_{e1}, \lambda_{er}\}$ by (3.14). However, values $\{\lambda_{e1}, \lambda_{er}\}$ are the eigenvalues of the correlation matrix ***R*** defined in (3.15)**.**

$$\sigma = \sqrt{\lambda_e} \tag{3.14}$$

$$\boldsymbol{R = HH^H} \tag{3.15}$$

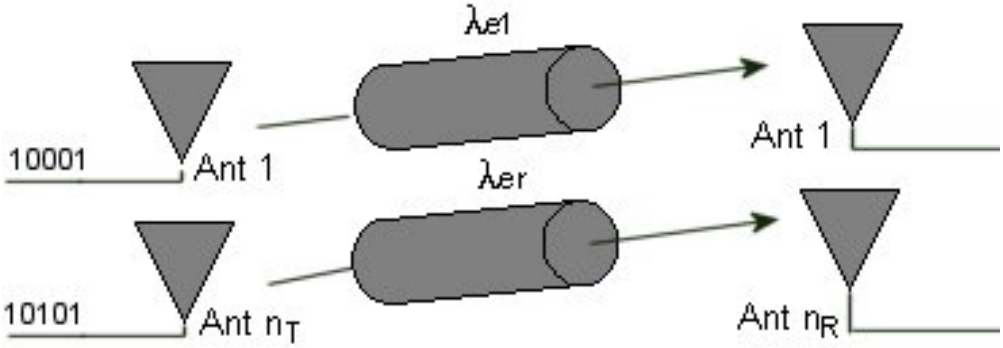

Figure 3.2 – Subchannels in a MIMO system.

When the state of the radio channel is known at the receiver before transmitting, input signals can be converted according to the elements of the singular vectors. After that, one can mark out several eigenmodes related with the parallel subchannels.

The existence of a high value of the parallel subchannels is possible only in environments that are rich in scatterers generating the multipath components. In this case, a correlation between the CIRs of the antennas pair is low enough. In this situation, the rank of ***H*** is high.

3.3 Capacity and BER performance

The main feature of MIMO is the ability to operate with a throughput greater than the capacity determined by Shannon's rule. The theoretical capacity for an AWGN channel is presented in [Proa01]

$$C = \log_2(1+\rho) \tag{3.16}$$

where:

- $C_{[b/s/Hz]}$: capacity of a radio channel
- ρ: signal to noise ratio

But, it does not mean that Shannon's bound is invalid. In specific conditions, in multipath environments, existence of independent subchannels causes the multiplication of the capacity. This is possible because in multipath environments, where a distribution of scatterers can be dense, multi element antennas at receive and transmit sides can create parallel channels, which can use the same carrier frequency and bandwidth simultaneous. The existence of the parallel channels is achievable because scatterers introduce randomness into the propagation environment, which is caused by the nature of scatterer, described by a complex reflection coefficient, see (2.21). The random character of the scatterers causes that the propagation of multipath components also has random direction but are dependent on the considered pair of input and output antennas.

In these circumstances, every input antenna can radiate different data streams in the same frequency bandwidth and at the same time. The transmitter can use a spatial multiplexing approach. The input data stream is divided into several substreams with lower bit-rate and each substream is grouped into a burst. After the demultiplexing phase, every burst from each substream is radiated by every transmit antenna. The sequence of transmitting depends on implementation. The multipath components from distinct input antennas have dissimilar ways of propagation. Thus, each substream actually experiences the best way of propagation and this is the reason why the capacity gain is possible. This situation is only possible when the CIRs at all pairs of input and output antennas are strongly decorrelated, otherwise the conditions of propagation are the same as in free space, where Shannon rule is valid in its convenient shape.

Another way to increase the capacity in a system exploiting MIMO is using space-time coding (STC). In the case of STC, the gain of capacity is obtained by adding some redundancy for the transmit signal. The example of STC is Space Time Block Coding (STBC) [GSSS03]. The blocks of input data are transformed into specific matrix $\boldsymbol{S}$. The rows of the matrix are related with the transmit antennas and the columns of the matrix correspond to the consecutive

moments of time. STBC does not provide the coding gain. A simple example of the matrix $\boldsymbol{S}$ for the system 2×2, presented by Alamouti, has the form [Alam98]

$$\boldsymbol{S} = \begin{bmatrix} x_1 & -x_2^* \\ x_2 & x_1^* \end{bmatrix} \tag{3.17}$$

where:

- $[]^*$: means complex conjugate
- x_1: signal for input antenna one
- x_2: signal for input antenna two

In case of using a non-normalised channel transfer matrix $\boldsymbol{T}$, which contains the channel transfer gains for each pair of antennas, the capacity of a MIMO system is given by (3.18), which is for the Rayleigh fading environment. Additionally, the equal distribution of power among all transmitting antennas (state of channel is not known at transmit side) has to be assumed [FoGa98].

$$C = \log_2 \left\{ \det \left[\boldsymbol{I}_{\boldsymbol{n_R}} + \left(\frac{E_{Tx}}{\mu^2} \right) \boldsymbol{T}\boldsymbol{T}^H \right] \right\} \tag{3.18}$$

where:

- $\boldsymbol{I_{nR}}$: is n_R-dimensional identity matrix
- E_{Tx}: energy sent by each transmit antenna
- $\boldsymbol{I}$: identity matrix has only the nonzero entries on the diagonal. All diagonal entries are equal to one.
- $\mu = \frac{P_{Tx}}{\rho^2} q^2$ and is defined for every received antenna
- $q^2 = E\left[\left|\boldsymbol{T}\right|^2\right] = \frac{1}{n_T n_R} \sum_{n=1}^{n_r} \sum_{m=1}^{n_T} \left|T_{nm}\right|^2$

With reference to Shannon's formula, the MIMO capacity has the form [Kyri01]

$$C = \log_2 \left\{ \det \left[\boldsymbol{I}_{\boldsymbol{n_R}} + \left(\frac{\rho}{n_T} \right) \boldsymbol{H}_n \boldsymbol{H}_n{}^H \right] \right\} \tag{3.19}$$

where:

- $\boldsymbol{H_n}$: is the normalised channel transfer matrix related to $\boldsymbol{T}$ as:
  $\boldsymbol{H_n}=\boldsymbol{T}/q$;

Upper and lower bounds of capacity for MIMO can be derived, corresponding to a channel that has a spatial correlation among the antennas between zero and one. For the former case,

$$C_{corr=0} = n_{\min} \log_2(1+\rho) \tag{3.20}$$

while for the latter,

$$C_{corr=1} = \log_2(1+n_{\min}\rho) \tag{3.21}$$

where:

- $n_{min}=\min(n_R, n_T)$

With knowledge of the radio channel, power can be allocated in the most profitable way [ATEM02]. Using the Channel State Information (CSI), the maximum capacity can be achieved, which is equal to the sum of capacities of all subchannels:

$$C = \sum_{m=1}^{n_R} C_m = \sum_{m=1}^{n_R} (1+\rho_m) \tag{3.22}$$

The average of the above equation leads to

$$\bar{C} = n_T \log_2(1+\rho) \tag{3.23}$$

By using the appropriate distribution of power, the radiated power is allocated only in eigenmodes, which have ρ above certain thresholds. In this way, power is not wasted by multipath components that are not pick up by the receive side. Equation (3.24) takes into consideration the distribution of the radiate power.

$$C = \log_2\left\{\det\left[\boldsymbol{I}_{\boldsymbol{n_R}} + \left(\frac{\rho}{n_T}\right)\boldsymbol{H}_n\boldsymbol{P}\boldsymbol{H}_n^{\,H}\right]\right\} \tag{3.24}$$

where:

- $\boldsymbol{P}$: is a distribution of power

The very important issue is the quality of the CSI, which describes the actual situation in a radio channel. In case the CSI is not perfect, the performance goes down at the receiver. All above considerations about the capacity are appropriate only under the assumption that the channel is constant for the duration of a burst. So for each burst there is a new CSI, otherwise an increase of bit rate is not possible.

Besides capacity gain, MIMO can be used for different reasons. MIMO also improves BER performance, and can be used only to minimise the probability of total outage, when the multi element antennas system is considered only in diversity reception aspect. This approach is common with known solutions, e.g., in IS-95 diversity reception is already applicable [CDGO05]. Using a few receive and transmit antennas, in a multipath environment, causes that in the receiver there are distinct versions of the same signal. The main difference is related with the power of the signal. The location of each receive antenna is a bit dissimilar, thus multipath components can influence on observed antennas in a distinct way. It means that every arriving ray gives a different contribution for the final shape of the received signal for a particular antenna on the reception site. The most unfavorable case is when arriving waves have a phase difference equal to $\pi/2$. In this situation two components subtract each other, and a decrease of the level of receive signal follows. The phase of one arriving multipath component is distinct for every antenna, Figure 3.3.

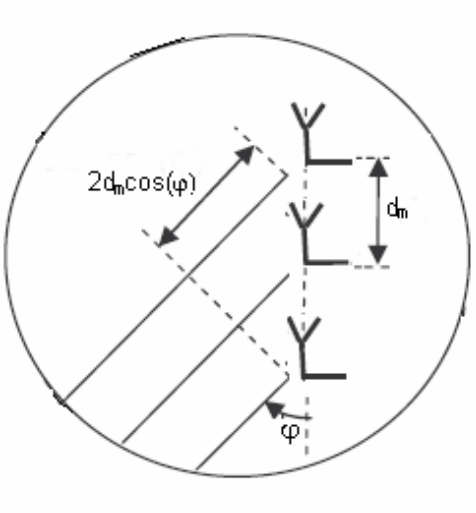

Figure 3.3 – Diversity reception aspect of MIMO.

Thus, it is more likely that there is an antenna, which mostly receives multipath components of the same phase. It is for this reason that the level of the signal is higher and an improvement of service quality follows.

The aspects described above are typical for a system that uses diversity reception, but MIMO additionally has several input antennas. It causes that there are more sources of multipath components. The number of multipath components is higher in environments that are rich in scatterers, and a greater gain generated by MIMO systems is observed.

3.4 GBSB model in MIMO

The GBSB model considered in Chapter 2 is used to describe the radio channel in a MIMO system. Each pair of input and output antennas can be treated separately. Like before, in this case, it is also possible to distinguish three different scenarios: pico-cell, micro-cell and macro-cell. The distance between antennas from the set is small so that some generalisations can be made.

If the micro-cell is considered, the GBSB with the elliptical deployment of the scatterers is suitable to estimate the condition in a radio channel. This model was analysed in Chapter 2. Every possible pair of receive and transmit antennas is treated like a singular example of a SISO system. Thus one can mark ($n_R \times n_T$) ellipses that represent propagation zones between a particular pair of antennas. The foci of the considered ellipse are placed on the location of BS single antenna and MT single antenna. The dimensions of each ellipse are defined by the longest delay of multipath components which is related with a size of the propagation environment, e.g., the width of the street and the distance between the BS and the MT.

Generally, each pair of antennas is associated with a set of clusters. But in this case, all pairs are located in very close surroundings, so that, all clusters of scatterers are common for the pairs of antennas. The described approach to deploy the clusters causes that every scatterer can be a source of a few multipath components. The number of the generated multipath components by the scatterer is related with the number of antenna pairs between transmit and receive sides. In order to calculate the number of multipath components in the considered environment, a multiplication of the number of the pairs by the number of the scatterers must be done. In comparison to the set of clusters, the multipath components are not common for all pairs of antennas. Each pair has its own set of multipath components, with different delay and amplitudes, which influence the received signal.

Each pair of antennas is attributed with its own LoS component which is only characteristic for the considered link. The LoS component is calculated as in free space, so that for a specific deployment of the transmitter and the receiver, i.e., sets of antennas are placed on parallel lines, some pairs of antennas have the same LoS components.

With reference to distance between single antennas, it is possible to generalise that there is only one ellipse common for every pair of antennas, Figure 3.4. But the independence of CIRs of the antenna-pairs is not violated. This phenomenon is possible because every scatterer can be described by a random reflection coefficient. The magnitude and phase of reflection coefficient have statistical values. More details about the reflection coefficient are presented in (2.21). The reflection coefficient is fixed for the considered scatterer. Taking into consideration the small spacing between antennas, one can suppose that the CIRs are similar. But, the significant number of the scatterer in propagations environment implies that the CIRs are distinct.

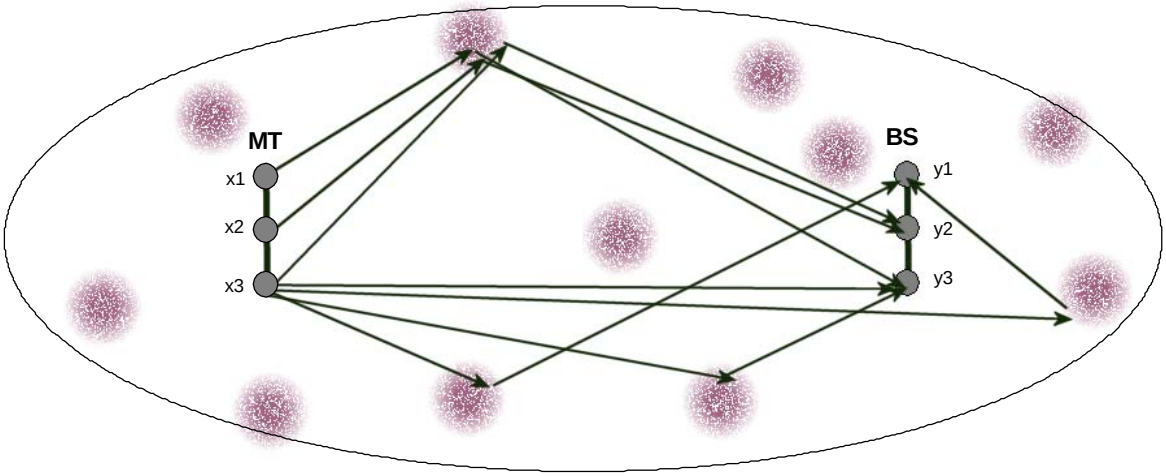

Figure 3.4 – Micro-cell for a MIMO system.

For the analysis of a macro-cell, the GBSB with the circular deployment of the scatters should be used, as described in Chapter 2. The characteristic for this scenario is depicted in Figure 3.5.

Similar as in the SISO case, also in the MIMO case scatterers are deployed in the surroundings of the MT, which is placed below the rooftops of buildings. In case there is one common circle for all MTs antennas, which indicates possible location scatterers causing the longest delay, the centre of the circle should be placed in the geometrical centre of the MT, as this approach is the most convenient. As for the micro-cell case, also here all scatterers are shared by all links between transmit and receive sides, because the distances between antennas are not significant

in comparison with the dimensions of the propagation environment. The number of multipath components depends on the number of the pair of antennas and the number of clusters. Also in this scenario, every scatterer is described by a random coefficient. The pairs of antennas do not have any LoS components, which is common with the SISO case.

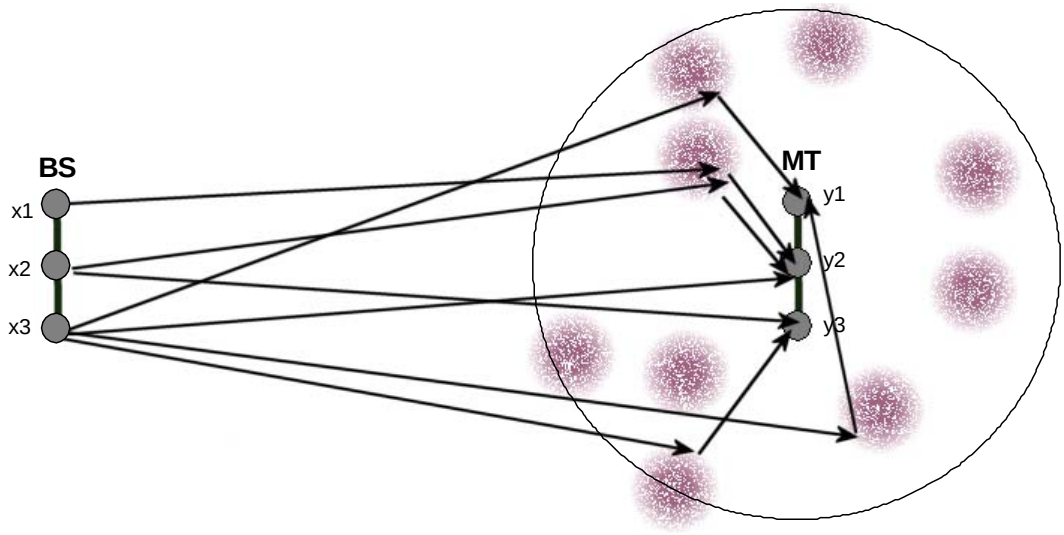

Figure 3.5 – Macro-cell for a MIMO system.

Pico-cell environments can be modelled as circular shapes. The MT and the BS are inside this shape. The centre of the circle is the position of the BS, Figure 3.6. Scatterers grouped in clusters are also inside the circle.

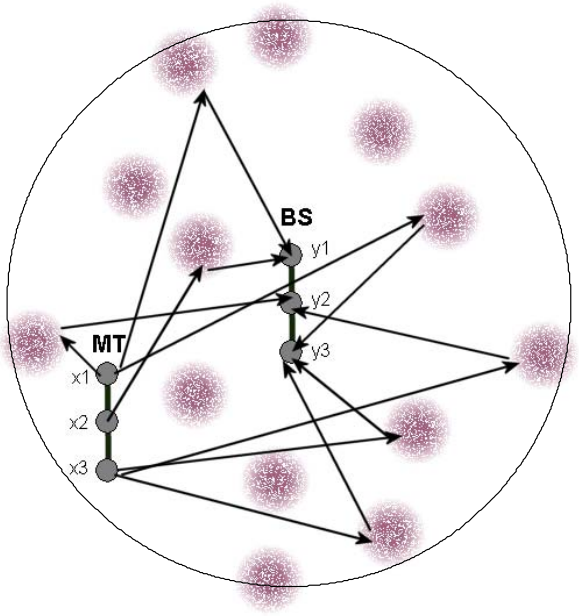

Figure 3.6 – Pico-cell for a MIMO system.

The dimension of the circle is determined by the size of the room, where the pico-cell is placed. In this scenario, the LoS component always exists, and it does not depend on the actual position of the MT related with the random deployment of scatterers in the propagation zone. Also in this scenario, as in the cases described above, all scatterers are common for all antennas, thus there is only one limiting shape.

For the macro- and pico-cell scenarios, the number of the multipath components is calculated in the same way as for the micro-cell.

4

Implementation

This chapter includes the description of the implementation of the simulator. Issues related with SISO and MIMO systems are presented separately. Input and output parameters, and a structure of the code can be found in this chapter.

4.1 General structure

In order to describe the implementation of the simulator the structure has been decomposed into a simple form, by breaking the radio channel simulator in blocks, Figure 4.1. The *Input Parameters* block represents input parameters of the simulator, which determine the way the program works, and allows choosing between different modes of the simulator.

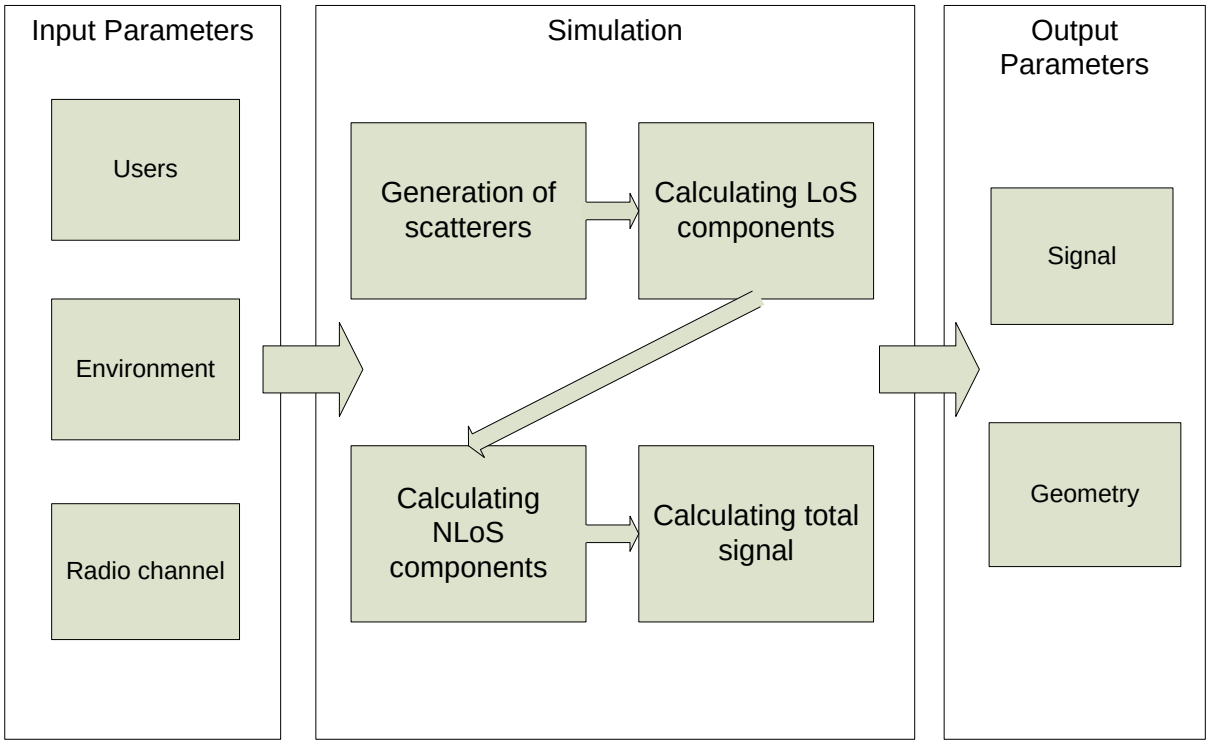

Figure 4.1 – General structure of the simulator.

The *Simulation* block contains the heart of the program, emulating the behaviour of the radio channel. This part includes the realisation of the algorithm in the simulator. In this part of the code, the sequence of steps is done according to the mentioned algorithm. It is worth noting that calculations are made separately for the LoS and the NLoS components. In the last block called *Output parameters,* the results are presented. Every part of the program is described in more detail in this chapter.

The above presented structure describes a relationship for the single pair of antennas, for which the SISO radio channel is taken into consideration. In the case of a MIMO system, for a particular pair of the input and output antennas there is a single independent radio channel, Figure 4.2. From a physical point of view, the channel is the same for each pair of antennas. The

deployment of the scatterers and their attributes are constant for every pair of the antennas. The features distinguishing the simulations are related to the considered pair of antennas.

In order to achieve a set of output parameters for the considered pair of antennas, input parameters related with the pair should be used for the calculations. Calculations are common for all pairs, but different input parameters generate different results. The decomposition can be done because a simulation for a MIMO system is a sequence of simulations for a SISO system. Each pair of antennas is an independent single system, thus, the result of the MIMO simulation is a set of output parameters.

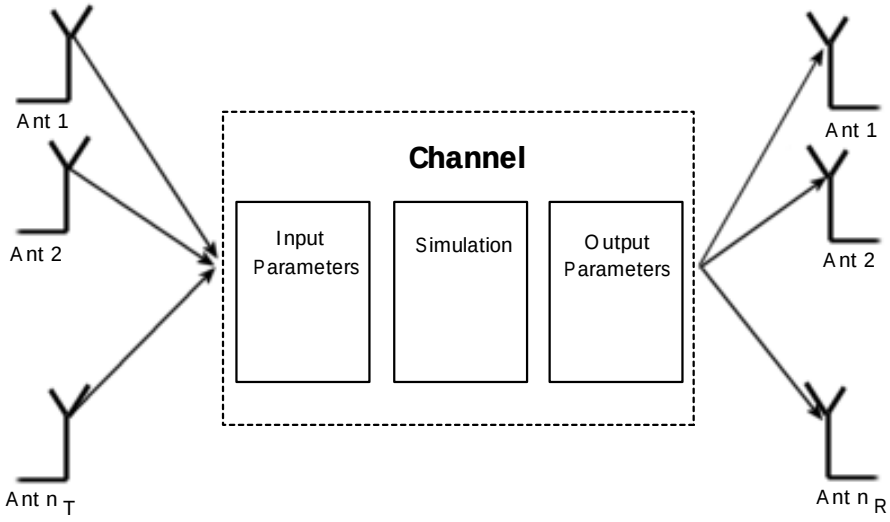

Figure 4.2 – Structure of the simulator for MIMO systems.

4.2 Channel

4.2.1 Input parameters

Input parameters can be organised in three groups. In the first group, there are parameters that describe the location and properties of the MT and the BS. The next group determines propagation environment and the type of scenario, and the last one illustrates some radio properties of the system. The groups of the parameters are presented in Figure 4.1.

In the *User* group, parameters describe some aspects connected with the users in the system. The positions of the MT and the BS are described by coordinates as [x,y], which determines a position in the x-y plane. Locations are deployed only in the 2-D plane, which is agreement with the assumption of the used propagation models. For the transmitter, it is important to determine the level of transmitting power; the receiver is defined by the noise level. Signals with power below the sensitivity of the Rx are not considered. The BS and the MT have a separately defined radiation pattern of the antennas. Every antenna can be a single radiator or an antenna array. In case of the antenna array, the parameters to determine the group characteristic are presented below. It is assumed that the radiation pattern for a singular antenna is defined by the radiation pattern for an omnidirectional antenna. Additionally, the radiation pattern of the antenna can be loaded from a file. So, a user of the simulator can define any radiation pattern, suitable for a considered application. The following parameters can be defined:

- $s_{dev[m,m]}$: position of the MT or the BS on the 2-D plane
- $P_{Tx[W]}$: transmit power of Tx
- $N_{Rx[W]}$: noise level of Rx

The antenna array can be described using the following parameters:

- N_a: number of antennas in the array
- $d_{[m]}$: spacing between antennas in case of linear array,
- $a_{[m]}$: radius of the circle in case of circular array
- $\Phi_{0[rad]}$: phase shift between consecutive radiators, it is assumed that all radiators are fed with the same amplitude (one feeding point)
- $\Phi_{n[rad]}$: phase feeding of n^{th} radiator (multiple feeding points)
- $I_{n[A]}$: amplitude of feeding of n radiator (multiple feeding points)

Antennas can have different names, which are helpful for sorting output files. The names of the output files consist of the names of the antennas between which radio links are established.

The Parameters from the *Environment* group, which describe a region of propagation, contain information on the scenario properties. The type of scenario is defined by choosing a pico-, micro- or macro-cell mode. The next parameter is the dimension of the scenario. For the micro-cell case, the scenario is defined by street width ratio, which describes an effective width of the region. The width of ellipse characteristic for micro-cell is multiplied by a constant factor. A pico- and macro-cell scenario is defined by the radius of an appropriate circle. The following parameters describe the distribution of reflectors within the region. The distribution of scatterers

is determined by the cluster density, and an average number of scatterers. The cluster density is used to calculate the number of clusters in a region and the average number of scatterers is used to calculate a number of scatterers within a cluster. The radius of the cluster determines the size of the cluster because every cluster has the shape of a circle. The parameters from the Environment group are:

- $dim_{[m]}$: a dimension of a scenario
- $d_{c[1/m^2]}$: cluster density
- n_{sc} : average number of scatterers per cluster

The parameters from the *Radio channel* group define propagation conditions and the transmitted signal. The radio signal is described by the carrier frequency:

- $f_{[Hz]}$: frequency

Some parameters are present in a config file, but are not consider among input parameters, because they are not related with a single run of the simulator.

In Figure 4.1, the structure does not take into consideration the modes of the simulator and the number of simulation once the environment has been defined. The mode of work is important when the number of simulations is greater than 1, because some changes of the environment are made for each run of the simulator. The structure presented in the figure is only appropriate for one run of the simulator. The description of the modes is presented in the following part of the work.

Parameters related with visualisation are not considered in the figure, as well. The parameters like time resolution, angle resolution and time sectors are only necessary for the present application of the simulation, so that the mentioned parameters are not placed in the general structure of the program. The Matlab environment was used to present results in graphic way, but, the parameters can be used by different environment for visualisation.

4.2.2 Description of the simulator

The simulator consists of some main processing blocks. In the beginning, based on the input parameters, the positions of the clusters are set in a random way using the uniform distribution. Both coordinates *x* and *y* are drawn apart. In this way, clusters are placed evenly distributed on the area of region. The shape of the region depends on the researched scenario. In case of the micro-cell, clusters are placed inside the ellipse, but in case of the macro-cell or the pico-cell, the clusters must be deployed inside a circle. During the drawing of the coordinates of the clusters, the considered shape of the scenario is limited by an appropriate rectangle. After drawing the parameters *x* and *y* are inside of the rectangle but belonging to a zone of the scenario is not sure, Figure 4.3. If the coordinates are not inside the considered shape of the scenario (circle or ellipse), another position of the cluster is drawn and considered. The number of clusters is defined by the dimension of the scenario and the cluster density related with the scenario. So, the number of clusters is fixed for every scenario.

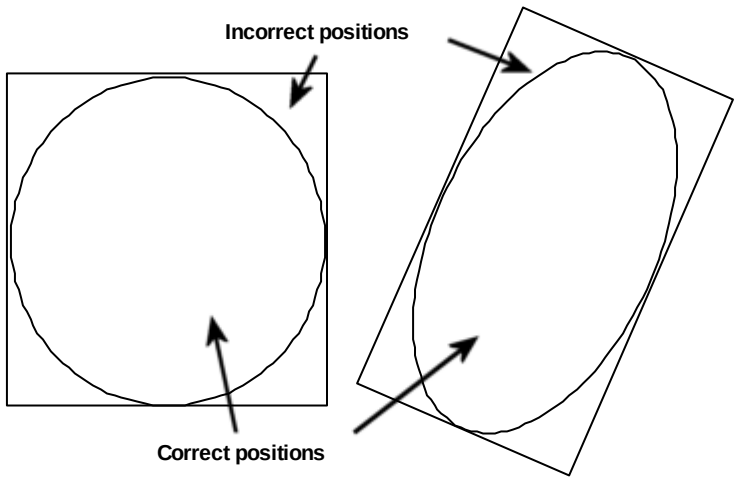

Figure 4.3 – Drawing of the positions of clusters.

In the next step, the simulator computes the location of the scatterers. Every scatterer belongs only to one cluster. The position of the considered scatterer is determined using the spherical coordinates. The distribution of the radius is determined by the Gaussian distribution. The mean value of the distribution is 0 and the standard deviation is determined by the radius of the cluster, but the angle is determined by the uniform distribution in the range $[0, 2\pi]$. Using the drawn angle and radius, the scatterer is deployed with reference to the centre of the cluster. Each cluster is defined by an average number of scatterers, so that in one scenario different

clusters may have different numbers of scatterers. The number of scatterers related with one cluster is described by the Poisson distribution. The flow of information in the first block is depicted in Figure 4.4.

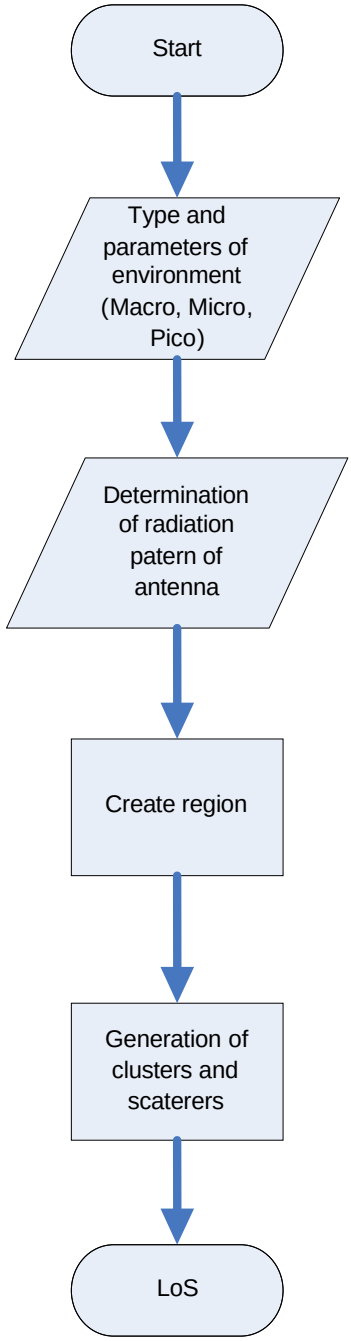

Figure 4.4 – Start of a simulation.

When the simulation environment is set, the calculations of the radio channel. In the beginning, the LoS component is taken into account. The scheme of data processing is depicted in Figure 4.5. The power picked up at the receiver is calculated using the formulation for free space. So,

only the positions of transmitter and receiver, transmitted power, and the radiation patterns must be known to estimate the received power. In some radio channel models, the path loss exponent is used. The path loss component is different for special terrain of propagation. In the simulator, the influence of the environment of the propagation is taken into consideration. The specific deployment of the scatterers for considering terrain makes the special shape of the final signal.

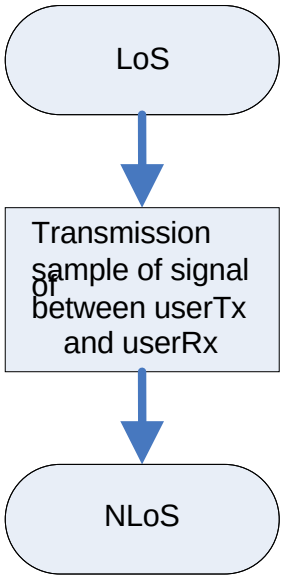

Figure 4.5 – Calculation of the LoS component.

After calculating the LoS component, the program goes on to the next part of the calculations, i.e., the NLoS components. An algorithm for this part of the program is presented in Figure 4.6. The simulation for the NLoS components is trickier, because all scatterers must be considered as check point for every ray in the considered environment.

Every scatterer is a source of one multipath component picked up at the receiver. The calculations for the NLoS components can be simplified. Every NLoS link can be treated like two LoS links, the first link being between the transmitter and the considered scatterer and, the second being between the scatterer and the receiver. The power picked up at the scatterer in the first link is radiated to the second link, but before transmitting, the power must be reduced by the magnitude of the reflection coefficient. Also the phase of the signal must be changed with reference to the phase of the reflection coefficient. This approach is possible, because the scatterers do not overshadow one another. The mentioned assumption guarantees the existence of the directional path between the transmitter and any scatterer. The same situation is true for the link between any scatterer and the receiver.

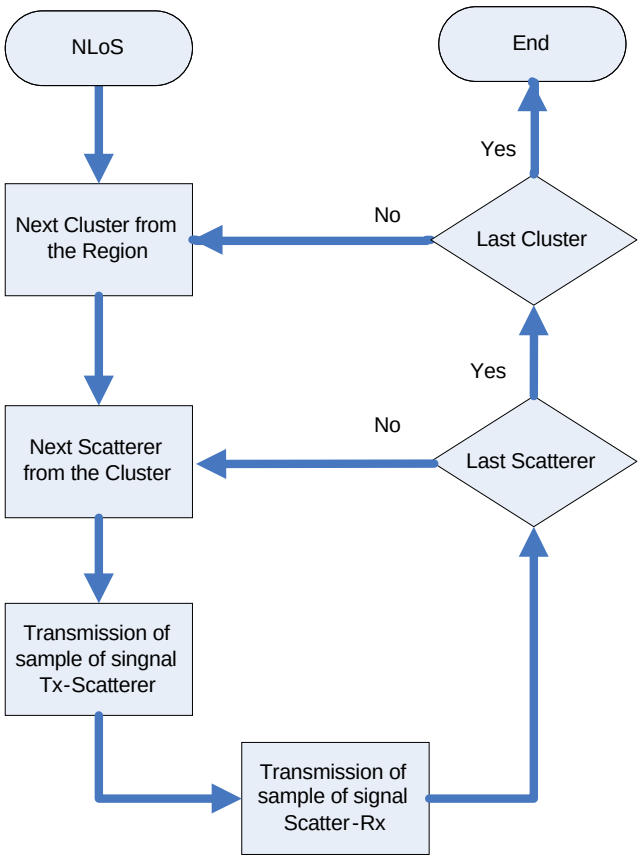

Figure 4.6 – Calculation of a NLoS component.

4.2.3 Output parameters

Output parameters are grouped as shown in Figure 4.1. The parameters from the first group represent Signal parameters. Every multipath component is associated to a set of parameters, so, the number of sets of parameters is equal to the number of the scatterers, plus one in scenarios where LoS exists, e.g.; a micro- and a pico-cell, whereas for a macro-cell the number of sets is constrained by the number of scatterers. The LoS component is not related with any scatterer. The mentioned set of parameters is listed bellow and the particular parameters were described in Subsection 2.2.1:

- Angle of Arrival (AoA) – from (2.26)
- Angle of Departure (AoD) – from (2.27)
- Amplitude of ray – from (2.31) or (2.32)
- Phase of ray – from (2.35) or (2.36)
- Time of Arrival (ToA) – from (2.37) or (2.38)

The parameters are given by the simulator in output files. One output is related with a radio link between single input and output antennas. The output file consists of parameters generated by all scatterers in an environment. The size of the output file is connected with the richness of the scatterers in the environment; for more complicated ones, heavier files are produced.

It is possible to restore the possible positions of the scatterers, using the above parameters and the position of the BS and the MT. In the case of the micro-cell, one multipath component can be described by the ellipse; the position of the scatterer, with which this multipath component is connected, is located on the ellipse. For the pico- and the macro-cell scenarios, the appropriate circle estimates the possible localisation of the related scatterer.

The group *Geometry* parameters presents the real position of all scatterers in the considered environment. These parameters can be helpful to confirm the correct position, achieved using the *Signal* parameters. The positions are saved in the file, which name can be defined by the user of the simulator. The file can be used in a direct way to run the simulator with the environment defined, and one or more changes can be done to check on influence of a disturbance.

Like mentioned above, every multipath component, which propagates directly from the Tx to the Rx or through the reflector, is described by a set of parameters. But these sets of parameters are not enough to evaluate the model and to make any conclusions. Having appointed all signal parameters to all ray components, it is necessary to process them in a statistical way. The statistical processing is made outside the simulator; in this work, it was made in Matlab environment. The statistical parameters used are (parameters were described in Chapter 2):

- $\overline{\tau}$: mean delay
- σ_τ : delay spread
- σ_φ , σ_θ : angular spread of AoA and AoD
- $\overline{P}$: mean power gain
- standard deviations for all these parameters

The raw output parameters are in filtered and unfiltered form. There are some ways of filtering One of them is refusing components, that have a level of amplitude below the sensitivity of Rx.

Another kind of filtering is overriding rays, which have angles out of the range of antenna. Every parameter from the mentioned set can be filtered in an appropriate way.

The results, which are obtained from the simulator, are more useful when they are averaged over many iterations. For each iteration, the simulator has to build a new scenario, which is changed with reference to a previous one. The simulator can be run in four modes, which define the way of changes the environment. The description of the modes is presented in Table 4.1.

Table 4.1 – Description of the simulator modes.

Mode	Description
0	For each run of the simulator, positions of clusters are kept in the same places. The only difference between the iterations is in a different reflection coefficient of scatterers. Output parameters from every iteration are generated.
1	The same changes are made as in mode 0, but for this mode, all results are averaged by the simulator, and only average results are generated as output parameters.
2	Positions of clusters remain the same, but scatterers within any cluster are independently generated for each run of the simulator. As a result, scatterers have different positions and reflection coefficients. The same as in the mode 0, all results from all iterations are written by the simulator.
3	Positions of terminals are kept in the same places. All clusters with scatterers are generated from the beginning for each iteration. Output parameters from all iterations are saved.

4.2.4 Assessments

The simulator was carefully checked, and some assessments were made, see Annex A and Annex B. These tests were made to assure that the calculations and the generation of the environment is done in a correct way. These include the following aspects:

- The environment was generated with the Rx, the Tx and only one scatterer. Having knowledge about parameters of the scatterer, calculations of all output parameters were made, which are described in Subsection 2.2.3. Results obtained from the simulator were verified.

- The entire environment is generated using random number generators, so the correctness of these generators is very important for the simulator. The simulator uses three kinds of statistical distributions: Gaussian, Poisson and Uniform. Every generator produced 1 000 000 of the samples, and after that, the histograms were plotted, see Annex C. Obtained shapes of the histograms agree with theoretical expectations.
- The correctness of the deployment of clusters within a region, and scatterers within a cluster, was checked. Clusters should be distributed uniformly in the region, which was generated with a few clusters, and the mean values of *x*- and *y*-coordinates of all clusters were calculated. These mean values, were the same (with some marginal error) as the centre of the clusters.
- Scatterers within a cluster are distributed with the Gaussian distribution, but also in this case, the mean values of *x*- and *y*- coordinates should be the same as the centre of the cluster. Obtained results confirmed, that the scatterers are generated correctly. Scatterers also have to prove some symmetry in the cluster. The cluster was divided into two identical regions in a vertical (up- and down-sides) and a horizontal (left- and right-sides) orientation. In every quarter of the region, scatterers were counted – the results for both regions in each pair were the same (with some marginal error).
- It was also checked that the way of averaging the raw results in the time domain. Some multipath components with the determined amplitude, phase and delay were generated, and after that they were processed by the averaging function. The obtained results agreed with the expectations.
- Some aspects related with a CIR were also checked. Every region has a finite dimension, so the maximum possible delay, which is obtained from the region, is strictly bounded and depends only on the dimension of the region. The three different scenarios were generated: micro-, macro-, and pico-cells, and for each of them, the maximum possible delay was calculated. After that, it was checked if there were any of the multipath components over exceeding these values.
- The correctness of the working of simulator in different modes was modes as well. The respective parameters of the scenario, connected with the different modes of the simulator, were checked for every iteration.

In Table 4.2, Table 4.3 and Table 4.4, one presents the influence of the different modes of the simulator and different number of the iterations on the computation effort. These tests were made on a PC PIII 1.2 GHz, 256 MB RAM. In every mode of the simulator, the same scenario

(macro-cell) was used, which consisted with of clusters with the average number of the scatterers equal to 20.

As it was mentioned earlier, in mode 2, the simulator returns the files with the averages of the output results from all iterations. Therefore, no matter how many iterations were made, always the same number of the files is obtained. For different number of iterations, the size of these files is similar. However, in other modes of the simulator, a large number of iterations causes a large number of the output files, therefore, the results occupy a greater space on the computer disk.

Table 4.2 – Comparison between the sizes of the files with the output results.

No. of iterations	Size of the files [kB]	
	Mode 0/1/3	Mode 2
1	32.5	32.5
10	184	32.5
50	862	32.5
100	1660	32.5
500	8280	32.5

In mode 2, the simulator calculates averages values, which is a reason why in this case more memory is used and simulations take a longer time. In other modes, almost the same value of the memory for different number of the iterations is used. In mode 3, the usage of the memory is slightly higher comparing with modes 0 and 1. In mode 3, in every iteration, the simulator generates the whole environment from the beginning, thus, the situation is more complicated than in modes 0 and 1.

Table 4.3 – The comparison between the memory usages during the simulation.

No. of iterations	Size of the memory [kB]		
	Mode 0/1	Mode 2	Mode 3
10	1296	1252	1292
50	1296	1296	1300
100	1296	2256	1300
500	1296	6348	1308

The relation between the number of iterations and the simulation time is linear for the different modes of the simulator. In every iteration, the simulator makes the same calculations, thus, the same computation effort is used. Every iteration within the same mode lasts the same time.

Table 4.4 – Comparison between the times of the simulations.

N. of iterations	Time of a simulation [s]			
	Mode 0	Mode 1	Mode 2	Mode 3
10	0.6	0.6	0.9	0.6
50	1.8	1.8	3.2	1.8
100	3.4	3.3	6.2	3.4
500	15.6	17.8	29.2	17.6

4.3 MIMO channel

4.3.1 Input parameters

For the MIMO case, parameters can be grouped into three groups: Users, Environment and Radio Channel. The general approach of Figure 4.1 showing the input parameters is also appropriate for the MIMO case. Only one difference can be noticed on the content of the group related with the user, which has extra parameters. The groups describing the propagation environment and the radio frequency channel are the same, because only the specification of user has a different characteristic for MIMO.

The MT and the BS are inside of the considered environment and both can function as either the transmitter or the receiver. The user of the simulator decides about the way of the radio link, so the situation is the same as in the SISO case. The main difference is the fact that both the BS and the MT can be associated to a set of antennas. The antennas of one system element are treated separately, which means that mutual influence between antennas is not considered. Each antenna in the set can have a unique radiation pattern. The antennas used in the MIMO system are omnidirectional by default, but the radiation pattern can be also described by using the input file.

In a general case, even an antenna array can be used as one element in a MIMO set. In the considered case, only single radiation elements are assumed. The size of the antenna array is larger comparing to a single antenna. The distance between edges of antennas from a MIMO set can be small, since the distance between the geometrical centres of antennas is taken into consideration during the deployment of the MIMO set.

A shift between the antennas of one system element has influence on the behaviour of MIMO systems. The distance can not be too large, because the system can transform itself to the MU (Multi User) case.

The modified parameters from the User group are presented below:

- $\boldsymbol{s}_{[m,m]}$: position of the MT or the BS on the 2D plane
- n_T: number of transmit antennas
- n_R: number of receive antennas
- $d_{T\,[m]}$: shift between transmit antennas
- $d_{R\,[m]}$: shift between receive antennas
- $P_{Tx[W]}$: power of Tx
- $N_{[W]}$: noise level

More details on the input parameters from the Environment Group and the Radio Channel Group are presented in Section 4.2.

It is impossible to define a power for each transmit antenna in a separate way. Power is obtained by dividing the power for all transmitters by the number of antennas. So, the quantity of power for eigenmodes that have the best gains can be amplified. Only an even distribution of power can be used in the simulator, which is a drawback of the program and should be developed further.

4.3.2 Description of the simulator

The description of the simulator presented in Subsection 4.2.1 has a general form, which does not take into consideration some aspects that are characteristic only of MIMO systems.

In the MIMO case, one transmitting user and one receiving user are considered, so that only one region can be taken into account. The mentioned region includes one MT and one BS and a set of clusters of scatterers, Figure 4.7. The way of deploying clusters is common to the description presented in the previous section, which is also valid for the deployment of scatterers inside the cluster.

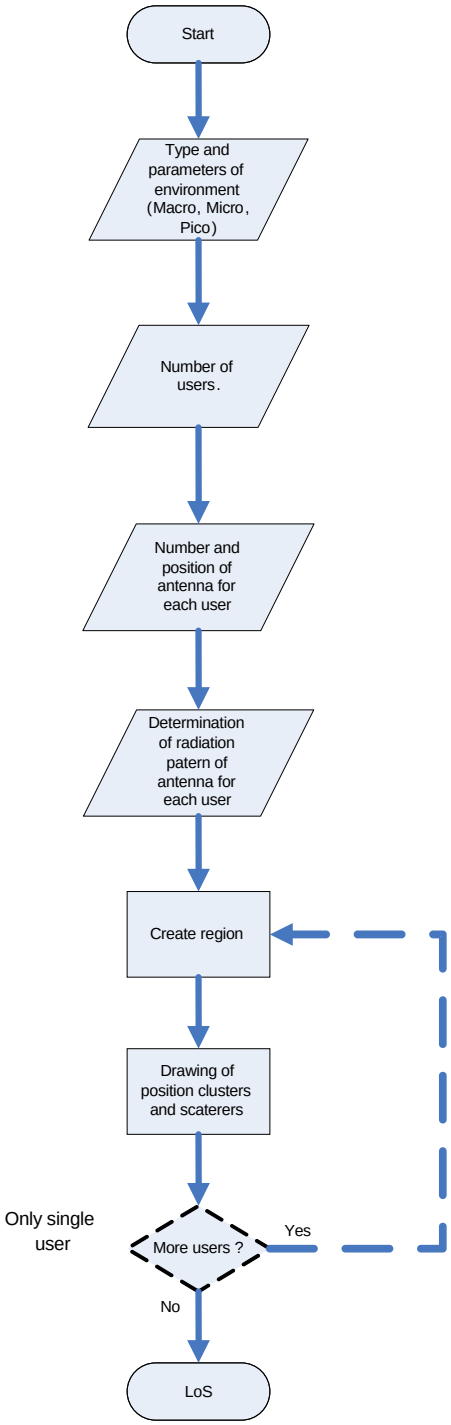

Figure 4.7 – Start of a simulation specified for MIMO.

The distributions for the clusters and for the scatterers are identical as in the previous part of the work. Also the definition of scenarios, and used ones are carefully described in Subsection 2.2.3. So, the aspects related with the area of propagation will not be considered in this part of the work.

All drawings showing the algorithm for the MIMO case are expanded with some extra parts. The additional parts, indicated by interrupted lines, show the algorithm for a system where MIMO and MU are used together. These kind of simulations are also possible with the simulator, but have not been further investigated here. The MU case is described in more detail in [Zuba05].

The characteristic feature for MIMO is the fact that both the MT and the BS can be associated to a set of several antennas. In the simplest case, the set of the antennas includes only one antenna. But to show the aim of using a MIMO system, the number of aerials should be increased, for both the input and output sides.

The existence of the set of antennas at each element of the system influences the calculation process in the program, Figure 4.8. Achieving the parameters for one pair of antennas is similar to the general case, therefore, some iteration of calculations must be done, for each pair of antennas. Every iteration has the same distribution of scatterers, so the propagation environment is common. Each pair of antennas has different positions of a transmitter and receiver, a location of either the BS or the MT is shifted in distance for a particular single antenna.

After implementing the described procedure, a few independent LoS components can be observed. The number of LoS components is determined by the numbers of input and the output antennas and is equal to the multiplication of these two numbers. The LoS path is available between each pair of input and output antennas, so, each pair has its own LoS component, which is a reference point for all calculations of that pair. All time parameters are stipulated with reference to the LoS component, amplitudes of multipath components are also considered with reference to the LoS component.

In the NLoS case, the number of links between input and output antennas depends on the number of the scatterers in the region. It follows that the number of all multipath components equals the multiplication of three factors: the number of input antennas, the number of output

antennas and the number of the scatterers in the environment, Figure 4.9. For every multipath component, the procedure of the general case is repeated.

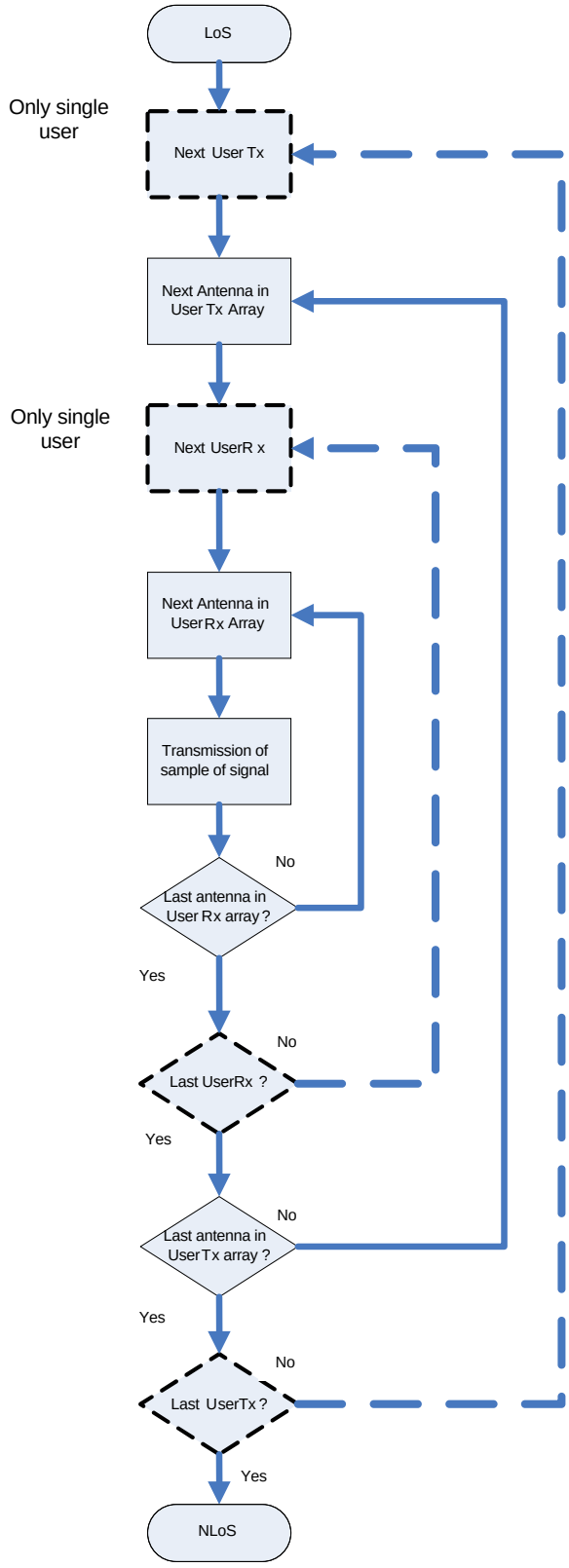

Figure 4.8 – Calculation of the LoS components specified for MIMO.

This is similar to the MU case, with some users on the transmit side and some users on the receive side. The quantity of users is like the number of antennas for each side of the radio link. An additional assumption is that every user has an antenna system with only one antenna. But for the MIMO case, the distance between antennas is smaller, because the set of MIMO antennas is placed on a real object.

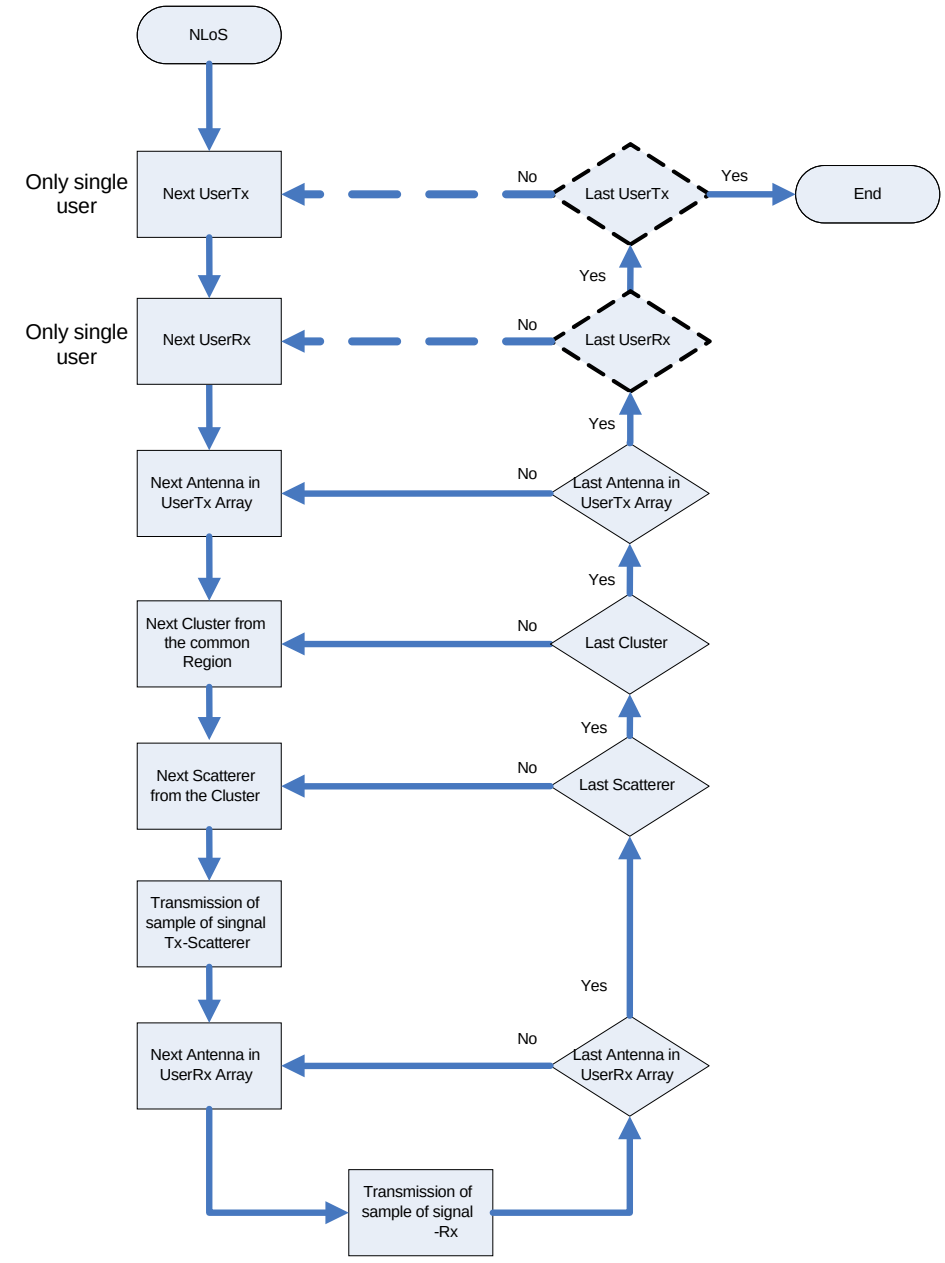

Figure 4.9 – Calculation of a NLoS component specified for MIMO.

4.3.3 Output parameters

The grouping of the output parameters will be the same as presented in the general considerations. The *Signal* group contains the raw results of the simulations for every link. The parameters as given in Subsection 4.2.3 are:

- Angle of Arrival (AoA) – from (2.26)
- Angle of Departure (AoD) – from (2.27)
- Amplitude of ray – from (2.31) or (2.32)
- Phase of ray – from (2.35) or (2.36)
- Time of Arrival (ToA) – from (2.37) or (2.38)

The main difference is in the number of sets of parameters. For a link between a transmit and a receive antenna, the number of sets of parameters equals the number of the scatterers in the propagation environment. If all input and output antennas are considered, the number of sets increases to the product of the number scatterers, and the number of transmit antennas by number of receive antennas. The data described above is needed to calculate the CIRs among all pairs of input and output antennas. The CIRs are necessary to calculated the correlation between paths to the output antennas.

Parameters for a particular pair of input and output antennas are saved in an output file. So, an increase on the number of antennas causes an increase on the quantity of disk space needed to keep the results of a simulation. If a research with a significant number of antennas needs a huge number of simulations (for a qualified average), a large disk space must be used. This fact should be respected during simulations.

The CIRs among all antennas are also needed to derive the spectral capacity of the system, which is helpful to evaluate MIMO under particular conditions. The way of calculating of the spectral capacity can be found in Annex J, where the whole process is described in detail.

The *Geometry* group of output parameters contains the deployment of scatterers in the propagation environment. This approach is the same for the general case.

Also the statistical parameters, which describe the radio channel, are calculated using Matlab. Parameters are obtained by using sets of raw parameters. As it was mentioned in Subsection

4.3.2, the number of multipath components depends on three factors: the number of transmit antennas, the number of receive antennas, and the number of scatterers. It is possible to make statistics for the chosen parameter with reference to one of the factors.

The radio channel can be described using the following statistical parameters:

- $\overline{\tau}$ [s]: mean delay
- σ_{τ} [s]: delay spread
- σ_{AoA} [rad], σ_{AoD} [rad]: angular spread of AoA and AoD
- $\overline{P}$ [W]: mean power gain
- standard deviations for all these parameters

4.3.4 MIMO Assessment

The correctness of results from the simulator, related with a MIMO system, is very important, because it is necessary to obtain proper values of the capacity, which is the subject of the research in the following chapter.

The number of links between transmitter and receiver depends on the number of antennas for each side of the system. Every link is related to the same clusters and scatterers, so the results for the particular link of a MIMO system differ one form another in an insignificant way. The reason of small differences is made by spacing between antennas on both sides of the radio link. The shift makes that the ray generated by the same scatterer has a different delay with reference to various links. If the delay is different, both amplitude and phase of the ray are different. These parameters have been checked in the present section. The shift between the antennas also influences both AoA and AoD, which have been investigated in the general assessments. The mentioned angels are calculated with reference to an LoS component, and each link has a different LoS component, so that any comparison can not be done.

For assessment, a simplified micro-cell was established. The scenario includes the BS and the MT, which are separated by 200 m. The MIMO 2×2 is chosen, so that 4 links will be taken into consideration. The environment of the propagation contains the cluster with 3 scatterers. The scenario is depicted in Figure 4.10. A simplification was made in order to focus only on taps

generated by single scatterers, which can be indicated in an easy way in an environment poor in clusters.

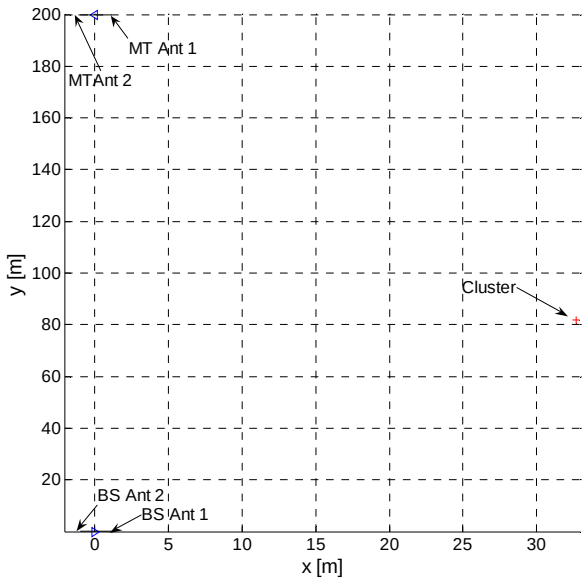

Figure 4.10 – The location of the cluster with reference to the MT and the BS.

The CIRs of the system are shown in Figure 4.11. For the following, only the taps from the nearest scatterer will be analysed which means that the first and second groups of taps on the graph are important; the first one corresponds the LoS components and the second one is generated by the closest scatterer. A small shift between the CIRs is observed, but from the graph is hard to notice which link has the smallest delay, so, the precise data is shown in Table 4.5.

Table 4.5 – Parameters of chosen taps from the analysed CIRs.

		h_{11}	h_{21}	h_{12}	h_{22}
LoS	delay [ns]	667.128190	667.128378	667.128378	667.128190
	Electric field [mV/m]	19.3649167	19.3649113	19.3649113	19.3649167
	Phase [^{0}]	92.297	92.432	92.432	92.297
First Scatterer	Delay [ns]	701.00	701.18	701.13	701.31
	Electric field [mV/m]	12.00701	1200390	1200478	1200167
	Phase [^{0}]	272	43	6	137

When the parameters of the LoS component are analysed, two groups with the same parameters can be indicated. The links related with the antennas placed in the front each other, have the smallest delays; the amplitudes for these links are the greatest, because rays cover the smallest distance; the phases are also the smallest, because they are related with the delays. The cross links have the greatest delays, so that the amplitudes of the rays are the smallest, but the phases

are the greatest. It shows that the simulator works correctly for the LoS components. The zooms of the LoS are placed in Annex B.

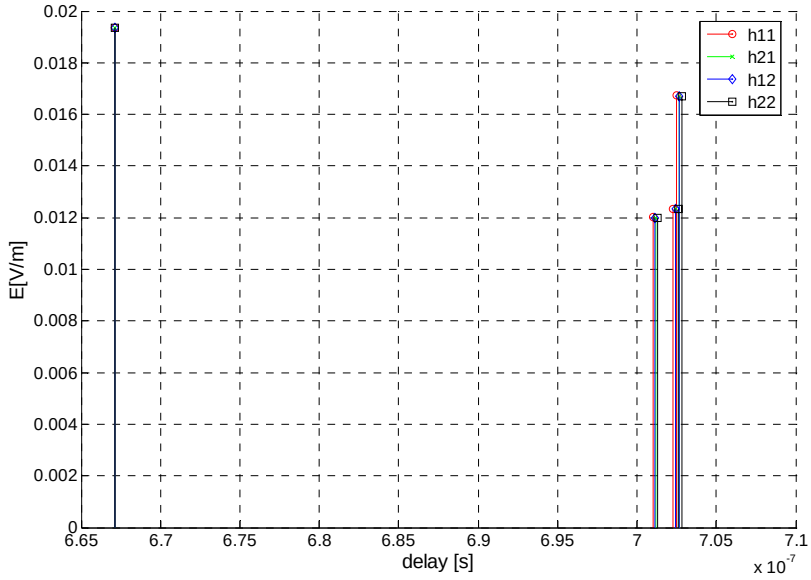

Figure 4.11 – CIRs for MIMO 2×2 in the scenario with cluster with3 scatterers.

The scatterer generates taps case is more complicated. All links have different parameters. The sum of distances from the MT towards the scatterer and from the scatterer towards the BS is different for each link. The scatterer is placed near antenna 1 from the BS and antenna 1 from MT, so that link h_{11} has the smallest delay; the amplitude of this link is the greatest. In the simulator, the phase is calculated in the range {0°, 360°} and the scatterer is near the border value, so in this case a jump of the phase is observed. However, if this value is compared with others related with greater delays, the rule is kept. The antennas 2 for both the BS and the MT are the farthest from the scatterer, so the delay related with this link is the greatest, which influences other parameters related with this link.

The analysis of this case confirms that the simulator is working properly. The simple environment for the simulation makes it possible to make a visual analysis of the results, and it shows that parameters are sensitive as expected.

One more experiment was carried out. Four regions with SISO systems were established. Positions of single users were the same as for the MIMO antennas from the previous test. The distance between users is so small that every region has the same deployment of clusters. In this case, only one cluster was considered. If the CIR from every region is related with the

appropriate link for the MIMO system the results are the same, which means that the simulator works correctly.

5

Analysis of Results

This chapter consists of descriptions of the used scenarios and results of simulations. The simulations have been made by varying three parameters: number of antennas, mutual positions of the BS and the MT and distances between antennas.

5.1 Scenarios for simulations

The advantages of a MIMO system strongly depend on where the system is applied. In order to make a realistic research, it is necessary to chose appropriate scenarios for the simulations. This approach helps to find places where applying a MIMO system makes sense and where the results are worse.

5.1.1 General criterions for selecting appropriate scenarios.

When searching for scenarios, all assumptions of the radio channel model of the implementation of the simulator were taken into consideration. Since the Doppler effect is out of the range for this work, MTs are static and have stable positions or change their positions with very small velocity, e.g., pedestrians. It is not possible to consider scenarios where vehicles are moving rapidly.

Every scenario can be considered for different users' penetration. So, the scenario should be also defined by the density of users and the density of active ones in the environment [DGVC03]. For this work, it is not necessary to consider this aspect, because interference among MTs is not considered. This dissertation investigates a single radio link between a receiver and transmitter, with multi element antennas, hence, the influence of mutual deployment of users in the scenario on the capacity is not analysed. Only one pair consisting of one MT and one BS is used, which is enough to calculate the capacity for a specific scenario.

For MIMO cases, the shape of the scenarios, the deployment of clusters and, the deployment of scatterers is important, and causes differences among the scenarios.

To find suitable environments for the simulations, a review of the FLOWS scenarios [DGVC03] was made. The following scenarios were taken for the simulations:

- The city street scenario,
- The railway station scenario,
- The highway scenario.

5.1.2 The city street scenario

The city street scenario is a micro-cell scenario, typical for an urban environment with many working people. The possible positions for the active MTs are depicted in Figure 5.1. The deployment of users is constrained by the structure of the buildings, which is characteristic for this kind of area, a grid of streets. Active users are located along the streets.

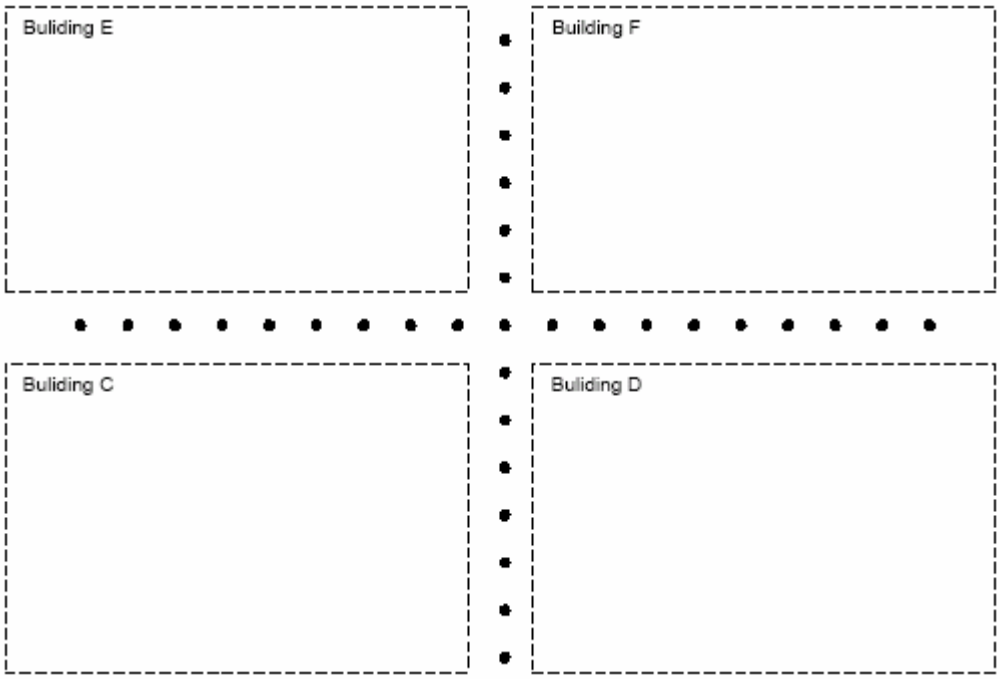

Figure 5.1 – The city street scenario – general [DGVC03].

For the MIMO case, only two points should be considered, the first one is the position of the BS and the second one is the position of the MT. When choosing the positions, the distance must be taken in consideration. The minimum separation between the BS and the MT is 200 m in a micro-cell scenario, Section 2.2.3. The position of the BS is at the crossroads and the MT is placed between the buildings as depicted in Figure 5.2, where the characteristic ellipse can be seen. The width of the ellipse is defined as 80 m, but the real width of the considered street is 40 m, the difference is induced by the effective street width ratio (for the city scenario the ratio equals 2).

Inside the ellipse, scatterers grouped in clusters are deployed. For the micro-cell scenario, the typical value for the number of clusters is 7, so that a cluster density for this scenario is $0.5 \cdot 10^{-3}$ m^{-2}. The influence of the number of clusters on capacity is depicted in Figure D.1. The average

number of scatterers per cluster equals 20 per cluster. An example of a deployment of a cluster is depicted in Figure 5.3.

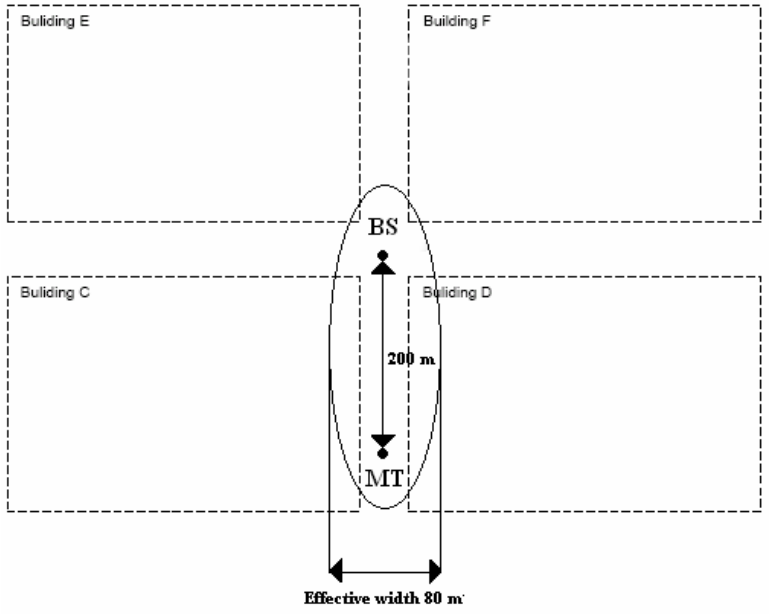

Figure 5.2 – The city street scenario – particular case.

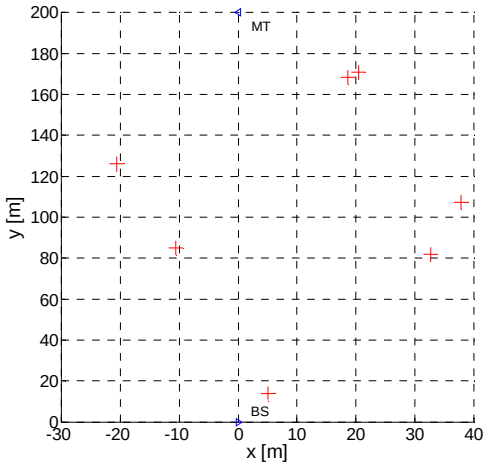

Figure 5.3 – An example of the deployment of clusters for the city street scenario.

A more detailed analysis of the number of clusters and the number of scatterers per cluster is presented in Annex D. All parameters for this scenario can be found in Table 5.1.

5.1.3 The railway station scenario

The railway station is located in a small city or in the suburbs of a big city. This environment can be used to simulate a pico-cell and micro-cell; in this work, only the pico-cell will be considered. Users are grouped in some places, e.g., waiting rooms, shops etc. Active users are also outside the building, on the platform close to the train, Figure 5.4. But these ones are not considered, since they can take service from the nearest BS in a micro-cell. This scenario may be enhanced to more complicated radio situations, by the combination of a few scenarios, but for this work the simple case is enough, because the main effort is to extract the capacity of a radio system for the pure pico-cell.

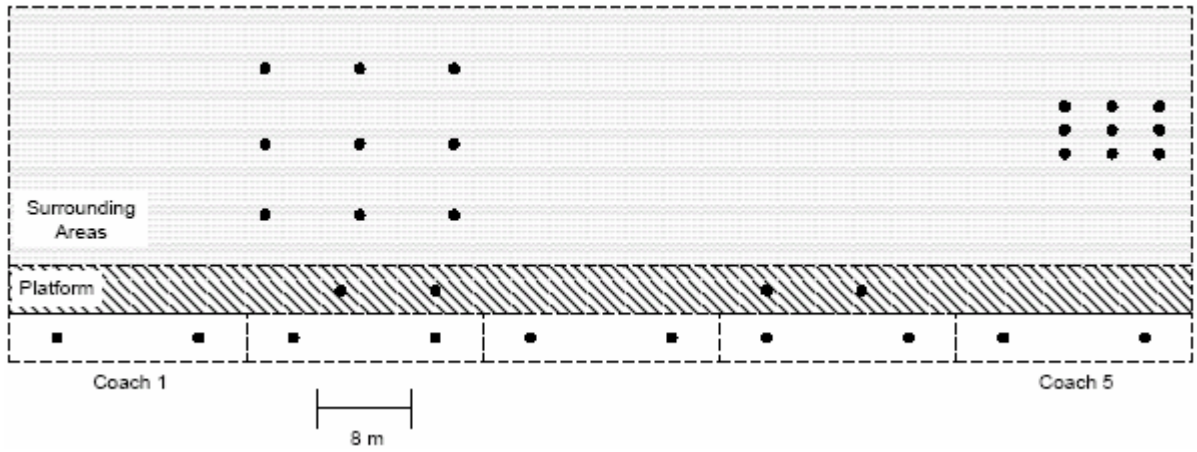

Figure 5.4 – The railway station scenario – general case [DGVC03].

The BS for the pico-cell with a radius of 50 m is placed in the centre of the main hall and the MT is placed 20 m from the BS. For the MIMO case, all railway station scenarios can be reduced to a circle with the BS in its centre. The MT is placed inside the circle as is depicted in Figure 5.5.

Scatterers are also placed inside the circle and are grouped in the clusters. The typical number for this kind of region is 15 [DGVC03], thus, for the considered area the cluster density is $1.91 \cdot 10^{-3}$ m^{-2}. The average number of scatterers equals 20, the same as for the micro-cell. All parameters for this scenario can be found in Table 5.1. An example of a deployment of a cluster is showed in Figure 5.6.

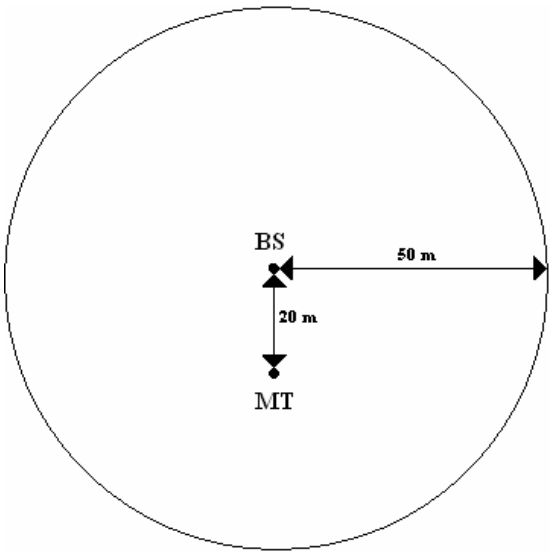

Figure 5.5 – The railway station scenario – particular case.

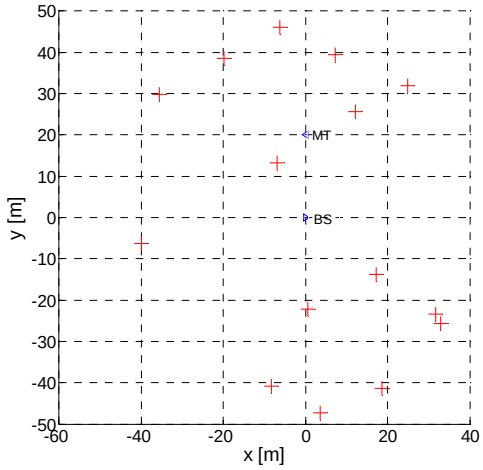

Figure 5.6 – An example of the deployment of clusters for the railway station scenario.

5.1.4 The highway scenario

The highway scenario describes the situation is a highway during a traffic jam, Figure 5.7, when the velocity of cars is very small or equals zero, which gives agreement with the assumptions of the radio channel model. In this scenario only the macro-cell is analysed.

The BS is placed far away from the highway, a distance of 2000 m being chosen, as depicted in Figure 5.8. MTs are deployed along the road and they are located on two lanes. One can notice that the distance between two adjacent MTs is significant with reference to a density of cars

distribution on a highway during a traffic jam. The reason of this situation is that on the picture only active users are presented, but, the real position of the MT is not important, because as was mentioned before the mutual influence of the MTs is out of scope of this work.

An important reason for using the scenario with cars is related to the size of the MT with MIMO antennas: a large number of antennas can be installed on the roof of a car. This approach is needed for simulations with a large number of antennas, so, for this scenario, MTs with 10 or 12 antennas are acceptable.

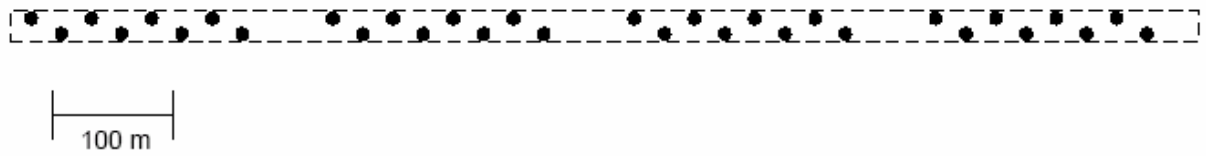

Figure 5.7 – The highway scenario – general case.

For the macro-cell with a radius of 200 m, the typical number of clusters is 5 [DGVC03], Figure 5.9. The cluster density equals to $0.04 \cdot 10^{-3}$. The average number of scatterers per cluster equals 20. This number is common for all scenarios, as is shown in Annex D. The number of scatterers has an insignificant influence on the capacity of a radio system.

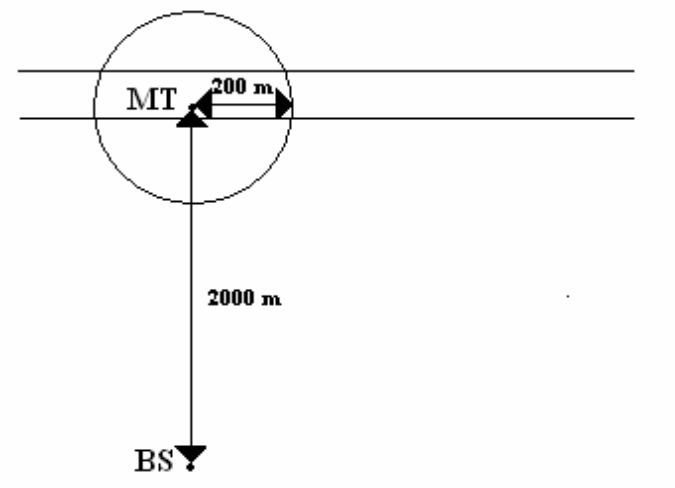

Figure 5.8 – The highway scenario – particular case.

All characteristic parameters of the scenario are shown in Table 5.1.

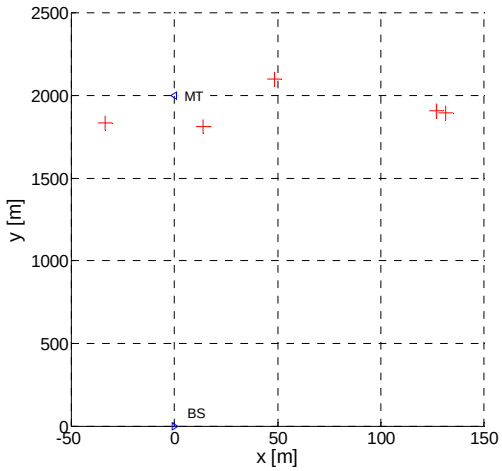

Figure 5.9 – An example of the deployment of clusters for the highway scenario.

Table 5.1 – Parameters of scenarios.

		The city	**The train station**	**The highway**
Type of scenario		Micro-cell	Pico-cell	Macro-cell
Scattering region	Shape	Ellipse	Circle	Circle
	Dimension [m]	w_{eff} = 40	R=50	R=200
Clusters	Clusters number	7	15	5
	Cluster density [1/m^2]	$0.5 \cdot 10^{-3}$	$1.91 \cdot 10^{-3}$	$0.04 \cdot 10^{-3}$
Scatterers	Average number of scatterers per cluster	20		
	Standard deviation around cluster [m]	1		
Mobility		Not considered		
Effective Street Width Ratio		2	-	-
Rx/Tx antenna types		Omnidirectional element		

5.2 MIMO capacity

5.2.1 Number of antennas

The main feature of a MIMO system, which distinguishes itself form other systems, is the fact of having multiple antennas on receive and transmit sides. This research starts with the analysis of simulations related with a varying number of antennas on the input and output sides of the radio link.

The distance between antennas is also important, which is analysed in detail in one of the following subsections. Now, the distance between adjacent antennas is fixed and equals λ, which is sufficient to give enough decorrelation between CIRs. The system in consideration is UMTS, thus the spacing between antennas equals 0.15 m, since the carrier frequency is assumed as 2 GHz.

For the capacity calculations also the bandwidth must be defined, because it affects the time separation for the filtered CIRs. The bandwidth is fixed as 5 MHz, so, the samples of the CIR after filtering are separated by 200 ns. The filtered CIR is used to extract capacity, the wider bandwidth the shorter separation time is, so the filtered CIR is more accurate, but this has no impact on capacity. Some simulations have confirmed this phenomenon. A more extensive description is placed in Annex I.

The average signal to noise ratio per every receive antenna is set to 10 dB, as it is one of the most frequent values found in the literature, and the noise margin was picked up from [GVCM03]. These values of bandwidth and signal to noise ratio are also valid for the reminder of this work, their impact on capacity is out of the scope of this dissertation.

All system parameters are given in Table 5.2. The combination of this table and Table 5.1 for the considered scenario provides all the information for the conditions of the radio environment.

Table 5.2 – System parameters for UMTS.

	UMTS
Carrier frequency [GHz]	2
Bandwidth [MHz]	5
Time resolution [ns]	200
Distance between antennas [m]	0.15
Noise margin [dBm]	-150
ρ[dB]	10

In the beginning, the number of antennas for both sides of the radio link is the same. This situation is not realistic, since a BS can have more antennas. The BS is static, and typically the size of this part of the system is larger than the size of any MT, thus, the BS can have a larger number of antennas. The following simulations have been made for checking a trend, how the various numbers of antennas influences capacity. The last analysis shows the capacity for

typical combinations of receive and transmit antennas for two systems: UMTS and HIPERLAN/2.

The number of antennas is taken from the set {2, 4, 6, 8, 10, 12}. The same simulations with the various numbers of antennas were made for all types of cells. All results are compared with the theoretical maximum and minimum capacity. The upper and lower bound are calculated using (3.20) and (3.21), respectively. The mentioned values are for the uncorrelated and full-correlated channel, so the extracted results have to be in between these bounds. The extremes are the same for all considered scenarios, but these constraints are appropriate only for symmetric systems, i.e., the same number of antennas for both sides of the radio link; to calculate any border capacity, the smaller number of antennas has to be taken into account. To assess the results, the asymmetric system can be compared with the symmetric one, but with the number of antennas equal to the smaller number of antennas of the asymmetric one. It shows the impact of the extra antennas for one of the sides of the radio link.

The results for the city street scenario are depicted in Figure 5.10. An increase of the number of antennas leads to a growth of capacity. The value of the capacity changes from 5.6 b/s/Hz for 2×2 up to 20.7 b/s/Hz for 12×12 MIMO system, which was expected, because a larger number of antennas makes a larger number of independent subchannels between the two ends of the radio link possible. The maximum number of subchannels is constrained by the number of receive antennas. A more extensive analysis of subchannels is presented in Section 3.2.

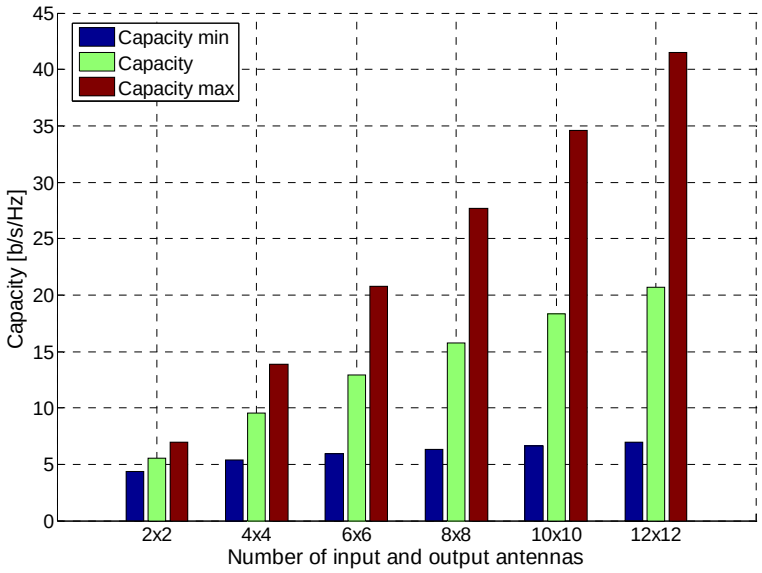

Figure 5.10 – Capacity for various numbers of antennas for the city street scenario.

The railway station scenario behaves in the same way as the city street one. Table 5.3 shows values of capacity for the considered scenario. A minimum value of capacity is 5.3 b/s/Hz for 2×2 MIMO system, and a maximum value equals 21.9 b/s/Hz for 12×12. In comparison with the city street scenario, capacity is slightly smaller for the 2×2 MIMO system, but for the largest set of antennas is slightly larger.

The highway scenario keeps the same trend as the previous ones. The smallest value is for the 2□2 MIMO system and equals 4.6 b/s/Hz, but, the value is slightly greater than the minimum capacity for a full correlated channel. The use of a MIMO system makes a sense in this condition, because capacity is larger than the one for a SISO system which equals 3.46 b/s/Hz, see (5.1). The capacity for 12×12 equals 12.8 b/s/Hz. The values for all combinations of antennas are presented in Table 5.3 and depicted in Figure F.2.

$$C_{1\times1} = \log_2(1+10) \approx 3.46 \ \text{[b/s/Hz]} \tag{5.1}$$

Results show that a MIMO system obtains the best results for the city street and railway station one, the comparison of all ones being depicted in Figure 5.11. For the two mentioned scenarios, the capacities for the particular sets of antennas are always greater than for the highway scenario.

Table 5.3 – Comparison of capacity for different cells.

	Capacity [b/s/Hz]		
Number of antennas	City street scenario	Railway station scenario	Highway scenario
2×2	5.6	5.3	4.6
4×4	9.5	8.9	6.7
6×6	12.9	12.2	8.4
8×8	15.7	15.4	9.8
10×10	18.4	18.7	11.4
12×12	20.7	22.0	12.8

The propagation phenomenon explains the difference in capacity for different scenarios. In highway scenario AoAs are in the smallest range comparing other ones, some examples of the angle ranges for particular scenarios can be found in Annex E. It implicates that the multipath components related with one output antenna have very similar conditions of propagations,

between a scatterer and the antenna. Also the multipath components received by all output antennas, but related with the same scatterer have the same feature as previous ones. If the distance between the BS and a scattering region is compared to the distance between output antennas, one can say that the paths towards all receive antennas are almost parallel, so this section of radio link give small impact on dissimilarity of multipath components. AoDs associated with all input antennas and a single scatterer are very similar as well. The reason is the same as for the section between the scattering region and the BS, i.e., the distance dividing a scatterer and input antennas is not comparable longer than a spacing between antennas. One can see that there are some potential sources of dissimilarity among links; however, it gives small gains of capacity relative to other scenarios.

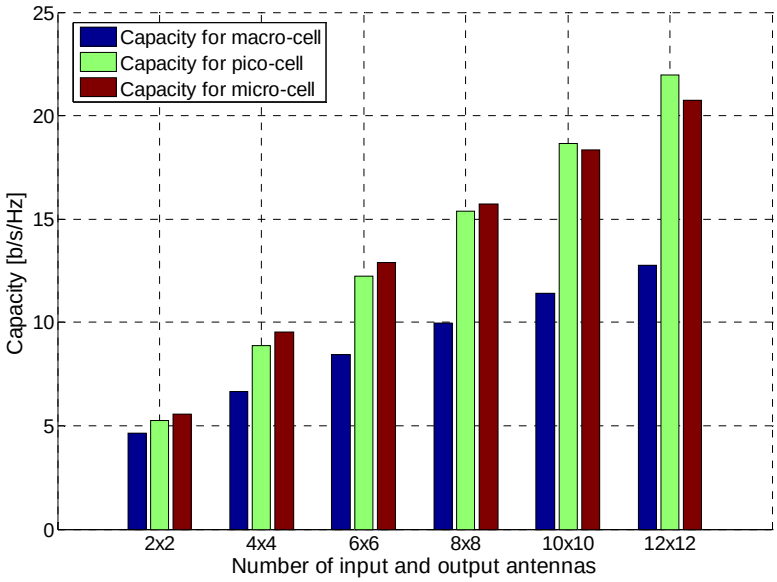

Figure 5.11 – Capacity for various numbers of antennas for different scenarios.

The range of AoAs and AoDs is definitely wider for the city street scenario and the railway station one. For the first one the range is defined by the width of a street and the distance between the BS and the MT. For the second one, the special deployment of clusters in the circle causes that the angles are in range $[0^{\circ}, 360^{\circ}]$. Those indicate that the multipath components related to all pair of input and output antennas, but to the same scatterer are more different than in the highway scenario, because the larger angles cause that the difference in lengths of covered ways by taps picked up by adjacent output antennas are more significant which implies that the parameters associate to particular taps differ one another. Also the distance between the

antennas is more comparable to the distance between the BS and the MT, and it is next reason of the larger gain of capacity for both mentioned scenarios.

The real capacity depends on the level of correlation among CIRs for all pairs of input and output antennas, since the stronger correlated the radio channel is the lower capacity becomes. Some examples of correlation for all scenarios can be found in Annex H. The above presented analysis shows the reason why the highway scenario has the most correlated radio channel. CIRs between all pairs of the input and output antennas are very similar. After comparing graphs form this annex, it is confirmed that the highway scenario is the most correlated one, since links with the same transmit antenna are almost the same. The mentioned graphs have been made for the UL case, so the transmitter is the MT. From the point of view of an input antenna, all output antennas are almost in the same locations, implying that links with the same transmit antennas are the most correlated. These conditions make that the highway scenario is most handicapped with reference to achieved capacities.

For city street and railway station scenarios, the level of correlation is similar, and one can see that the higher correlation is between links that have either a common transmitter or a common receiver. However, the correlation is far below one, which shows a not so large dose of similarity. In this case, a larger quantity of independent subchannels can be established.

For city street scenario, the difference between maximum capacity and the capacity from a simulation for a specified antenna array increases with the number of antennas. The increase depends on the actual size of antennas set. The growth on the number of antennas from 2 to 4 causes an increase of the capacity of 4.0 b/s/Hz, but in case from 10 to 12, gain equals 2.4 b/s/Hz, Figure 5.12.

After reaching some value, extra antennas have a smaller influence on capacity. For the city street scenario, 8 antennas for each side of the radio link seems to be adequate, the increase is smaller above this value and the cost of upgrading system elements may be significant comparing the achieved increase in capacity.

For the railway station scenario, extra antennas have the same impact on capacity. Two extra antenna give almost a constant growth of capacity. The mentioned phenomenon is depicted in Figure 5.13. The increase always is greater than 3 b/s/Hz, the maximum value being for the change from 2 to 4.

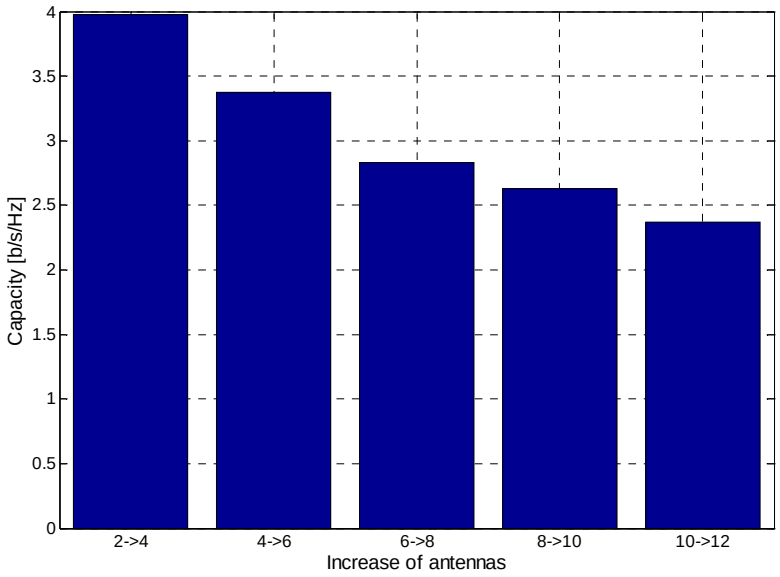

Figure 5.12 –Increase of capacity for the city street scenario.

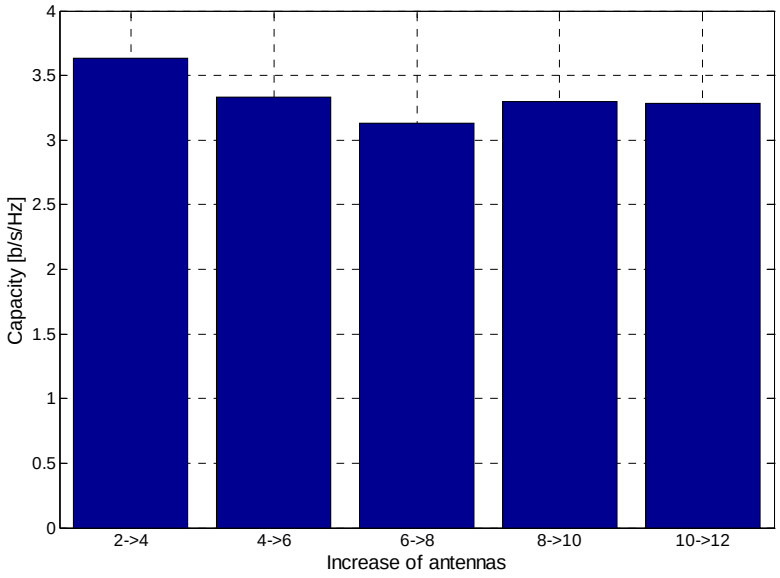

Figure 5.13 – Increase of capacity for the railway station scenario.

The above described effect is caused by fact that in the railway station scenario clusters are around the BS and the MT and that the density of clusters is the largest for this scenario, which causes a greater decorrelation of the radio channel (for larger sets of antennas). A greater number of clusters allows that more independent subchannels can be established for the extra antennas. A larger number of clusters enables links between new antennas to be different enough yielding an increase in the capacity of the system.

For the highway scenario, the increase depends on the actual number of antennas, so that the effect is similar to the city street scenario. Also, here the number of clusters is not enough to give a high decorrelation of links established by new antennas.

For the highway scenario, smaller values of increase of capacity are observed. All values, except the first one, are below 2 b/s/Hz, the first has a value of 2.0 b/s/Hz, and the last one equals 1.4 b/s/Hz.

A comparison of the growth of capacity is shown in Table 5.4. The railway station scenario has a constant increase, giving largest capacity for the largest number of antennas.

Table 5.4 – Comparison of increase of capacity for different cells.

	Capacity [b/s/Hz]		
Increase of a number of antennas	City street scenario	Railway station scenario	Highway scenario
2->4	4.0	3.6	2.0
4->6	3.4	3.3	1.8
6->8	2.8	3.1	1.5
8->10	2.6	3.3	1.4
10->12	2.4	3.3	1.4

The main differences between UMTS and HIPERLAN/2, from the point of view under analysis in this work, are the various carrier frequencies and bandwidths. HIPERLAN/2 has two and half times larger carrier frequency than UMTS. If a distance between antennas is assumed as λ for both input and output sides, the distance in meters is much smaller for HIPERLAN/2 and equals 0.06 m. The bandwidth does not have impact on achieved results which was above mentioned.

All system parameters for HIPERLAN/2 are given in Table 5.5. The same scenarios are used for the two systems, but only two are taken into consideration. HIPERLAN/2 makes sense only in a micro-cell and pico-cell scenario, so that the city street and railway station scenario have been chosen. The distance between an MT and a BS is not accepted in a macro-cell scenario for the mentioned WLAN.

Table 5.5 – System parameters for HIPERLAN/2

	HIPERLAN/2
Carrier frequency [GHz]	5
Bandwidth [MHz]	20
Time resolution [ns]	50
Distance between antennas [m]	0.06
Noise margin [dBm]	-150
P[dB]	10

For the present analysis, real combinations of antennas are considered. The following sets of antennas have been simulated: 2×2, 4×2, 8×2, 8×4, 16×2, 16×4; the first number of each set is related to the number of antennas for the BS side, the number for the MT being limited to 4.

For both UMTS and HIPERLAN/2, the achieved capacities are almost the same. Only approximately a 1% difference can be observed. A similar situation occurs for both city street and railway station scenarios, so, only the graphs related only with the city street scenario are presented in the present section, the others being given in Annex F. In order to compare both systems, all necessary values are presented in Table 5.6.

The results show that if the spacing between antennas expressed in wavelength is constant, the achieved capacities for the same combination of the antennas and in the same scenarios are almost equal. Any significant difference is hard to notice.

A correlation between CIRs is related to the distance expressed in wavelengths, not in a metric scale. This is caused by fact that differences in shapes of the CIRs come from by a shit in phase of signals picked up by the receiver. The phase is related to the wavelength, so the spacing in the metric scale has no influence on capacity. Delays of taps generated by the same scatterer but for two systems are insignificant different, and for some cases even the same, so that after CIR filtering corresponding taps are in the same place of the time axis. Thus, filtered CIRs for both systems have similar samples in the same instant of time. Also the amplitudes of the signal are almost the same, because they are related to delays. Only phases of multipath components are different, which have an impact on filtered CIR. It means that a MIMO system can find good conditions for application when the multipath component phenomenon exists.

If the UL and DL is considered, some interesting phenomenon common for both systems can be observed. Mentioned before the MT is associated to a smaller number of antennas.

Figure 5.14 shows the capacity for the UL in the city street scenario. The increase of receiving antennas has the main influence on the achieved capacity. Increasing twice of input antennas always gives worse results than output ones.

In the DL case, capacity is constrained by a number of MT antennas, Figure 5.15. Even if the number of BS antennas is different, the achieved capacity is almost the same. The small difference between capacities of systems is associated to the same number of output antennas, however, a greater number of the input antennas has small influence of the capacity. As expected, all that is radiated must be received. In the case of constant number of output antennas, a larger gain can not be achieved by adding extra input antennas. Only a small increase is perceptible, because the situation is a bit better from the correlation point of view. The propagation environment is richer in multipath components.

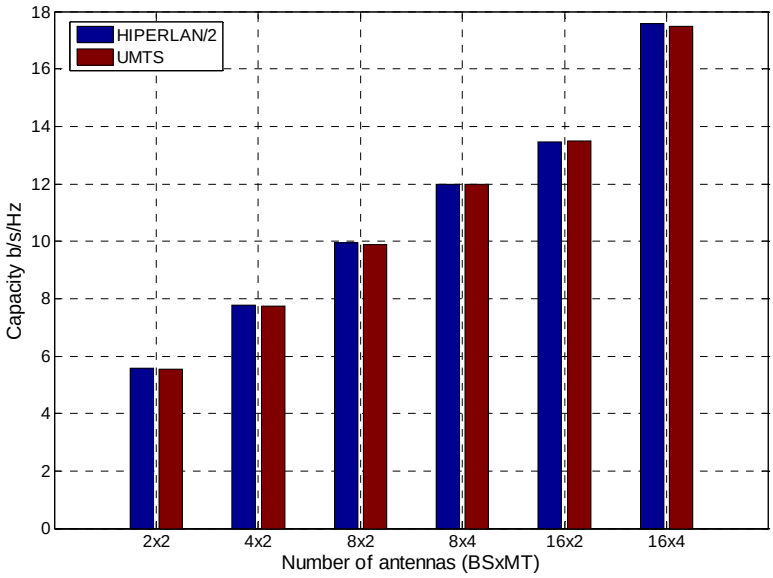

Figure 5.14 – Comparison of capacity for the city street scenario (uplink).

This is very important from the practical point of view, because the throughput from a BS to an MT is limited. This is unfavourable, because download is the typical link of traffic in the radio channel for this kind of systems, especially for UMTS. In the mentioned conditions, the radio channel is not used in full range. In typical conditions, capacity is divided by some MTs and one BS. In this way, asymmetric sets of the antennas are acceptable.

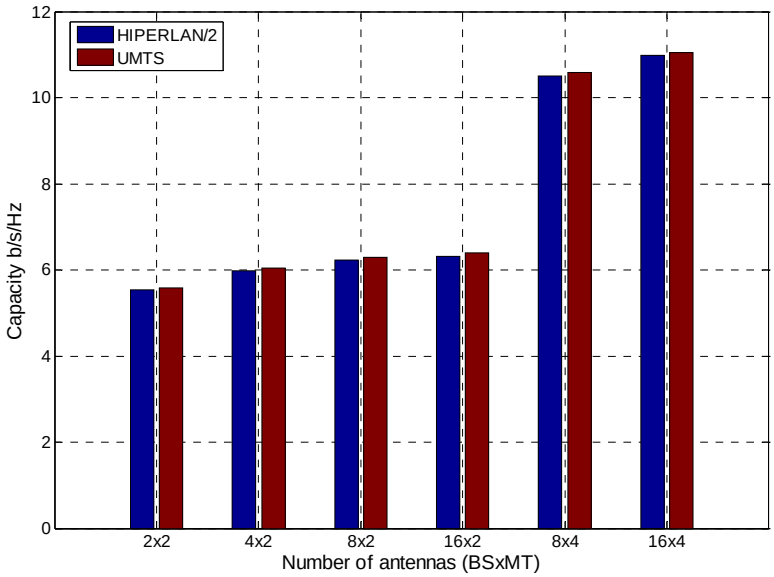

Figure 5.15 – Comparison of capacity for the city street scenario (downlink).

Table 5.6 – Comparison of capacity for UMTS and HIPERLAN/2.

		City street scenario		Railway station scenario	
		UMTS	HIPERLAN/2	UMTS	HIPERLAN/2
Uplink	2×2	5.56	5.58	5.27	5.34
	4×2	7.75	7.78	7.37	7.43
	8×2	9.88	9.93	9.46	9.52
	16×2	12.00	12.00	11.64	11.59
	8×4	13.50	13.48	12.70	12.61
	16×4	17.49	17.58	17.00	16.72
Downlink	2×2	5.59	5.54	5.26	5.54
	4×2	6.05	5.97	5.74	5.79
	8×2	6.29	6.23	5.96	6.00
	16×2	6.39	6.32	6.14	6.11
	8×4	10.59	10.50	9.84	9.77
	16×4	11.04	10.98	10.56	10.36

5.2.2 Capacity for different angles

The mutual positions of the BS and the MT are analysed in the present section. This aspect is important for a real situation. The previous simulations have been made for antennas in the BS and the MT in parallel, but this kind of situation is very rare in real conditions, so, a change of orientation of antennas should be considered. The way of changing the orientation for the MT is depicted in Figure 5.16. In the same way, the orientation for the BS is changed.

For the following analysis, some assumptions are established. In the first case, the orientation of the MT is constant and shows the line of an orientation zero. Only the orientation of the BS is changed. It emulates a situation when the MT makes a move around a BS. The orientation of the MT antennas keeps the right angle with the line that joints the BS and the MT. In the second case, the orientation of the BS is constant and indicates the line of an orientation zero. However, the orientation of the MT is varied. Here, the MT spins itself around its own axis. An angle of an orientation is change in the range [0°, 360°], with 10° step. Used antennas are omnidirectional for both BS and MT.

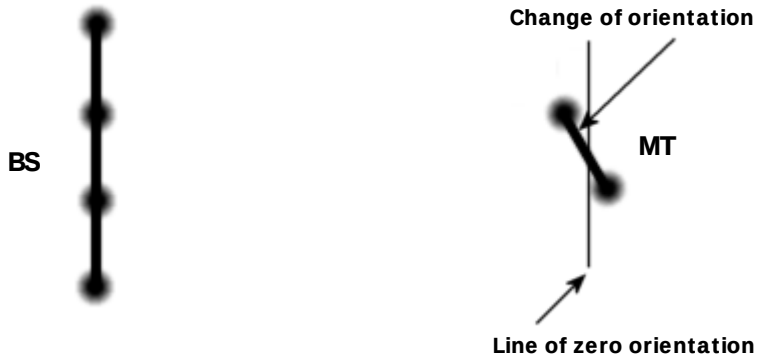

Figure 5.16 – Change of the orientation of antennas.

All graphs consist of two curves: one shows the change of capacity for a 4×2 MIMO system, and the other is related with to capacity for a SISO system. For this case, the SISO capacity is calculated using (3.19). A CIR for SISO is defined between the first antenna of the BS and the first antenna of the MT. The channel impulse response matrix is uni-dimensional. It was made to show the spatial gain of a MIMO system.

Figure 5.17 shows a change of capacity for various orientations in the city street scenario. For the MT case, the greatest capacity is for orientations 0° and equals 7.8 b/s/Hz. The parameter goes down to a 90° orientation, where reaches 6.1 b/s/Hz. The difference between the upper and lower value is 1.7 b/s/Hz. It means that the 90° rotation of the MT causes a 21.9% loss of capacity. A correct mutual position of the BS and the MT gives a significant increase of capacity. Almost the same results are obtained for the rotation of the BS. It was expected, because the clusters of scatterers are mainly placed between the BS and the MT, and the scenario is symmetric.

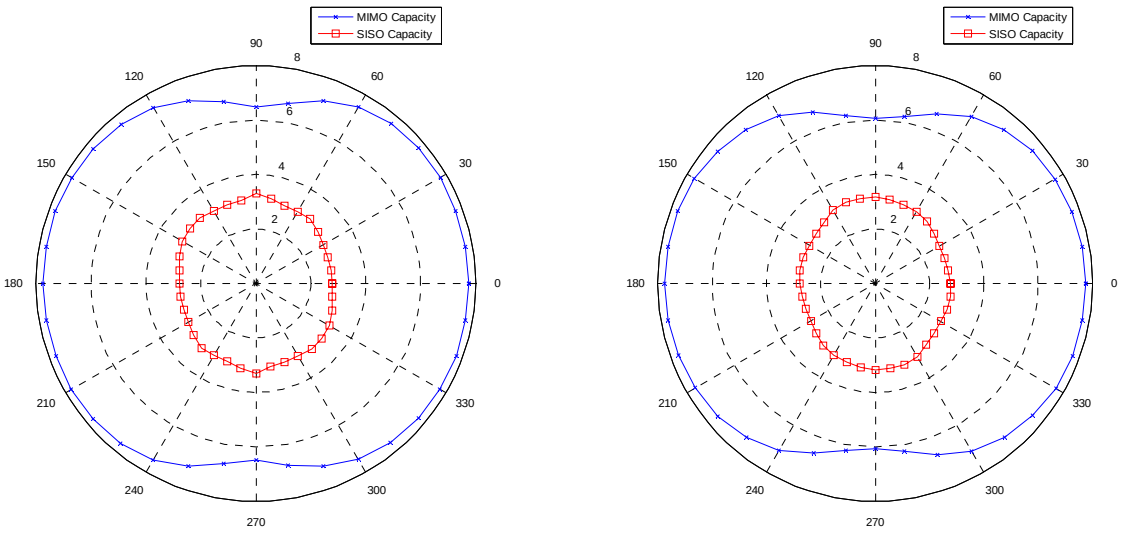

(a) Rotation of BS. **(b) Rotation of the MT.**

Figure 5.17 – Capacity for different rotations of antennas for the city street scenario.

The MIMO curves for the city street scenario consist of four the same parts. Both MT and BS are attributed with omnidirectional antennas, so that for analysis is enough to carry out the experiment only for the range [0, 90°]. But for real antennas, with specific antenna pattern, this kind of simplification is not acceptable.

For the railway station scenario, the shape of the graph of the capacity as a function the orientation angle is similar to circle, see Figure 5.18. A small deviation of the radius is observed. For the MT case, the greatest value of the capacity is for $30^0$and equals 7.7 b/s/Hz; however the smallest one appears for 290^0 and equals 7.2 b/s/Hz. So the change of the capacity is 6.25% with reference to the maximum value. The loss of capacity is significant smaller with reference to the city street scenario, which is a valuable feature of this scenario.

A rotation of both BS and MT gives almost the same results, but this is valid only for the railway station scenario. Clusters are deployed around the BS and the MT, so changes of the orientation has a small impact on capacity.

The curves for the railway station scenario are asymmetric relative to axis y, which seems be caused by deployed scatterers. The shape of the curves in Figure 5.18 seems only to be characteristic for the distributions of clusters, which were considered during the simulations. So, a huge number of the simulations should make the curve very similar to a circle. But, the same

simulation was made for 1000 different realisations of the radio channel, with various distributions of scatterers for each. The deviation of the radius of the circle keeps the same level, see Figure 5.19. The minimum value is 7.2 b/s/Hz and the highest one equals 7.7 b/s/Hz. The loss of capacity relative to the maximum value is 6.16%.

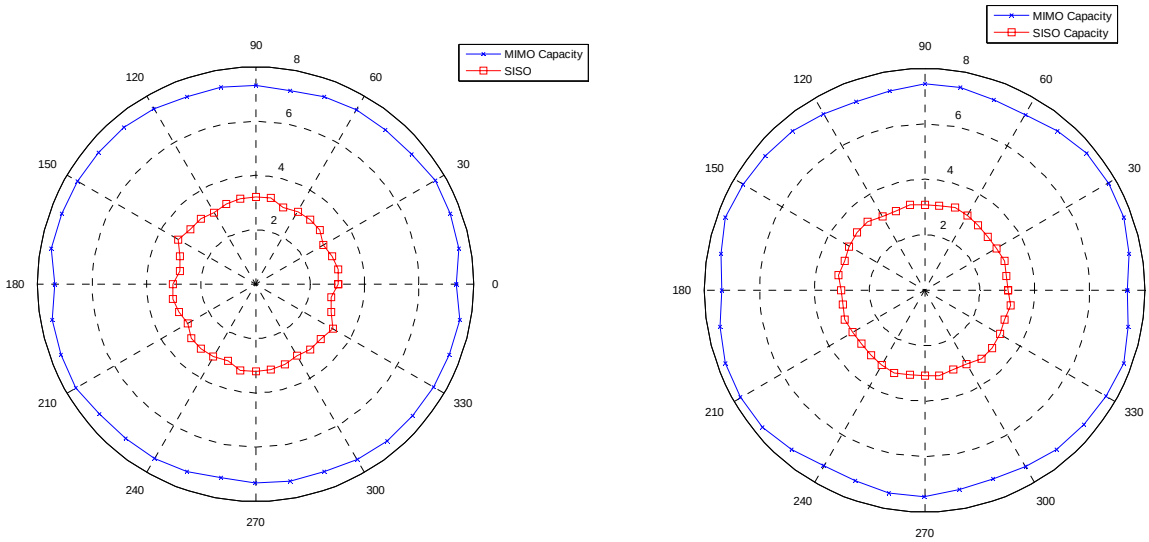

(a) Rotation of the BS.

(b) Rotation of the MT.

Figure 5.18 – Capacity for different rotations of antennas for the railway station scenario.

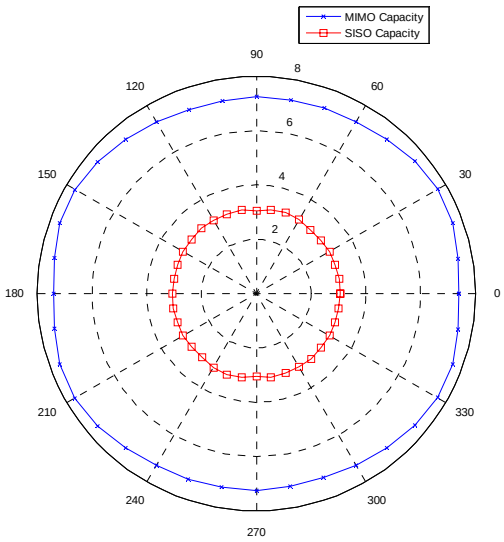

Figure 5.19 – Capacity for different orientations for the railway station scenario for 1000 simulations.

For the highway scenario, a spinning MT generates a curve that is also circular. But for the highway scenario, the deviation of the radius is almost imperceptible as depicted in Figure 5.20. This phenomenon is caused by part of the radio link, which is free of scatterers. The distance

between the BS and the scattering region is larger, and the radius of the scattering region is significantly larger than the size of antennas arrays, so that a small displacement, generated by the change of orientation, has no influence on capacity.

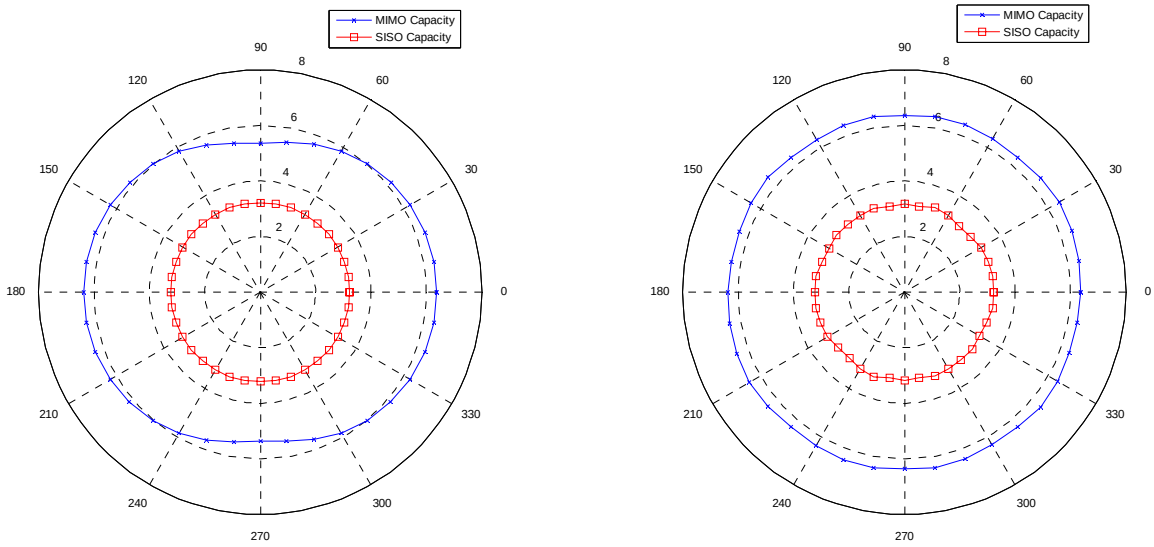

(a) Rotation of the BS. **(b) Rotation of the MT.**

Figure 5.20 – Capacity for different orientations for the highway scenario.

In case of the highway scenario, but for a change in the orientation of the BS, the fluctuations of the capacity are greater. The minimum of the profile is for 90° and 270°, when the lines of deployment of the antennas are perpendicular.

The scenarios with the circular-shaped scattering region tolerate better the changing of the orientations of the antennas, except the rotation of the BS in the highway scenario. Scatterers are always deployed around either the MT or the BS, so the change of orientation has a small influence on capacity. In this work, the simplest example with the omnidirectional antennas is analysed, but for circular cells, even antennas with non omnidirectional radiations patterns do not change the shape of the curve. For each realisation of the channel, some multipath components are smooth by the radiation pattern of the antenna, but others are amplified. If a distribution of clusters is even, for each realisation of the radio channel, both number of smooth taps and the number of amplified taps are constant. So, after averaging, the circular shape of the curve is kept.

For the city street scenario, the situation is trickier. Scatterers are placed mainly between the BS and the MT. So, the change orientation of the antennas has a substantial impact on capacity. If the orientation of the MT is laid under a right angle with reference to orientation of the BS, the situation is the worst. Rays toward different receivers cover almost the same path. The antennas are on the line that is parallel to direction of the radiation, so, the CIRs from particular input antennas differ themselves only in time shift which equals one period for the considered wavelength. For UMTS the period is 0.5 ns and the mean duration of CIR for the considered city street scenario is 30.46 ns, thus, the shift is insignificant relative to the duration time. This is the reason why CIRs are more correlated to one another, which follows a drop of capacity.

For the highway scenario with the rotation of the BS, the situation is the same. But here rays are more parallel because the distance between the BS and the MT is greater, thus, this phenomenon should have stronger impact on the achieved capacity. The mean duration of the CIRs for the highway scenario is approximately 1μs, thus the previously mentioned shift between CIRs is smaller relative to the average length of CIR.

The situation is worse when the system has non omnidirectional antennas. If the orientation causes that a minimum of a radiation pattern is aimed towards the region where most scatterers are located, capacity goes down noticeable. The worst situation is for a highway scenario, where all multipath components are focused in a small range of angles, as depicted in graphs in Annex E. If all taps are in a minimum of a radiation pattern, the power of a signal is smooth in a significant way. For this reason, antennas should be almost omnidirectional, which is not so easy.

For systems like UMTS or HIPERLAN/2, a user changes orientation during a session, because it is not comfortable to keep it constant, so, in some conditions, especially in a city street scenario, a drop of capacity can be observed.

5.2.3 Spacing between antennas

In the present section, the influence of spacing between antennas on capacity is analysed. It is important to find an appropriate distance separating the antennas, but it must be a result of a compromise. A large spacing gives a high decorrelation of links between input and output

antennas, because they are placed in distant points of a scattering region. A single scatterer has more impact on more separated antennas, but, this is not a global solution. On the other hand, the greater the spacing is the greater the size of a MT is. If the MT is too large, it loses its main feature, i.e., mobility. Additionally, a greater spacing constraints a number of antennas in an antenna array if the size of the device is limited. Therefore, the best case depends on a number of parameters.

Distance is taken from the range [0.025, 0.3] m with 0.025 m step. If the range is compared with the wavelength of 0.15 m, one has [λ/6, 2λ] with the λ/6 step. Simulations have been made for all scenarios and for different combinations of antennas, 2×2, 4×4, 8×8 MIMO systems have been considered.

All results are presented in Table 5.7 and graphs for the 2×2 MIMO system can be found in the present subsection. Other graphs are given in Annex G.

Figure 5.21 shows the behaviour of capacity in the city street scenario. An increase of the distance between antennas causes an increase of capacity. A growth of the spacing up to λ is more important for capacity comparing to the increase above λ. The change of the distance from 0.025 m to 0.15 m gives 1.07 b/s/Hz increase of capacity, when the global increase is 1.25 b/s/Hz in this scenario.

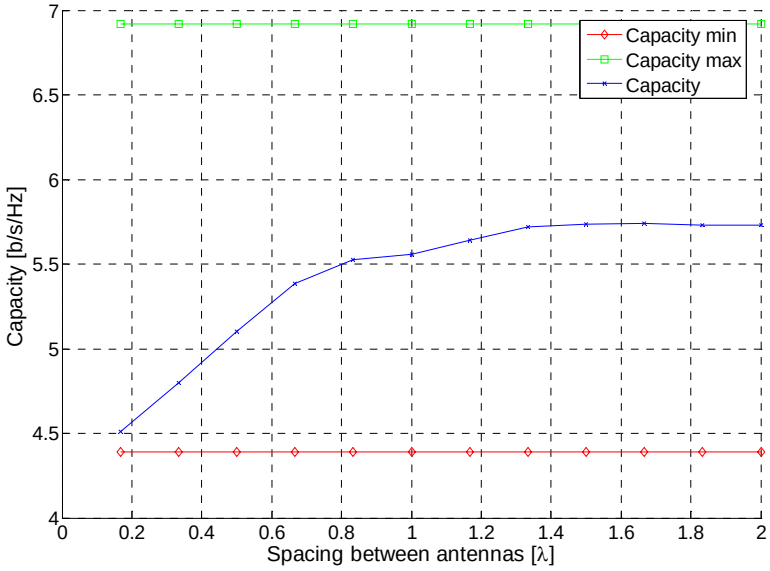

Figure 5.21 – Capacity of MIMO 2×2 for different spacings for the city street scenario.

For the other sets of antennas the trend is the same, and capacity increases intensive below λ. At the end of the spacing scale, capacity asymptotically goes toward a border value, which is characteristic for each scenario. The border capacity is significant smaller than the theoretically defined maximum capacity, since a full decorrelated radio channel is not achievable.

In the railway station scenario, an increase of the distance between antennas also gives an increase of the capacity and the most important part is below λ, see Figure 5.22. Capacity changes itself from 4.8 up to 5.6 b/s/Hz for the 2×2 MIMO system in this scenario. The behaviour for the railway station scenario is not as smooth as for the city street scenario.

The profile consists of local extremes of capacity. A distribution of these points is related to a mutual deployment of the BS and the MT. In the pico-cell scenario, as depicted in Annex E, AoAs and AoDs are the largest and the distance between antennas of one side of the radio link is the most comparable with the one between the BS and the MT. So, even a small change in the spacing has a significant influence on the angles, which leads to changes of delays generated by a single scatterer. This is the reason why some irregularity in the shape of the curve is observed.

For the case related to a larger set of antennas, the irregularity is smaller, because capacity is calculated based on larger number of antennas. Some antennas can be located in points, where irregularity exists, but others may have positions related with places without it. So, results are more averaged when the number of antennas is larger, e.g., a 8×8 MIMO system, see Annex G.

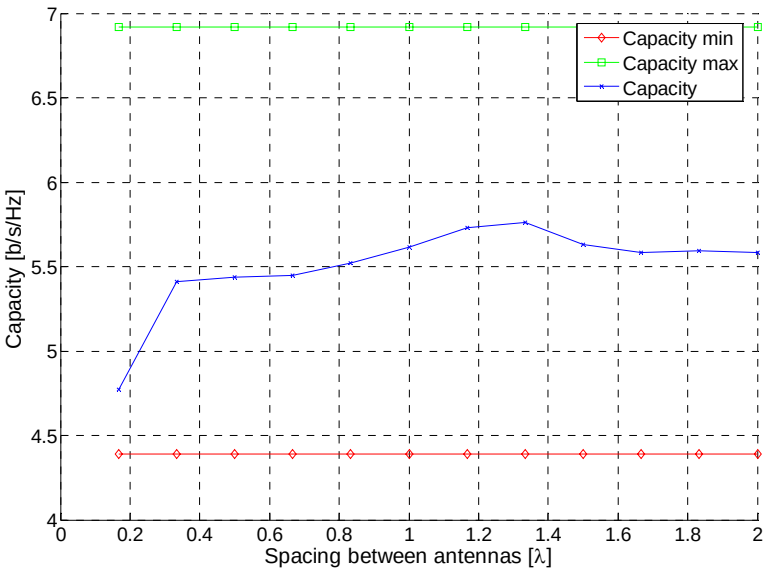

Figure 5.22 – Capacity of MIMO 2×2 for different spacings for the railway station scenario.

Figure 5.23 shows the profile for the railway station scenario, but the MT is placed in different points. The distance between MT and BS is kept to 20 m. Capacity has similar values as for the first deployment of the BS and MT, the only changes being where the local minima and maxima are observed.

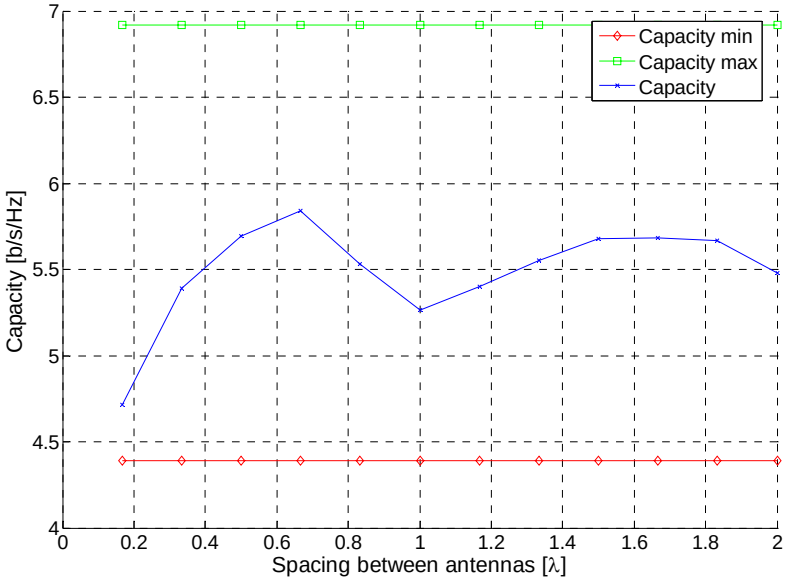

Figure 5.23 – Capacity of MIMO 2×2 for different spacings for the railway station scenario. The MT is placed in a different position.

The curve for the highway scenario is shown in Figure 5.24. Also for this scenario, a growth of capacity caused by the increase of spacing is observed. But, the shape of the curves is a bit different comparing to previous scenarios; an almost linear progress of capacity can be seen in the graph. The saturation of capacity occurs at the end of the scale, but the curve is almost linear below 1.8λ.

The increase of capacity is caused by the increase of spacing between antennas of the BS. Figure 5.25 shows two curves for the highway scenario that are almost constant but parallel shifted. Capacity is independent of the spacing between MT antennas, i.e., an increase of the distance between antennas of the MT does not have any influence on capacity. Only small fluctuations of the curves caused by various spacing between MT antennas are observed. The curves are distinguished by the spacing for the BS, i.e., the levels of the curves are regulated by the spacing between antennas of the BS. This is confirmed by Figure 5.26, where capacity is dependent on the spacing of antennas of the BS. In the figure also two curves are depicted, each one is associated with a different spacing between MT antennas. The difference has no impact

on the shapes and values of the curves, and they are almost superimposed. The shapes of the curves are almost the same as the curve from Figure 5.24, where the spacing is changed for both BS and MT.

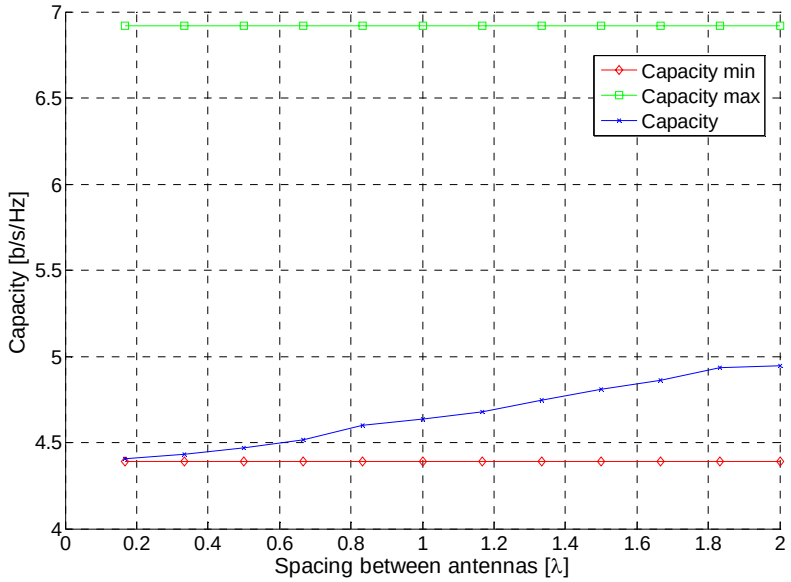

Figure 5.24 – Capacity of MIMO 2×2 for different BS spacings for the highway scenario.

The above presented results show that a link between an MT and a scatterer does not make a significant decorrelation between CIRs for the highway scenario. If two taps related to a single scatterer are taken into consideration and they are transmitted from adjacent antennas, the differences in values for their parameters are small. Each scatterer is described by a random complex reflection coefficient, which is common to all taps related with the scatterer. So after bouncing, the parameters of the taps are changed by two factors. The covered distance and the reflection coefficient have impact on the parameters, but, the reflection coefficient influences in a stronger way. The influence of the distance between MT and scatterer can be neglected comparing to the impact of the scatterer. After meeting with the scatterer the multipath components from two input antennas have almost the same parameters. The case of two adjacent antennas can be generalised for all input antennas. Multipath components related to the same scatterer, but transmitted by different input antennas are described by very similar parameters. This is the reason why spacing between MT antennas does not influence on the capacity of the system.

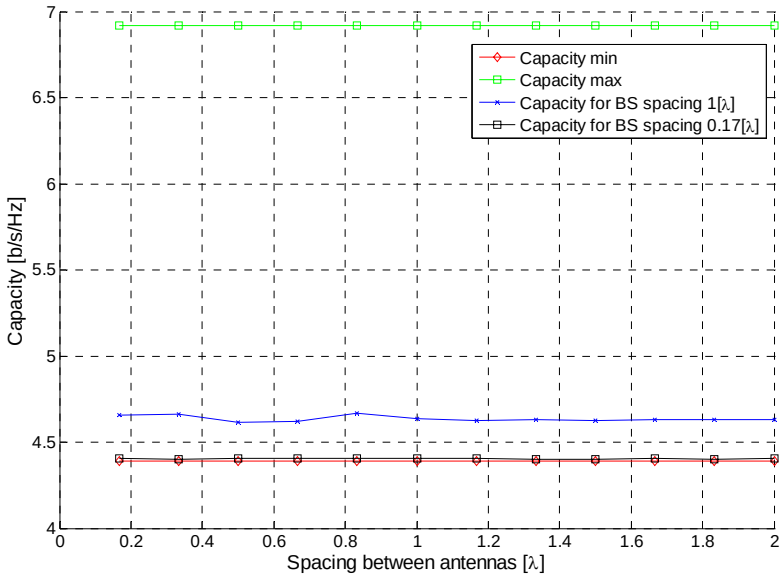

Figure 5.25 – Capacity of MIMO 2×2 for different MT spacings for the highway scenario.

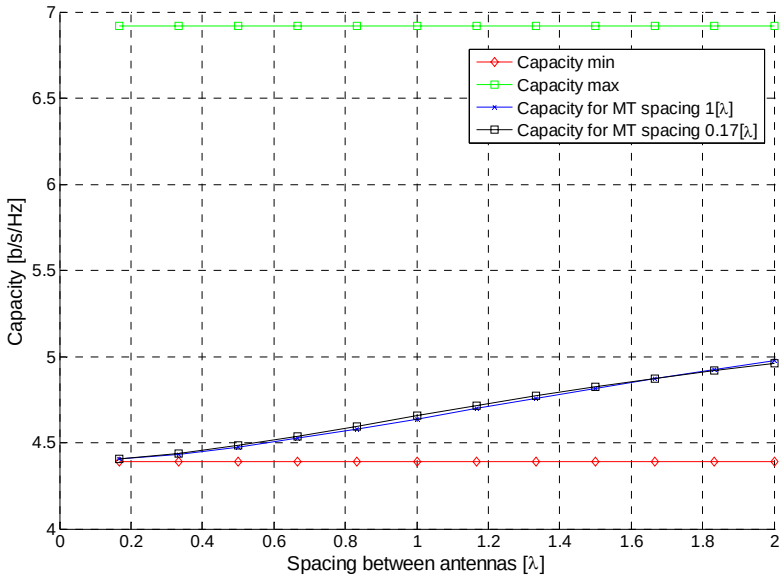

Figure 5.26 – Capacity of MIMO 2×2 for different BS spacings for the highway scenario.

After covering the distance between a scatterer and the BS, taps can be distinguished, because at the end of the way there is no random phenomenon. The spacing between the BS antennas distinguishes taps towards various MIMO antennas and the decorrelation of the radio channel appears just here. Hence, the spacing between BS antennas is very important and influences on the achieved capacity.

Table 5.7 – Comparison of capacity for various spacings, different scenarios and combinations of antennas.

		Capacity [b/s/Hz]		
$n_R \times n_T$	Spacing [λ]	City street scenario	Railway station scenario	Highway scenario
2×2	0.17	4.5	4.8	4.4
	0.33	4.8	5.4	4.4
	0.50	5.1	5.4	4.5
	0.67	5.4	5.4	4.5
	0.83	5.5	5.5	4.6
	1	5.6	5.6	4.6
	1.17	5.6	5.7	4.7
	1.33	5.7	5.8	4.7
	1.50	5.7	5.6	4.8
	1.67	5.7	5.6	4.9
	1.83	5.7	5.6	4.9
	2	5.7	5.6	4.9
4×4	0.17	6.1	7.1	5.5
	0.33	7.2	8.7	5.7
	0.50	8.1	9.4	5.9
	0.67	8.8	9.5	6.2
	0.83	9.3	9.8	6.5
	1	9.5	10.0	6.7
	1.17	9.7	10.2	6.9
	1.33	9.8	10.2	7.0
	1.50	9.9	10.2	7.2
	1.67	9.9	10.5	7.4
	1.83	9.9	10.3	7.5
	2	9.9	10.1	7.6
8×8	0.17	9.0	11.2	6.9
	0.33	11.4	14.4	7.8
	0.50	13.2	15.8	8.5
	0.67	14.5	16.0	9.0
	0.83	15.2	16.9	9.6
	1	15.7	17.2	10.0
	1.17	16.0	17.7	10.5
	1.33	16.4	17.9	10.8
	1.50	16.6	18.1	11.1
	1.67	16.8	18.6	115
	1.83	16.8	18.9	11.7
	2	16.8	18.5	11.9

For others scenario, impact of spacing both MT and BS are comparable, because the distance between an MT and a scatterer is smaller relative to the macro-cell scenario. The above described disproportion is only characteristic for the highway scenario. All results are presented in Table 5.8.

Table 5.8 – Comparison of capacity for various spacings for one side of the radio link for different scenarios.

		Capacity [b/s/Hz]		
	Spacing [λ]	City street scenario	Railway station scenario	Highway scenario
Constant spacing λ for the MT	0.17	4.6	4.9	4.6
	0.33	5.0	5.4	4.6
	0.50	5.3	5.6	4.6
	0.67	5.4	5.6	4.6
	0.83	5.5	5.5	4.6
	1	5.5	5.6	4.6
	1.17	5.5	5.7	4.6
	1.33	5.5	5.7	4.6
	1.50	5.5	5.7	4.6
	1.67	5.6	5.6	4.6
	1.83	5.5	5.6	4.6
	2	5.5	5.6	4.6
Constant spacing λ for the BS	0.17	4.7	4.9	4.4
	0.33	5.1	5.4	4.4
	0.50	5.4	5.4	4.4
	0.67	5.5	5.6	4.5
	0.83	5.5	5.5	4.5
	1	5.5	5.6	4.6
	1.17	5.5	5.7	4.6
	1.33	5.6	5.7	4.7
	1.50	5.6	5.7	4.8
	1.67	5.6	5.6	4.8
	1.83	5.5	5.6	4.9
	2	5.5	5.6	4.9

While the increase of the capacity for some first values of the simulated scenarios is not surprising, one could wonder why the asymptotic curve does not get the ideal capacity. This is caused by fact that the statistical characteristic of the propagation environment is independent of the spacing between antennas. The scattering region gives a minimum correlation of the signals at arrival. An average number of the scatterers, a deployment of them, the shape and the size of the scenarios make that the channel is Gaussian, without any relation with antennas characteristics. The Gaussian model represents the least restrictive channel model [Debb03].

In all scenarios, the general trend indicates that an increase of capacity with an increase of the spacing between antennas is valid. Of course, there some subtle difference in the shapes of

curves, but this does not change the general conclusion. It is not possible to establish a special limit, which is characteristic for each scenario, because each one gives its own correlation of the radio channel. After observation, the spacing of λ seems to be the most appropriate one for use in model of the radio channel. The mentioned distance gives enough decorrelation to achieved satisfactory results.

It is worth noticing that using a twice larger number of antennas is more valuable than using a twice greater distance between antennas. This rule is true for all scenarios, therefore, the increase of the number of antennas gives a greater decorrelation of the channel than the increase of the spacing between antennas.

In real conditions, the radiation patterns of antennas will have some influence. The change in spacing causes a variation in the distribution of AoAs and AoDs, which is related to way of influencing a real antenna on transmit and arrival rays. This situation is most serious in a railway station scenario, where the angles change in the widest range.

5.3 General conclusions

The results of above presented analysis of MIMO systems in different scenarios are helpful to show the locations where the application of the systems is the most profitable.

An increase of the number of antennas leads to a growth of capacity, but the range and dynamic of the change are unique for each scenario. The change of the mutual orientation of the BS and MT is characteristic for each one as well. However, an increase of spacing between antennas for each scenario generates increase of capacity, and it is common for all scenarios.

The city street and railway station scenarios have the largest gain of using MIMO systems. For each set of antennas, the values of achieved capacities are comparable, however, the largest ones are better used for the railway station scenario, and capacity is a bit larger for this scenario. It is related with the constant increase of the capacity in the railway station scenario. Extra antennas for both side of the radio link gives the same increase of the capacity, and it is not dependent on the actual size of antenna set.

Comparing all scenarios, the application of a MIMO system in the highway scenarios gives the smallest gain of the capacity which related with the largest correlated radio channel. The difference is especially large for the biggest set of antennas.

If the mutual orientation of the MT and the BS is considered, the railway station scenario has the best characteristic. Regardless of the actual positions of the BS and MT, capacity is almost constant, and only a small deviation can be observed. It shows that this scenario is most prepared for provision of services for mobile users.

For the city street scenario, in some situation, the drop of capacity is observed. The worst case is when the lines of antennas deployment for the MT and BS make a right angle, and the largest decrease of capacity appears.

The highway scenario joints the features of other scenarios. The rotation of the MT does not influence capacity, as for the railway station scenario. However, the rotation of the BS gives the same results as for city street scenario, so, a large drop of capacity is noticed when antennas are deployed on the perpendicular lines.

The greater distance between antennas is the larger capacity exists. For all scenarios, one can see that the most important increase is below λ, and above λ the one is slower. Additionally, the curve of the railway scenario is associated to numerous extremes which sometimes break the general tendency.

6

Conclusions and future work

This chapter includes some conclusions on the radio channel model and implementation of the simulator. The results from the three scenarios are summarised here. Some clues for future work are presented in this chapter as well.

The main purpose of this work was to investigate MIMO systems in three different scenarios that emulate different situations in mobile communications. The purpose generated some intermediate ones. First, a propagation model was selected, after which it was implemented in a simulator written in C++. Finally, some research related with MIMO systems was preformed.

Among the existing models fulfilling main goal of this work, the GBSB was chosen, but some improvements were necessary. Some corrections have already been done by GROW which simplified the work.

The main advantage of the GBSB model is simplicity, but it does not mean that it does not describe reality correctly. The extension made by GROW regarding grouping scatterers in clusters emulates a real behaviour of the radio channel, where taps related with one obstruction are associated to similar parameters. Scatterers are described in a random way, which increases similarity to real conditions. Unfortunately, the model does not consider rough surface scattering, diffraction, and multiple bounce multipath components which is a drawback. However, the rough surface scattering is quite well emulated by the scatterers grouped in to clusters, because parameters of each tap are changed by a random coefficient describing a scatterer which can be related to different angles. All elements of the environment are deployed on a 2D plane which is a substantial constraint of the model. Nevertheless, the GBSB model serves perfectly for the purposes of this work.

In order to implement the MIMO radio channel, a simulator has been developed. The simulator implements the GBSB model, extended by the feature that scatterers are grouped into clusters. Both BS and MT can be attributed with a set of MIMO antennas. Multipath components for each pair of input and output antennas are calculated, so all radio link between transmit and receive sides can be defined by CIRs. The last version of the simulator developed by IST/TUL did not consider a MIMO channel and simulated only a SISO system. To simulate MIMO systems, the converter from SISO to MIMO has been created. The converter takes a multipath component from a SISO radio channel and changes a phase of it by a shift defined with reference to a distance between antennas in a MIMO system. This procedure is made for all links between input and output sides of the system. Amplitudes and delays are identical for all receive antennas what is not true with reality.

The simulator implements MU aspects, so that in a propagation environment any number of users can be placed. Mutual relations between users can be analysed. The simulator gives the

ability to analyse MUI among users with a MIMO system. Consideration about MUI for SISO systems can be found in [Zuba05] which was based on the same simulator.

The capability to deploy clusters and scatterers in a determined way is a very useful feature of the simulator. A real scenario can be processed by the simulator and its results can be helpful before a measurement campaign. Some locations of obstacles can be researched, and an optimum deployment of clusters can be found. A change of the BS position related with the change of location of the scatterers can be useful to find the best conditions of propagation in a scenario. This application is especially important for a pico-cell scenario, given its dimensions.

A MIMO system has been analysed under different aspects. The behaviour of the system in three scenarios has been investigated, and it is a source of knowledge, where receivers and transmitters with multi element antennas can be applied with the greatest gain.

Spectral capacity was chosen as the criterion of a comparison of scenarios. Results show the capacity per unit of the frequency bandwidth and indicate maximum throughput of the radio channel, which can be achieved in ideal conditions. The capacity is a sum of throughputs related with transmission established in the radio channel, or it is the maximum throughput that can be obtained. The actual implementation in any system reduces this value, because the required technologies have an impact on the real maximum throughput; achieving the capacities as shown in Section 5.2 in a real system is impossible, because additional scaling factors related to the used solutions must be considered. For example, the modulation scheme has significant influence on the throughput of a system; using more a complex modulation give better results, and approaches the performance of the system to the limiting value.

First, the influence of various numbers of antennas for both sides of the radio link has been checked. Two types of combinations of antenna arrays have been considered. One is related to a symmetric link, where both receiver and transmitter have the same number of antennas; the following MIMO systems have been taken into consideration: 2×2, 4×4, 6×6, 8×8, 10×10, 12×12. The other regards an asymmetric deployment of antennas, since a BS is always associated to a greater number of antennas, which is obvious, because it has dimensions larger than any MT, for this case, five different combinations of antennas have been researched: 4×2, 8×2, 8×4, 16×2, 16×4. The asymmetric case has been analysed for two wireless systems: UMTS and HIPERLAN/2.

In the symmetric case, an increase in the number antennas generates a growth of capacity, which was predictable. A large number of antennas leads to a larger number of independent subchannels which is related to the gain of MIMO systems. The increase depends on the scenario where a MIMO system is applied. The best results are obtained in the city street and the railway station scenarios. Smaller sets of antennas are better for the city street scenario. For the 2×2 MIMO system, the city street scenario achieves 5.6 b/s/Hz, whereas the railway station scenario has 5.3 b/s/Hz. However, for the largest set the situation is reversed, and the smallest scenario gives the best gain of capacity, 22.0 b/s/Hz comparing to 20.7 b/s/Hz for the city street scenario. This phenomenon is caused by fact that in the railway station scenario there is a constant increase of capacity, and adding two extra antennas to the present set gives almost the same growth of the capacity, approximately 3 b/s/Hz. In the city street scenario, capacity drops with the number of antennas, this shows that receivers with a significant number of antennas in the railway station scenario make sense.

The highway scenario is a distinct case, because results are significant smaller comparing to the previous scenarios. For the 2×2 MIMO system, capacity equals 4.6 b/s/Hz, whereas for MIMO 12×12 one has 12.8 b/s/Hz. The difference is especially high for the largest set of antennas and equals 38% for the railway station scenario. The increase of capacity is not constant and goes down with a growing number of antennas, so that the situation is analogous to the city street scenario.

Capacity is regulated by the correlation of the radio channel, which shows a similarity between CIRs of all pairs of input and output antennas and defines the gain of the radio channel. The highway scenario has the most correlated radio channel, which is related to the smaller number of clusters and the larger dimension of the scattering region. The level of correlation in the city street and the railway station scenarios is similar, which is why results are almost the same.

If non equal numbers of antennas for the receiver and transmitter is considered, capacity is mainly regulated by the dimension of the receive antennas set. However, the number of transmit antennas has some impact on capacity. There is only one limitation, i.e., the number of transmit antennas must be smaller than the number of receive ones which is case for UL. This situation is more favourable, because a BS is associated to larger number of antennas, so the receiving side is dominant regarding the number of antennas. For the DL case, when the number of input antennas is smaller than the output one, a strong dependence on the receive side is observed. Even a substantial growth of transmit antennas brings an insignificant increase of capacity. If

MIMO systems 4×2 and 16×2 are considered, a four-time increase on the number of input antennas gives only a 5% gain of capacity. For systems where a DL is dominant, this is a strong constraint.

Two systems, UMTS and HIPERLAN/2, have been compared, which have different carrier frequencies and bandwidths. Results achieved for the same scenarios and with the same number of antennas for both sides of the radio link are almost the same. Differences are insignificant, because the distance between antennas was established as λ for both systems. Of course, the distance in a metric scale is different, but it has no influence on the results. The bandwidth does not influence capacity.

The impact of mutual position of a BS and a MT has been analysed as well. MIMO antennas are deployed on a line, so that the mutual relationship between lines related with both MT and BS influences capacity.

In the railway station scenario, a rotation of both the MT and the BS has insignificant influence on capacity. Only a small deviation of capacity is observed, which is obvious, because scatterers are deployed around both MT and BS, so, change of antennas orientation does not change the fact that the scatterer are still around. A high deviation of capacity in a real condition can be observed only in a situation, when an even distribution of clusters is disturbed in a circular scattering region. In the case of non omnidirectional antennas, a change of orientation does not influence capacity. The change selects only multipath components which are either amplified or smooth, but if an even distribution of clusters is considered, after the average the result is the same. This feature is a substantial advantage of the railway station scenario.

For the city street scenario, where scatterers are mainly placed between the MT and the BS, a change of orientation has a considerable influence on capacity. This influence is similar for both MT and BS, because this scenario has a symmetric characteristic. Positions of both BS and MT are placed in symmetric points of the scattering region. Neither the BS nor the MT is privileged, because they are in the same situation relative to the deployment of the clusters. The worst case is when the lines of the antennas deployment are perpendicular. In these circumstances, the radio channel is the most correlated one. The difference between minimum and maximum capacity equals almost 22%. The deployment of clusters mainly between a transmitter and a receiver is a source of serious consequences. In case the minimum of the radiation pattern of the antennas is directed into the region, where clusters are mainly deployed, a significant part of the

power of the signal is lost, which surely influences capacity. So, correct orientations of antennas are especially important in the city street scenario, or the used antennas must be almost omnidirectional, which reduces the consequences of a wrong orientation of antennas.

The analysis of the highway scenario has given different results for the MT and the BS. A change of orientation of the MT does not influence capacity, which is similar to the railway station scenario. The MT is inside a circular scattering region and the change of the orientation can be neglected. The use of non omnidirectional antennas has a great impact on capacity which is related to with the small number of clusters. If a maximum of the radiation pattern is directed into a space where no cluster exists, there is a total outage, but if results are derived by using a large number of simulations, this can be neglected. A change of orientation of the BS reduces capacity, when antennas deployment lines are perpendicular, so this situation is similar to the city street scenario. The change of orientation generates a 16% loss relative to the maximum value.

The increase of the spacing between antennas has a similar influence in all considered scenarios: when antennas are more separated, capacity is larger. The most intensive increase is for a spacing below λ. This phenomenon is especially visible for the city street scenario, because for the railway station one the curve presents a few local extremes but the tendency is kept. For the highway scenario case, the different between an increase of capacity in the range below λ spacing and above is the smallest among all scenarios. The increase is almost linear and mainly defined by the distance between the antennas of the BS. Change of spacing for an MT has no impact on capacity. This tendency is good, because the size of the MT can be reduced, but for the BS it is not so important and can be enlarged.

The above consideration shows that a λ spacing seems to be optimal. A too large distance between antennas enlarges the dimensions of the equipment, which is especially important for an MT, because it is related with the main feature of it, i.e., mobility.

The number of MIMO antennas and the spacing between them are factors that regulate capacity of the system. Both of them influence the dimension of equipment. After comparing results, the increase of the number antennas always has a greater impact on capacity.

If all scenarios are compared, taking all analysed parameters into consideration, the scenario with the best results can be chosen. Comparing only the number of antennas, the city street and

the railway station scenarios give almost the same results. The spacing between antennas also influences capacity in more or less the same way. However, if the change of antennas orientation is taken into consideration, a significant advantage of the railway station scenario can be noticed. The capacity of the railway station scenario does not depend on a mutual position of the BS and the MT. This is very important in mobile systems, where MTs are always in motion. For the highway scenario, using a MIMO system is also sensitive. In each scenario, some gain of the capacity is observed, but in the highway scenario it is the smallest one. The use of MIMO systems makes sense everywhere, because the achieved capacity is greater than the one for SISO systems.

In this work, a MIMO system has been researched regarding three parameters related with the configuration of antenna sets. The research can be expanded by some aspects.

All simulation have been made for omnidirectional antennas hence, it seems adequate to use other antennas patterns. Especially, patterns of real MTs or BSs should be used, which is possible, because the simulator has the ability to define an antenna pattern by an appropriate file. Non omnidirectional antennas should have influence in some cases, especially related with a rotation of antenna sets.

Another interesting feature of the simulator, which can be used for MIMO system research, is that antennas can be defined as arrays.

The impact of different values of signal to noise ratio has not been studied in this work, and the sensitive of the receiver has not been analysed as well. A research showing the dependence of capacity on these parameters should bring interesting results.

The considerations carried out in this work do not consider the mutual coupling between antennas. If a spacing between antennas is large enough, the mutual coupling has a small influence on capacity, however, for small distances between antennas, a disturbance should be observed and the profile for various distances will be changed.

Considering the radio channel model, in future work, some improvements can be done in order to approach the model to real conditions. The propagation environment can be established in a 3D space. A mechanism of multiple bounces can also be considered which seems to be closer to reality, because this type of multipath components, changed by a few bounces, is frequent.

Also some enhancements can be done to improve the functionality of the simulator, related to both capabilities, and the way of it operates.

The simulator places antennas along a line. This solution is only good for a system with a small number of antennas. It is not appropriate for MTs, where a number larger than 8 can not be distributed along a line, because it occupies too much space. So, the simulator should be able to distribute antennas on a 2D plane.

New types of scenarios can be implemented in the simulator. So far, three are supported by the simulator. Circular and elliptical scenarios are considered in the present realisation of the simulator, but, an upgrade of the simulator to rectangle scenarios seems adequate.

To increase the randomness of the radio channel a varying phase of the reflection coefficient can be implemented. Depending on the amount of phase deviation, an increase of capacity will be observed. The research related with this phenomenon can be found in [Fern04].

The simulator is controlled by a config file. Parameters for simulation are defined by single values, so that any research related with variation of parameters loads to a huge number of config files. This process is quite complicated and laborious. The possibility to change any parameter in a defined range is the solution to this problem.

Annex A. Assessments

In order to the simulator, the example presented in Figure A.1 was simulated. In this case, the environment has only one scatterer, the BS and the MT. In this example UL is considered, thus, the MT works as the Tx and the BS as the Rx.

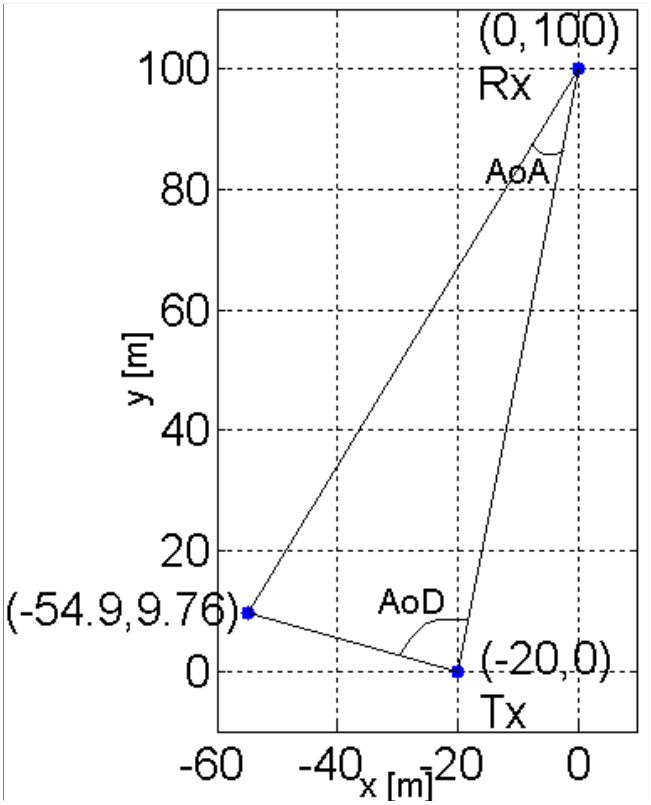

Figure A.1– Example of calculations

The positions of the objects are depicted in Figure A.1. Other parameters of this example are:

- $|\Gamma| \cdot e^{j\Phi_{sc}} = 0.154 \cdot e^{j51.06}$: reflection coefficient of the scatterer
- $f = 1.87$ GHz: frequency

In Table A.1 two files are listed, which describe the positions and functions of the terminals, as well as the parameters of the scatterer.

The program returns the results that are listed in Table A.2. These parameters are obtained using the equations presented in Chapter 2. The AoA and AoD for the LoS component are obtained relative to the *x*-axis on the *x*-*y* plane. The entirely NLoS parameters are presented in a non normalised form.

Table A.1 – Files describing the environment of the test scenario.

File with the terminals:	p,1,1.87e+009 t,0,1 o,-20,0,0,10,MT1,0 a,0,1,180 m,1 n,a1,0,0 e o,0,100,0,0,BS1,1 a,0,1,180 m,1 n,a1,0,0 e
File with the scatterers:	c0,-54.9,9.76,1,0,1 s0,-54.9,9.76,0.154,51.06

After making the calculations, it was confirmed that the program works correctly.

Table A.2 – Output parameters.

	LoS	NLoS
Amplitude [mV/m]	169.84	18.80
Phase [deg]	42.42	278.88
Delay [ns]	340.17	133.04
AoA [deg]	258.69	20.01
AoD [deg]	78.69	85.68

The other tests involved the correct generation of the deployment of clusters within the region, and scatterers within clusters. The clusters within the region should be distributed uniformly, to check this aspect, a circular region with a radius of 100 m was generated and inside of it, 94 clusters were deployed. A mean value of coordinates of all clusters was calculated: $(\bar{x}, \bar{y})$ = (1.91534 m, 1.50414 m). Every coordinate can change in the range [-100, 100], thus, an ideal mean coordinates should be (0 m, 0 m). The results have an error (1.92 %, 1.5%) are acceptable to confirm that clusters are distributed uniformly.

Similar tests were made for the distribution of scatterers. A cluster with a radius of 5 m was generated. Within these clusters, 500 scatterers were generated using the Gaussian distribution, with the centre of the cluster being (0 m, 0 m) also for this case the mean value of the coordinates was calculated ($-12.222 \cdot 10^{-3}$ m, $-3.332 \cdot 10^{-3}$ m), which are acceptable.

Also other tests were made. The cluster was divided into symmetric parts, upper and lower sides, and right and left sides. Within all these quarters, the scatterers were counted, and the results are presented in Table A.3. The deployment of scatterers is not ideal symmetric and one can see some disproportion between the upper and lower sides, the amount of scatterers being different (4.8%). But one should not forget that the distribution of scatterers is generated by using a statistical distribution, and this level of disproportion for such a low number of samples is typical. The function generating the deployment of scatterers is affirmed to be correct.

Table A.3 – The scatterers within the cluster.

Side	No. of scatterers	Error [%]
Up	238	4.8
Down	262	
Right	256	2.4
Left	244	

Finally, the function generating the Channel Impulse Response was checked. This function divides time into bins, and sums coherently all components that are inside the bin. The delay of the ray after sum is determined as the middle of the bin. Some multipath components were generated, Table A.4.

Time was divided into 1 ns bins. The operation of summing can be considered on the complex plane. The results, which were confirmed by external calculations, are presented in Table A.5.

Some other tests connected with the CIR where done as well. Every scenario has a maximum time delay, due to the fact that locations of clusters are bounded by the region. For every scenario, one can use an equation that calculates the maximum time delay relative to the LoS component. For the pico- and the macro-cell scenarios (A.1) can be used, while for the micro-cell scenario (A.2) is used.

Table A.4 – Multipath components – example of calculations.

No.	Amplitude [V/m]	Phase [deg]	Delay [ns]
1	1	0	5.1
2	1	90	5.9
3	1	90	6.1
4	1	180	6.9
5	1	180	7.1
6	1	270	7.9
7	1	270	8.1
8	1	0	8.9

Table A.5 – The rays of the CIR.

No.	Amplitude [V/m]	Phase [deg]	Delay [ns]
1	1.41	45	5.5
2	1.41	135	6.5
3	1.41	225	7.5
4	1.41	315	8.5

$$\tau_{\max} = \frac{2R}{c} \tag{A.1}$$

$$\tau_{\max} = \frac{2\sqrt{b_{ell}{}^2 + f_{ell}{}^2} - 2f_{ell}}{c} \tag{A.2}$$

where:

- $f_{el[\mathrm{m}]}$: focal length of the ellipse
- $b_{ell[\mathrm{m}]}$: minor axis of the ellipse
- $R_{[\mathrm{m}]}$: radius of the circle

These three types of regions were generated, and every region was defined in the same way:

- Cluster density: 10^{-3} per 1 m^2
- Dimension:

    - 50 m – radius of the circle in the pico-cell scenario
    - 100 m – minor axis of the ellipse in the micro-cell scenario
    - 200 m – radius of the circle in the macro-cell scenario
- Cluster radius: 1 m – this is the standard deviation for the Gaussian distribution
- Average Number of the scatterers: 20 per cluster
- Positions of the BS and the MT:
    - (0, 0) and (10,10): pico-cell scenario
    - (0, 0) and (200,0): micro-cell scenario
    - (0, 1000) and (0,0): macro-cell scenario

The values of the maximum time delay (normalised to the delay of the LoS component) that are obtained from the simulation and that are calculated using (A.1) and (A.2), are presented in Table A.6.

Table A.6 – Maximum time delay [ns].

Cell	Values calculated	Values simulated
Pico-cell	333.3	341.5
Micro-cell	276.1	277.4
Macro-cell	1333.3	1297.1

One can see that the values obtained from simulations are larger than the calculated ones. This is caused by the assumption that only the centres of the clusters have to be inside of the region. When the cluster is located near the boundary of the region, it is very possible that some scatterers are placed outside, and these outside scatterers are the source of the increase of the maximum time delay.

One can then say that the simulator passed all the tests hence, it is considered to work properly.

Annex B. MIMO Assessments

This annex is contains the assessments from Section 4.3.4, where the simulator for MIMO is checked. In Figure B.1 the multipath components generated by the nearest scatterer are shown. The larger delay, related to the positions of antennas, generates the smaller amplitude The multipath component with the smallest delay corresponds to input and output antennas that are placed near the scatterer. A small shift between antennas has influence on parameters, such as delay, amplitude and phase. The difference between parameters for multipath components related to a scatterer is small, and any decorrelation between radio links does not exist. Nevertheless, a single cluster is associated to approximately 20 scatterers, which implies that the some decorrelation is obtained.

In Figure B.2 a comparison of LoS components is presented; two groups of LoS components can be observed. One is corresponds to links between antennas that are in front of each other, so that the distance is the smallest; another one is associated with radio links that are crossed to each other. The components of the latter have longer distances, so they have greater delays and smaller amplitudes.

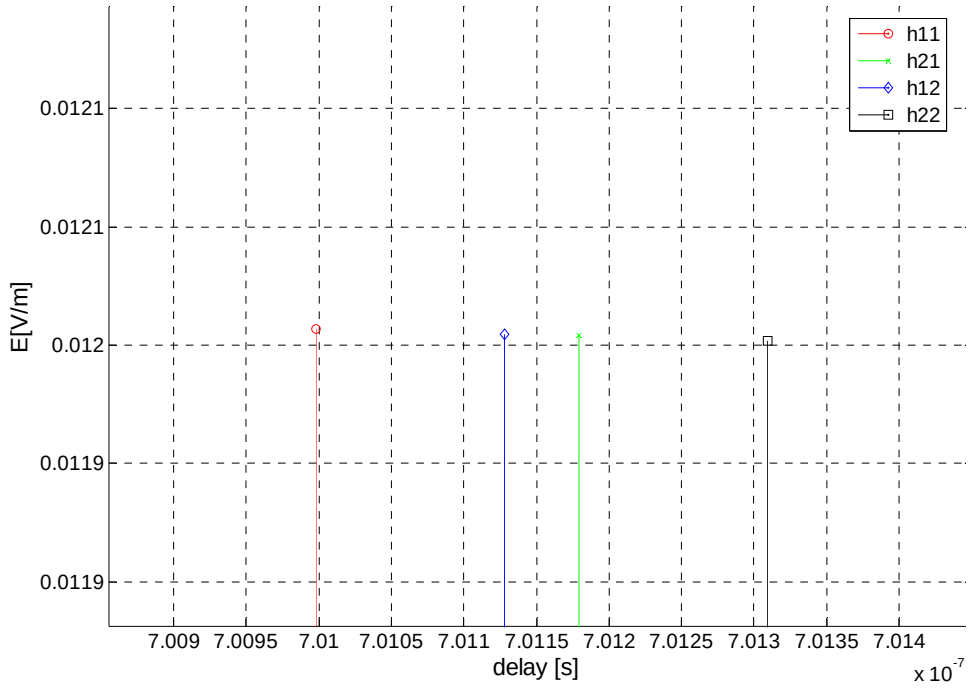

Figure B.1 – Zoom of the CIRs for different links.

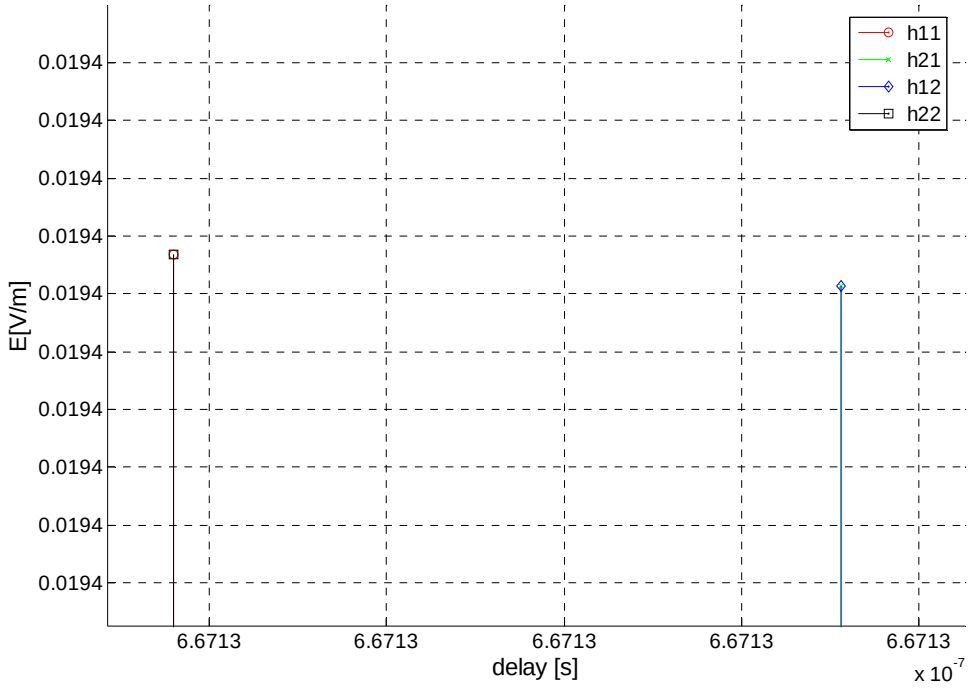

Figure B.2 – Zoom of the LoS for different links.

Annex C. Random numbers generators

Further tests were made to ensure that the simulator is working in the correct way. These tests involved checking the randomise functions. Histograms were prepared using 1 000 000 samples, which generated pseudo-random values in Gaussian, Poisson and Uniform distributions. Every histogram is similar to theoretical ones.

Figure C.1 concerns the Gaussian distribution.

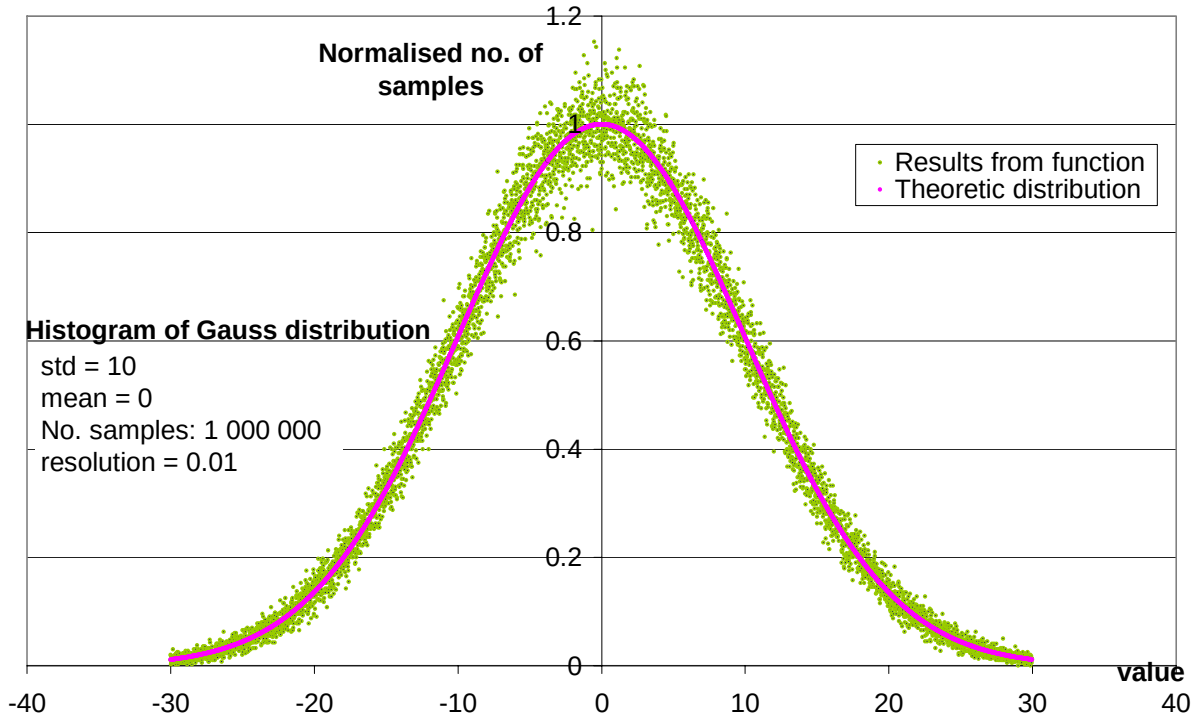

Figure C.1 – The histogram of Gaussian distribution.

The Gaussian distribution is described [Math05] by:

$$f(x) = \frac{\exp\left(-\frac{(x-\mu_G)^2}{2\sigma_G^2}\right)}{\sigma_G\sqrt{2\pi}} \qquad \text{(C.1)}$$

where:

- μ_G: mean value
- σ_G: standard deviation

The histogram was obtained with the following parameters:

$\mu_G = 0$

$\sigma_G = 10$

Both the shape of the histogram and the shape of the theoretical curve are the same, so one can consider that the function works correctly.

Random numbers with a Poisson distribution are generated using a separate function, Figure C.2. The histogram is normalised to the number of times λ_P (parameter of Poisson distribution) occurs. The theoretical Poisson distribution, which is described [Math05] by:

$$f(x) = \exp(-\lambda_P)\left(\frac{\lambda_P^x}{x!}\right) \qquad \text{(C.2)}$$

where:

- λ_P: parameter of Poisson distribution, in this example $\lambda_P = 10$

The results, which are obtained from this function and from the theoretical equation are the same.

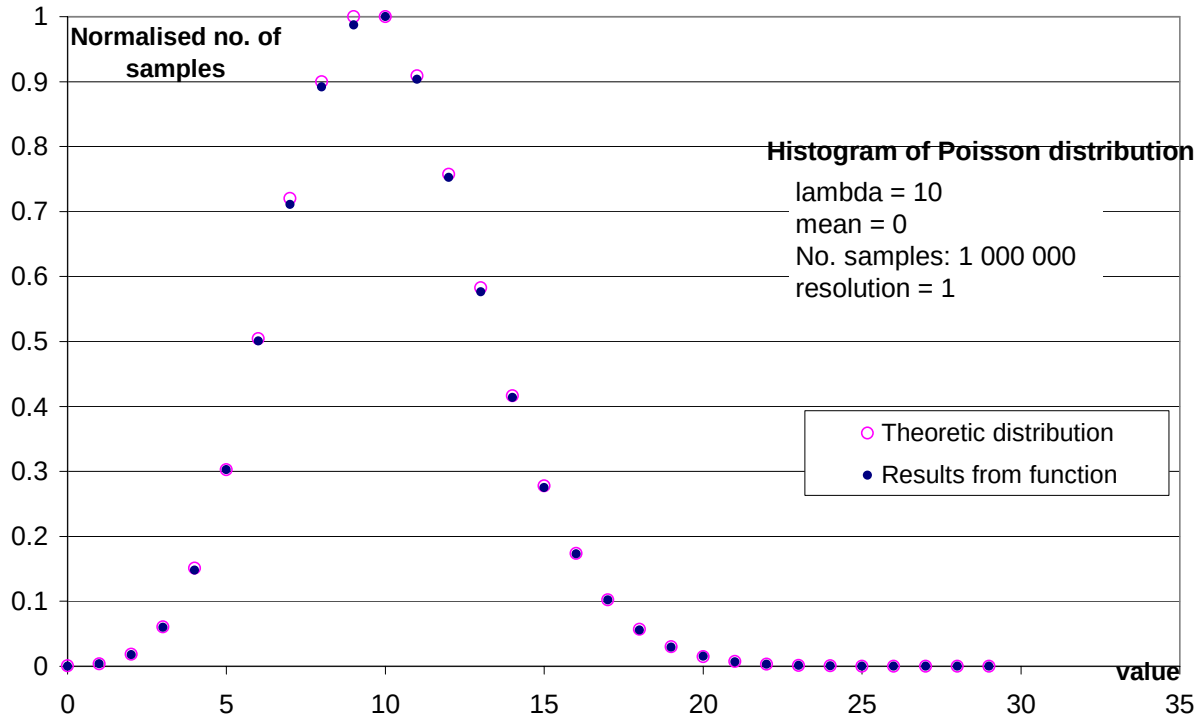

Figure C.2 – The histogram of Poisson distribution.

Figure C.3 contains the histogram associated to the uniform distribution, normalized to the average number of times all values occur. The shape of this histogram is uniform for all values, which shows that the function works correctly.

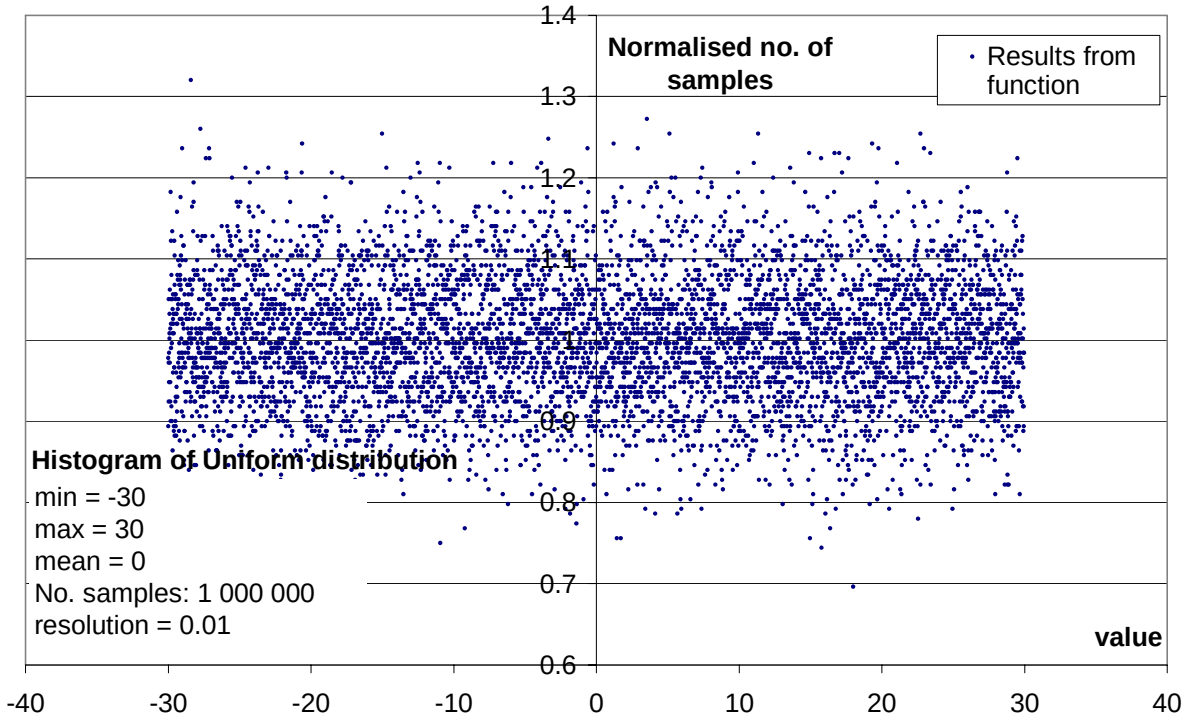

Figure C.3 – The histogram of uniform distribution.

Annex D. Influence of number of clusters and scatterers

Some simulations were made to check the influence of the density and the deployment of scatterers in the propagation environment on capacity. Two different types of simulations were considered: with a constant average number of scatterers per cluster, and with a constant number of clusters in the environment but various average numbers of scatterers. For the former, the number of scatterers was fixed as 10 and the number of the clusters was in the range {1, 39}. The latter were made with the number of the clusters fixed as 7 and the average number of the scatterers in the range {2, 40}. To simulate the above cases, three modes of the simulator were used: mode 0, mode 1, and mode 3. The description of the simulator modes is in Subsection 4.2.3. For specific conditions, 100 simulations were made, and after that statistic parameters were calculated. Three scenarios were considered: city street, railway station and highway. Full details about the scenarios are presented in Table D.1.

For this kind of simulations, mode 3 is the best, since average results are the most stable. The drawback of the mentioned mode is fact that the standard deviation (std) is the biggest. For every type of simulations, the values of std for mode 3 are higher than for mode 0 and mode 1, of course, if whole propagation environment is changed from one to another simulation, this is natural (all scatterers are new). In mode 3, for each simulation, the realisation of channel is different, but in agreement with the assumption for the considered scenario. Hence, only mode 3 will be used.

For all scenarios, if the number of clusters varies, capacity goes up with the growing number of clusters, Figure D.1, Figure D.5, and Figure D.9. The main difference is the amount of increase of capacity (4.3 b/s/Hz for the railway station, 3.3 b/s/Hz for the city street,and 1.8 b/s/Hz for the highway). For the railway station, there is the largest difference between the capacity for the smallest number of clusters and for largest one. The highway scenario has the smallest one. The figures with std for the mentioned relations are shown in Figure D.3, Figure D.7 and Figure D.11.

The smallest difference between the spacing for MIMO antennas and the distance dividing the BS and the MT occurs in the railway station scenario, thus, spacing between antennas makes a difference in the delays corresponding to adjacent receive antennas, which is significant relative to the full delay between transmitter and receiver. Additionally, the magnitudes of rays taht

come from the same scatterer have the greatest difference. In that case, every extra cluster of scatterers increases the decorrelation of the radio channel, leading to an increase of capacity.

Table D.1 - Environment for the research of influence of a number of scatterers and a number of clusters.

		City street scenario	Railway station scenario	Highway scenario
Scattering Environment	BS to MT distance [m]	200	20	2000
	Dimension of scenario [m]	b=80	R=50	R=200
	Number of clusters	7	7	7
	Average number of scatterers	10	10	10
	Std of the scatterers within clusters [m]	1	1	1
MIMO System	$n_R \times n_T$	4×4	4×4	4×4
	d_m [λ]	1	1	1
System Parameters	f(bandwidth) [GHz(MHz)]	2(5)	2(5)	2(5)
	P	10	10	10
	Mobility	Not considered	Not considered	Not considered
	Delay resolution [ns]	200	200	200
	Number of Channel Realisation	100	100	100

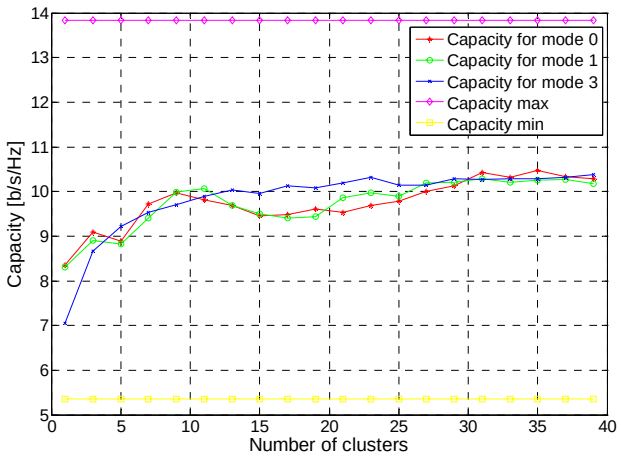

Figure D.1 – Capacity for different number of clusters for the city street scenario.

The next feature, which is common to all scenarios in fact, is that the biggest increase of capacity is for number of clusters, which is below a typical value for each scenario, e.g., 5 for the highway scenario, 7 for the city street, and 15 for the railway station. After reaching this point, the channel is "satured", and extra clusters have a small influence in capacity, because the

increase of decorrelation of the radio channel is more or less the same level. The std for the mentioned relations are depicted in Figure D.4, Figure D.8 and Figure D.12.

If the average number of scatterer is above 5, capacity is not related with it, which is depicted in Figure D.2, Figure D.6 and Figure D.10. Only for the railway station, a small increase can be observed. For the city street and especially for the highway, single scatterers are not distinguished, since scatterers tied to any clusters are deployed inside a circle with 1 m radius. For the railway station, which dimension is only one range more, they can be distinguished, but generally, scatterers related to a cluster generate multipath components with more or less the same delay and amplitude. Thus, extra scatterers do not make large difference between CIRs for pairs of input and output antennas. In these conditions, the decorrelation of the channel is invariable.

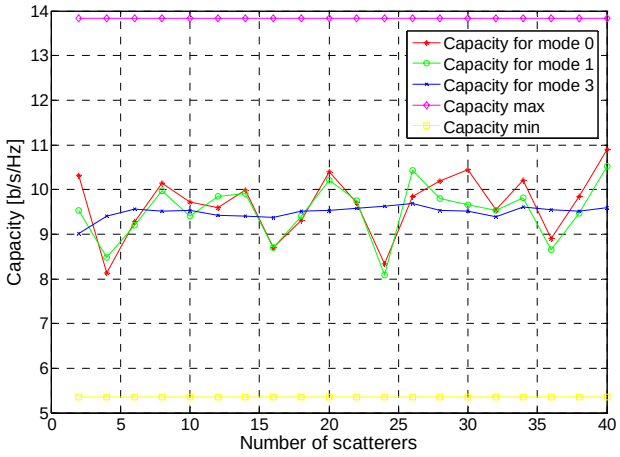

Figure D.2 – Capacity for different number of scatterers for the city street scenario.

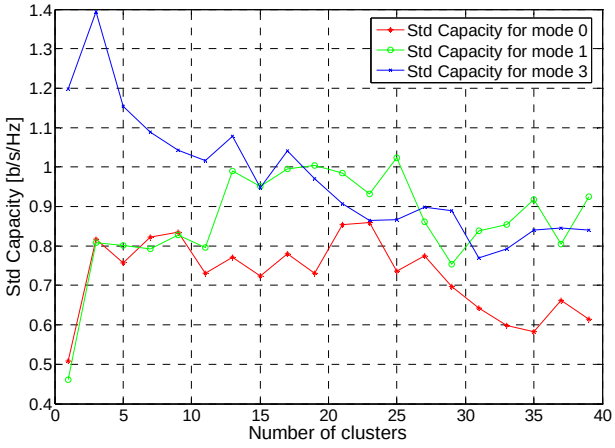

Figure D.3 – Std Capacity for different number of clusters for the city street scenario.

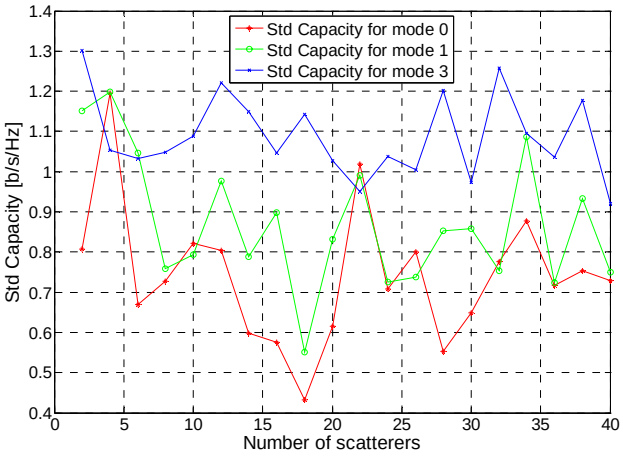

Figure D.4 – Std Capacity for different number of scatterers for the city street scenario.

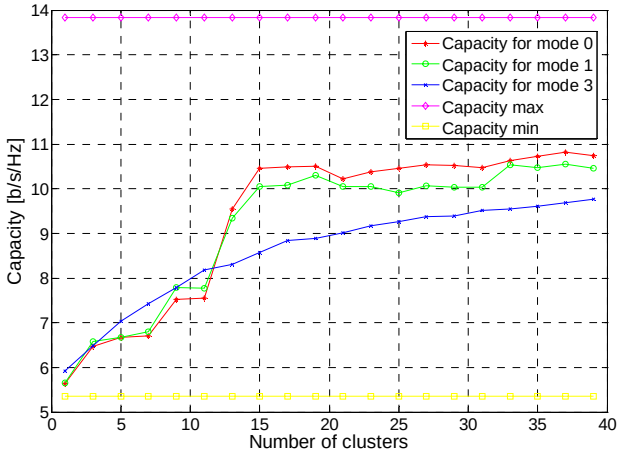

Figure D.5 – Capacity for different number of clusters for the railway station scenario.

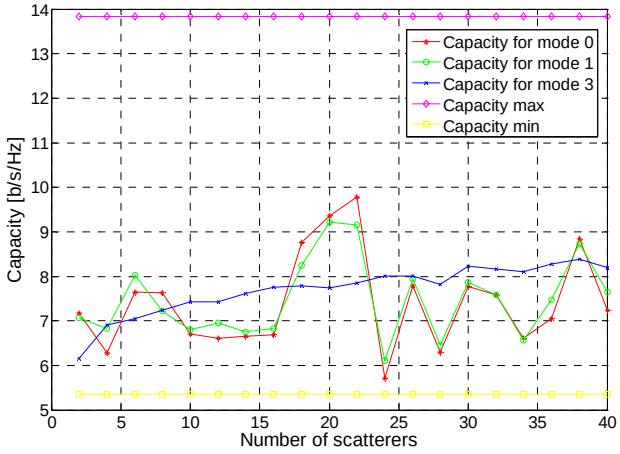

Figure D.6 – Capacity for different number of scatterers for the railway station scenario.

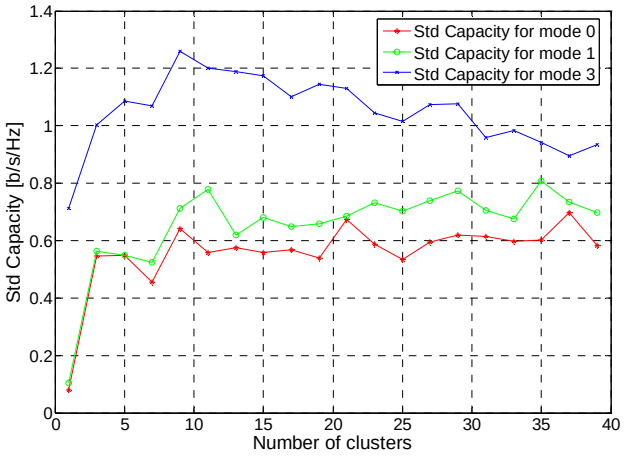

Figure D.7 – Std Capacity for different number of clusters for the railway station scenario.

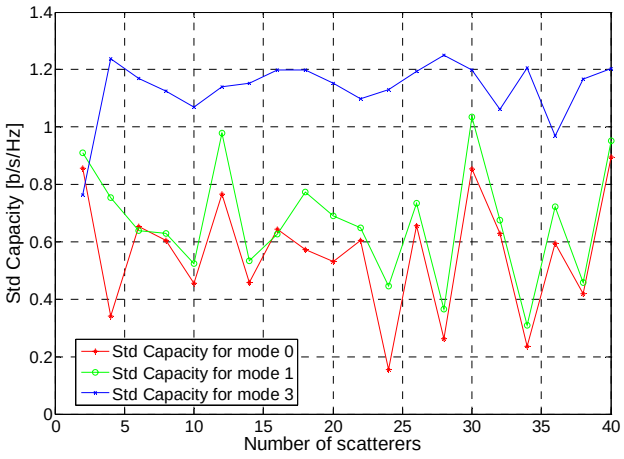

Figure D.8 – Std Capacity for different number of scatterers for the railway station scenario.

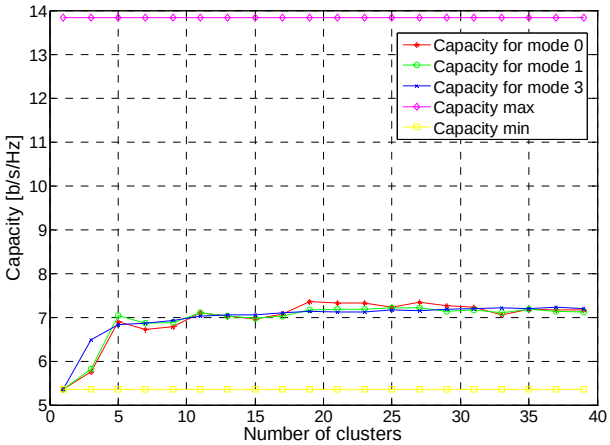

Figure D.9 – Capacity for different number of clusters for the highway scenario.

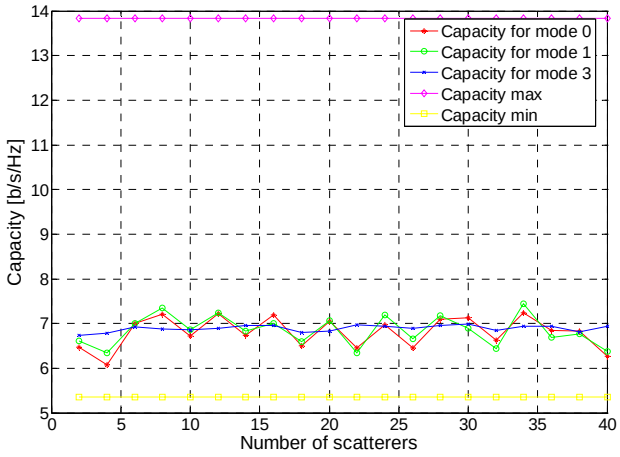

Figure D.10 – Capacity for different number of scatterers for the highway scenario.

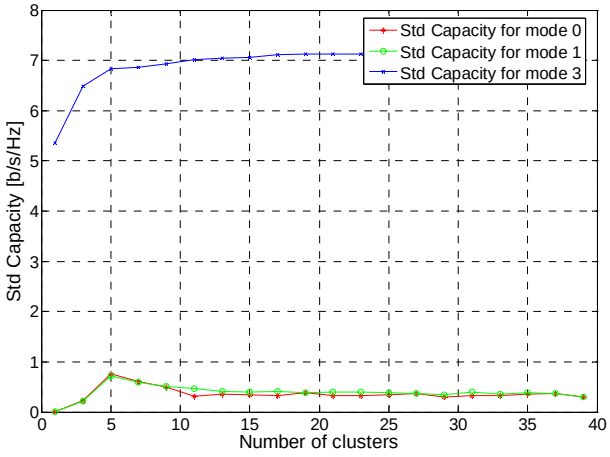

Figure D.11 – Std Capacity for different number of clusters for the highway scenario.

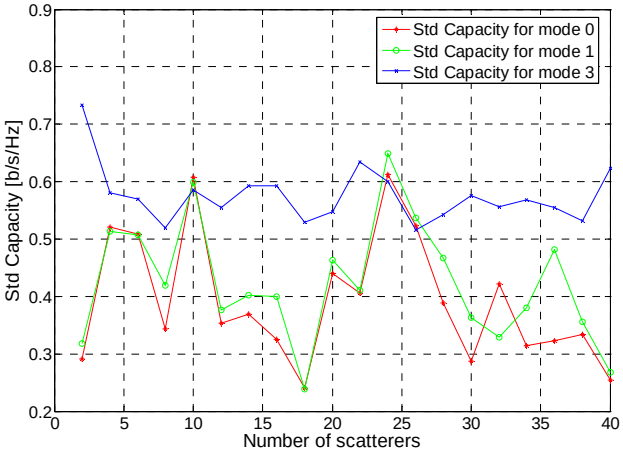

Figure D.12 – Std Capacity for different number of scatterers for the highway scenario.

Annex E. CIR and PDAP for the used scenarios

The present annex includes the CIRs and the Power Delay Angle Profiles (PDAPs) for the considered scenarios. The observation of the profiles is only necessary to recognise the scenarios, because each one has special characteristics. All these differences have an impact on the achieved capacities.

In the graphs, the amplitude is presented with reference to the LoS component, which has the biggest amplitude equal to 1. Also the delay is compared to the LoS component which has the delay equal to 0. For the highway scenario, which has no real LoS component, the same calculations are made using the artificial LoS, which is extracted as it would exist.

In the graphs with PDAP, only AoA is shown, and only the uplink is considered, so only angles for a BS are shown. The graphs are divided on three time zones, and 5^0-resolution angle is used.

In Figure E.1, the CIRs between all input and output antennas for the MIMO 2×2 city street scenario are presented The CIRs are very similar, but small differences can be found, which are caused by the λ-shit between antennas. The CIRs can be divided into a few parts, since scatterers are grouped in clusters. The city street scenario has 7 clusters, but it is impossible to recognise 7 groups impulses, because some of the clusters are at the same distance from the receiver and transmitter, hence, they superimpose one another and make one group of rays. In every group of scatterers, the level of particular multipath components is strongly diverse. The amplitude of each multipath component is regulated by the distance and also by a magnitude of a reflection coefficient. If the components with the maximum level are considered, it can be said that there is a small difference between the level of the LoS component and the highest multipath components. It is caused by fact that the scatterers are placed inside the ellipse, and the difference in the distance between the LoS component and any different ray is small.

The time parameters for the city street scenario can be seen in Table E.1. The mean excess delay is the smallest comparing the other cells which only confirms the smallest difference between the LoS and the rest of the taps. The RMS delay shows that the power of the signal is spread evenly along the CIR. Even the last taps give power comparable to the first ones. From a practical point of view, inter-symbol interferences appear here with the highest probability.

The PDAPs for the city street scenario are depicted in Figure E.2. All multipath components are focused around the LoS one. The range depends on the effective width of the ellipse which

indicates where the scatterers are located. For this scenario, scatterers are mainly between the receiver and transmitter. The mentioned range is limited between -30^0 and 30^0 with reference to LoS.

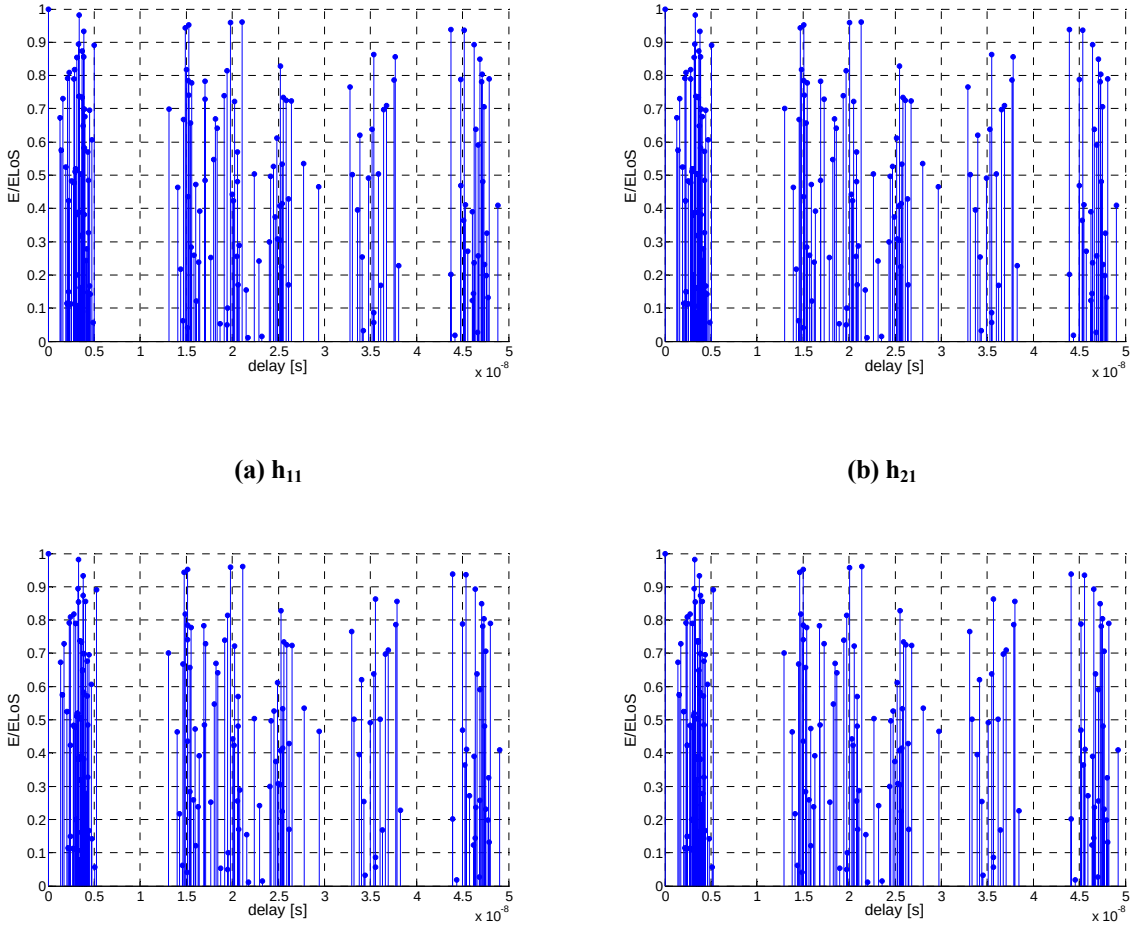

(a) h_{11} **(b) h_{21}**

(c) h_{12} **(d) h_{22}**

Figure E.1 – CIRs for MIMO 2×2 for the city street scenario.

The CIRs for the railway station scenario are depicted in Figure E.3. The LoS component is significant by higher than the rest of the multipath components. The difference in distance, which rays must cover between transmitter and receiver, is significant between the LoS component and the rest of the taps. AoA and AoD are the largest for the present scenario, which comes from the mentioned difference in the distance. This phenomenon is only characteristic of the railway station scenario and is not observed in the other cases.

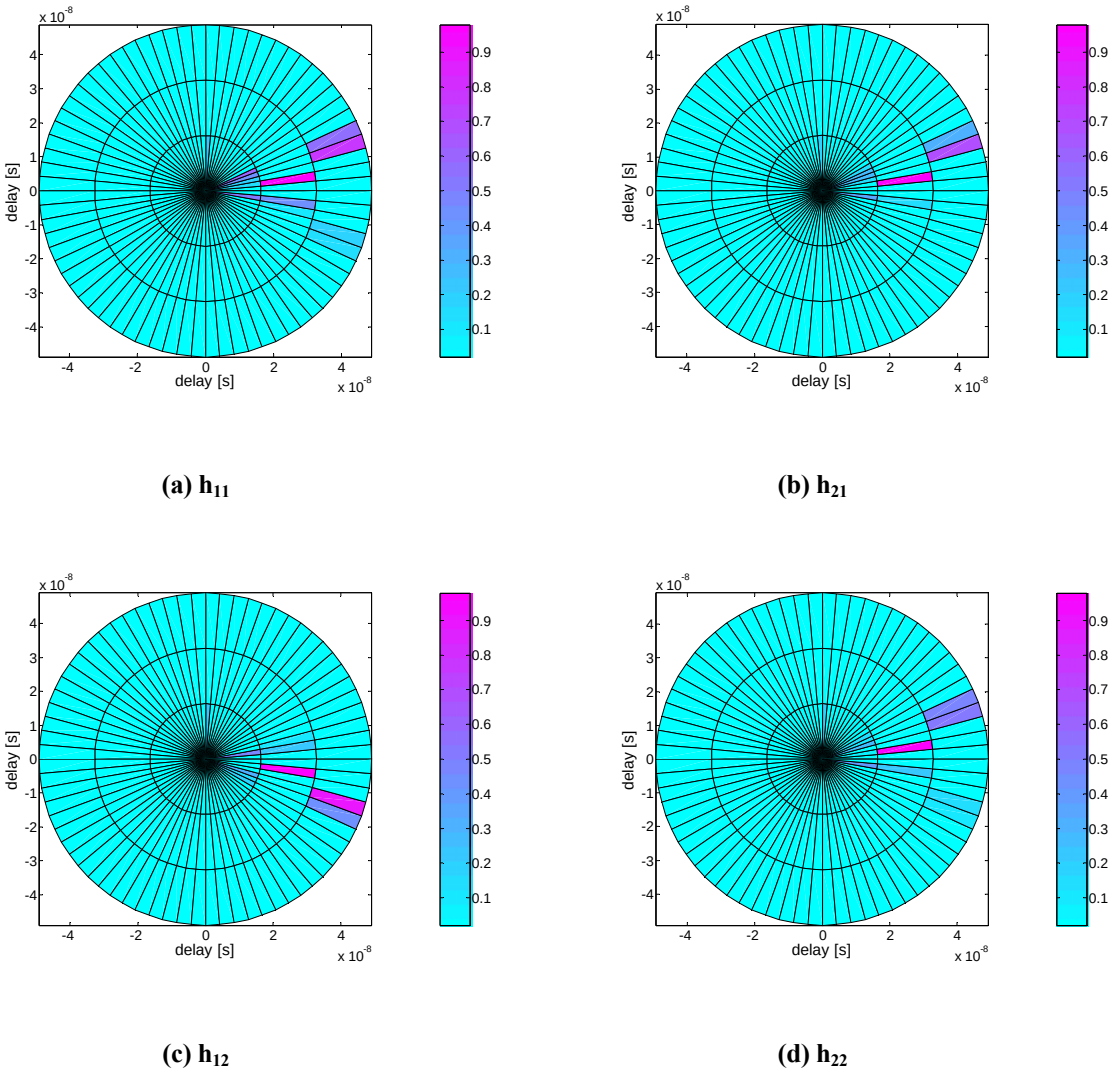

(a) h_{11} **(b) h_{21}**

(c) h_{12} **(d) h_{22}**

Figure E.2 – PDAP for MIMO 2×2 for the city street scenario.

Also here, it is impossible to recognise single clusters. Scatterers are grouped, but figuring out 15 clusters is not possible. The groups of scatterers are wider, because the radius of a cluster is comparable to the distance between clusters. As a consequence, the CIR for the railway station scenario is strongly spread.

The BS in the railway station scenario receives rays from all directions, Figure E.4. Scatters are placed around the BS, so power is distributed around.

The analysis of the parameters from Table E.1 shows that the main power is brought by multipath components that are at the beginning of the CIRs. The last taps are strongly faded.

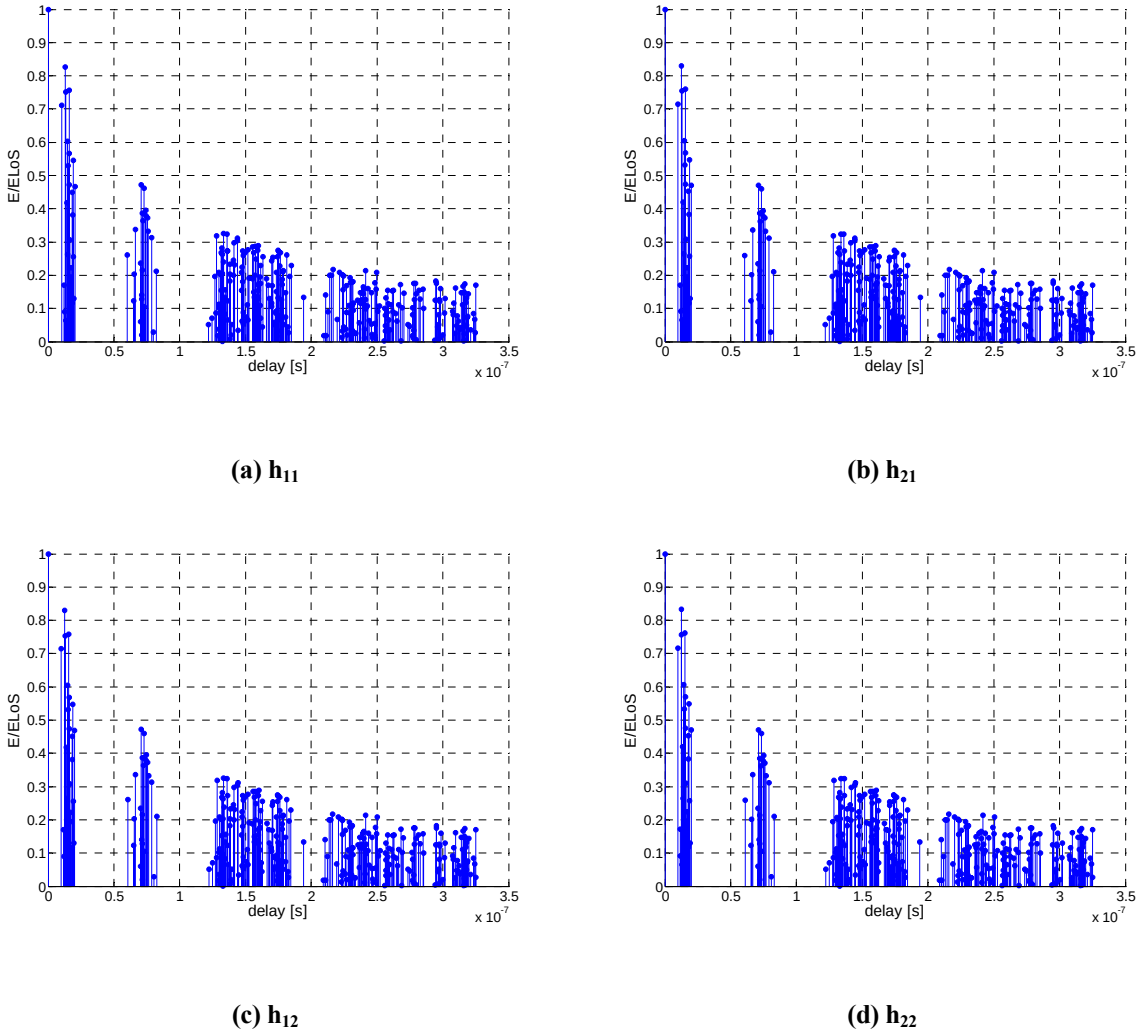

(a) h_{11} **(b) h_{21}**

(c) h_{12} **(d) h_{22}**

Figure E.3 – CIRs for 2×2 for the railway station scenario.

In the highway scenario there are 5 clusters. After analysing Figure E.5, all 5 clusters can be indicated. Clusters are deployed on a huge area, so there is enough separation The CIRs show in an easy way, how many clusters are in the scenario. However it is not possible to recognise single scatterers, because delays in the highway scenario are the biggest among all scenarios. The accuracy of the time axis is not enough to extract single scatterers. The highway scenario does not have a LoS component, so the taps with highest amplitudes appears not only at the beginning of the time axis.

All taps in the highway scenario are tightly focused around the artificial LoS component, in the range between -10^0 and 10^0. The distance between the BS and MT is significant bigger than the radius of the scattering region around the MT. After the analysis of PDAP, Figure E.6, only the position of the MT can be shown, with a low accuracy.

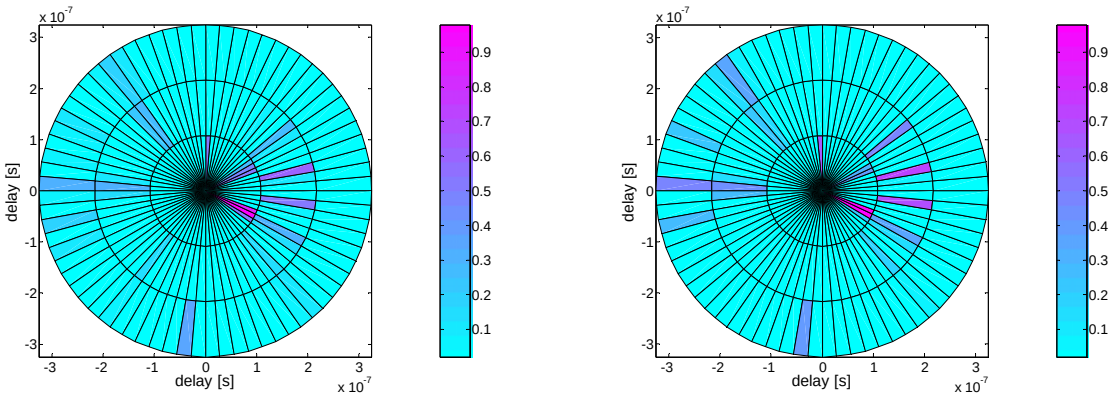

(a) h_{11} **(b) h_{21}**

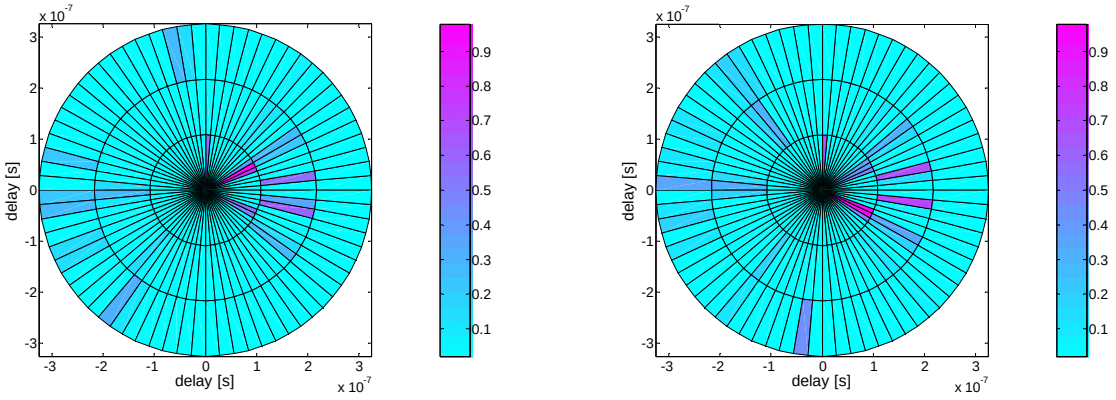

(c) h_{12} **(d) h_{22}**

Figure E.4 – PDAP for MIMO 2×2 for the railway station scenario.

Table E.1 – Time parameters for the considered scenarios.

		Highway scenario	City street scenario	Railway station scenario
$\bar{\tau}$ [ns]	h_{11}	532.6	20.1	96.9
	h_{12}	532.5	20.2	96.6
	h_{21}	532.6	20.2	96.7
	h_{22}	532.5	20.2	96.4
σ_τ[ns]	h_{11}	358.7	15.7	89.7
	h_{12}	358.8	15.8	89.8
	h_{21}	358.7	15.7	89.8
	h_{22}	358.8	15.8	89.9

In this scenario case, the delays are the longest, as predictable, because the scattering region is the biggest. For this scenario, the CIRs for the links with the same transmit antennas make pairs that are more similar. From the point of view of a transmit antenna in the MT, two different antennas in the BS are the same point, because the spacing between antennas is not comparable to the distance between the MT and the BS.

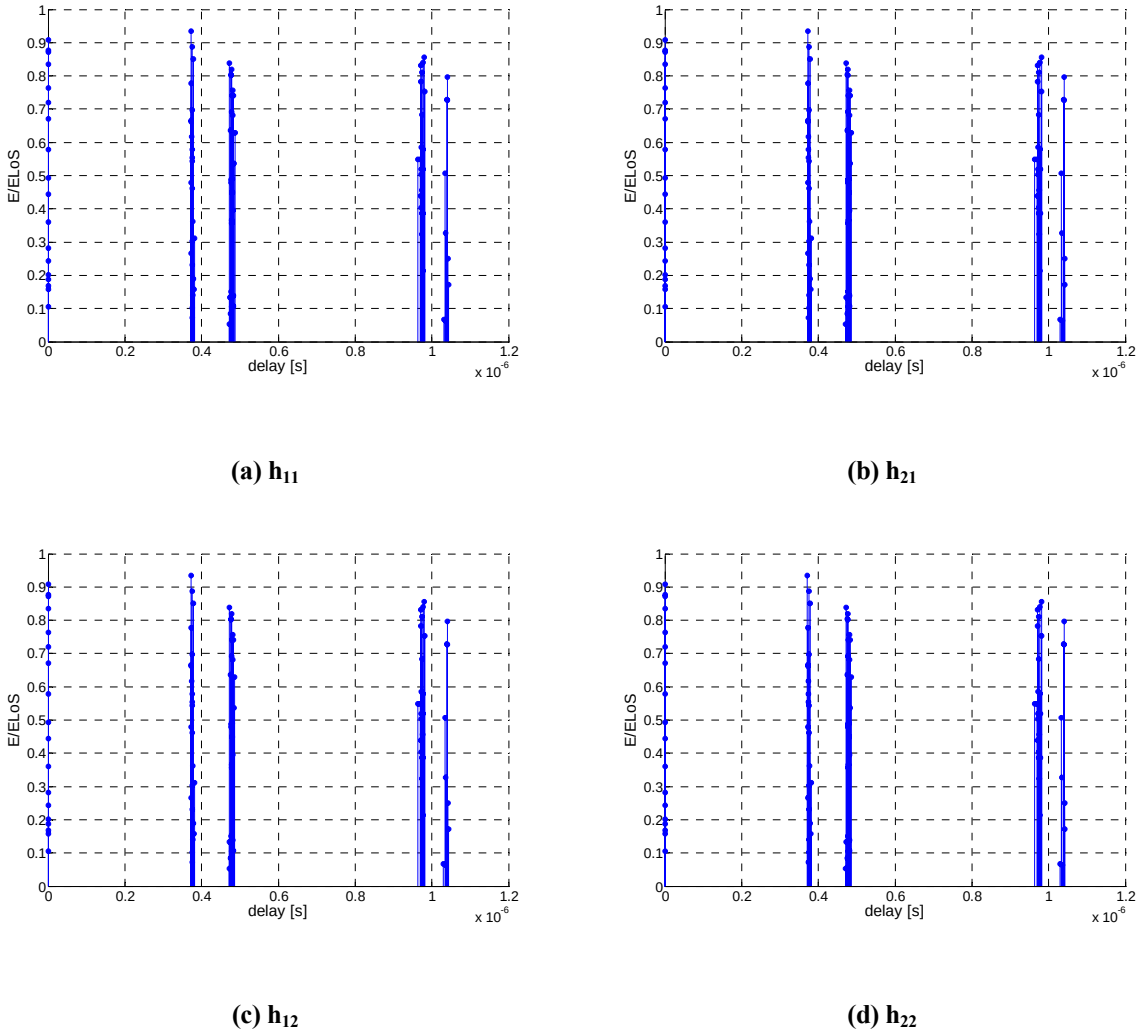

(a) h_{11} **(b) h_{21}**

(c) h_{12} **(d) h_{22}**

Figure E.5 – CIRs for MIMO 2×2 for the highway scenario.

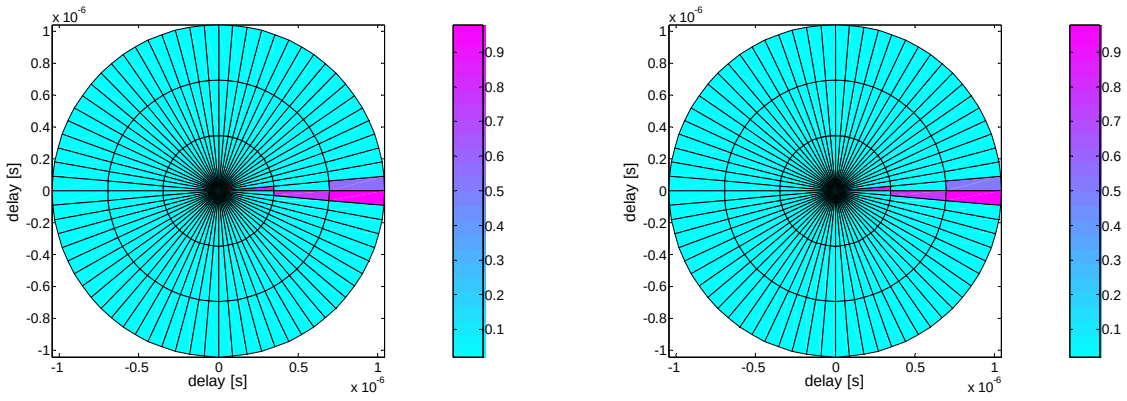

(a) h_{11} **(b) h_{21}**

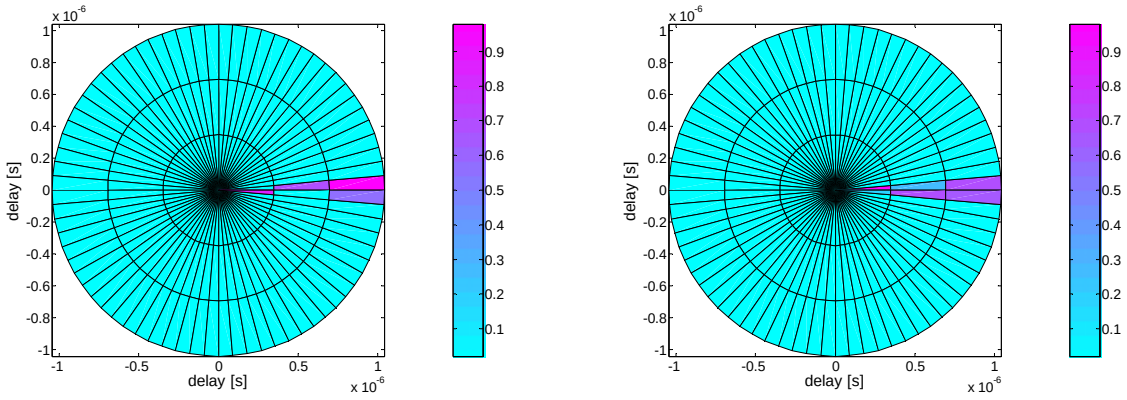

(c) h_{12} **(d) h_{22}**

Figure E.6 – PDAPs for MIMO 2×2 for the highway scenario.

Annex F. Graphs of the capacity for various number of antennas

This annex extends Section 5.2.1, where results related to different numbers of antennas for both sides of the radio link are presented. The following graphs shows data that is presented in tables in that section. In the graphs, capacity for different numbers of antennas can be observed. The increase of capacity, caused by adding extra antennas, is shown as well. A comparison of capacity for UMTS and HIPERLAN is also presented.

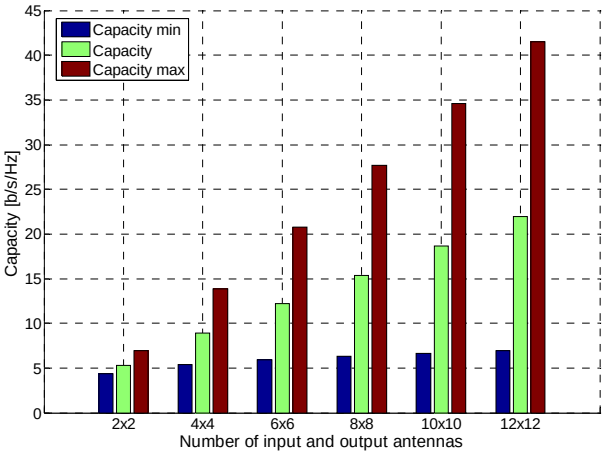

Figure F.1 – Capacity for various numbers of antennas for the railway station scenario.

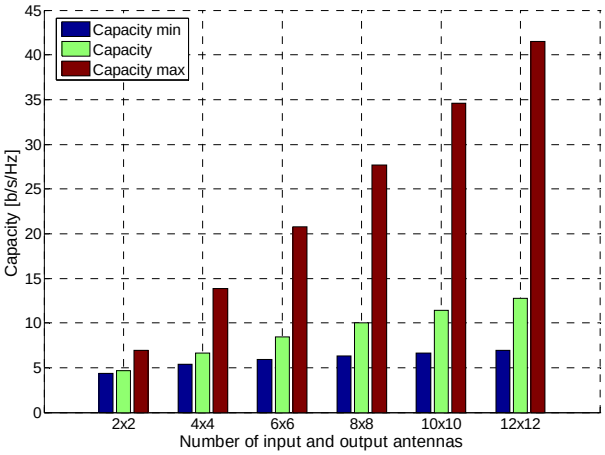

Figure F.2 – Capacity for various numbers of antennas for the highway scenario.

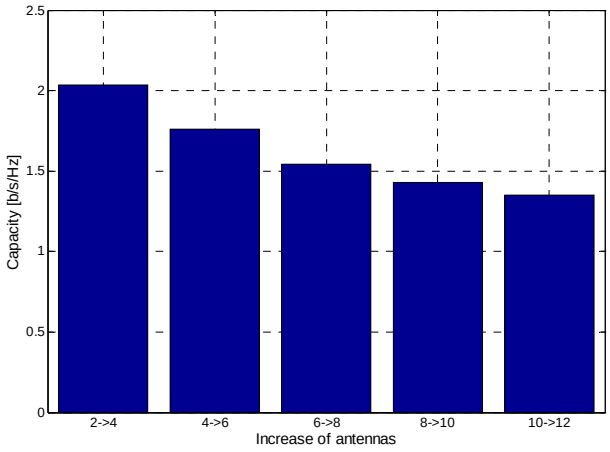

Figure F.3 – Increase of capacity for the highway scenario.

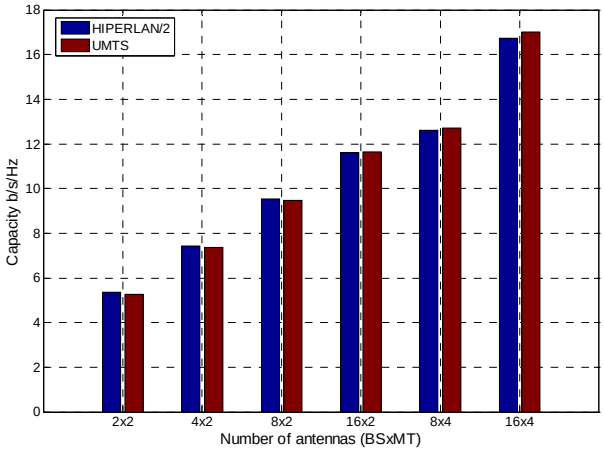

Figure F.4 – Comparison of capacity for the railway station scenario (uplink).

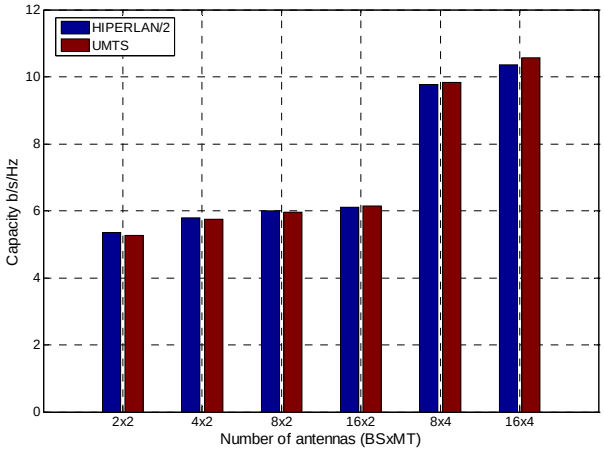

Figure F.5 – Comparison of capacity for the railway station scenario (downlink).

Annex G. Graphs of the capacity for various spacing between antennas

This annex extends Section 5.2.3, where results related to various spacings between antennas for both sides of the radio link are presented. The following graphs shows data that is presented in tables in that section. Below, graphs for all considered scenarios can be seen. MIMO systems with 4 and 8 antennas for both sides of the link are considered here.

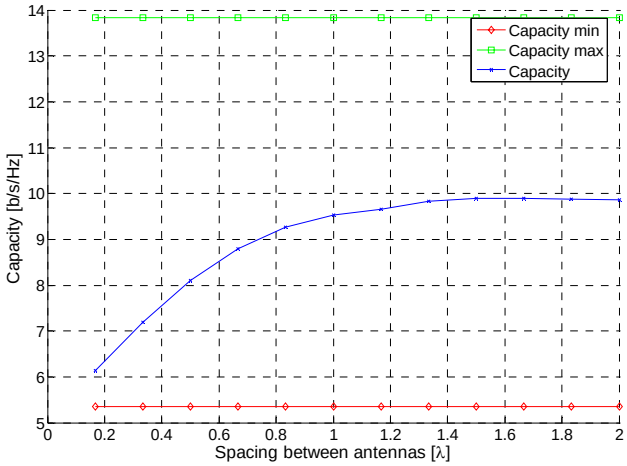

Figure G.1 – Capacity of MIMO 4×4 for different spacings for the city street scenario.

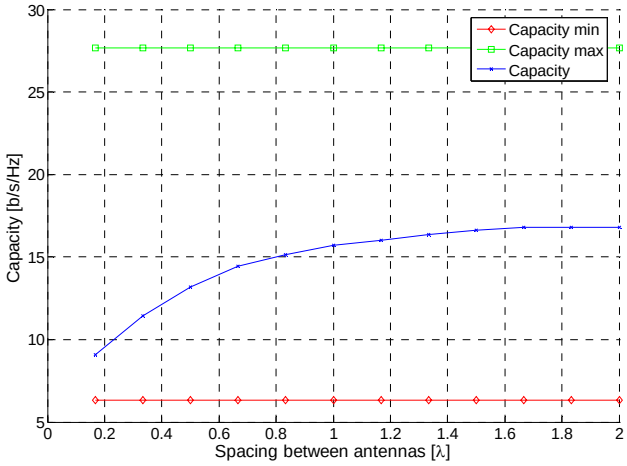

Figure G.2 – Capacity of MIMO 8×8 for different spacings for the city street scenario.

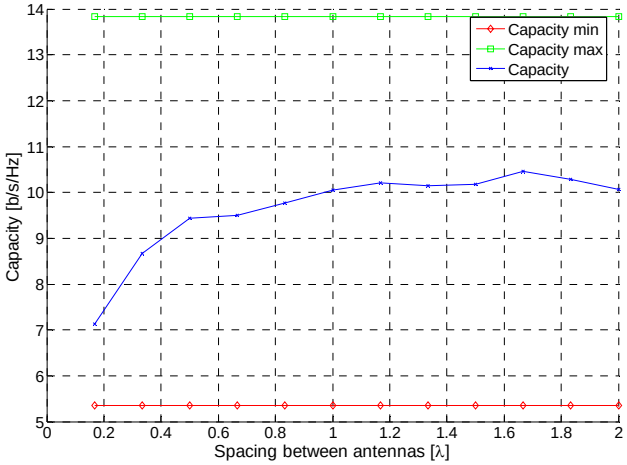

Figure G.3 – Capacity of MIMO 4×4 for different spacings for the railway station scenario.

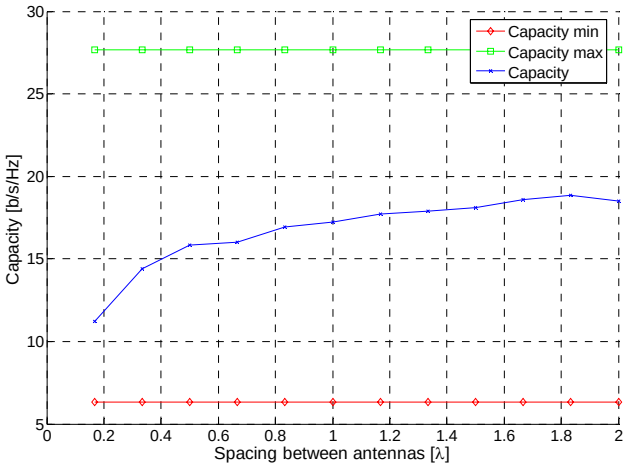

Figure G.4 – Capacity of MIMO 8×8 for different spacings for the railway station scenario.

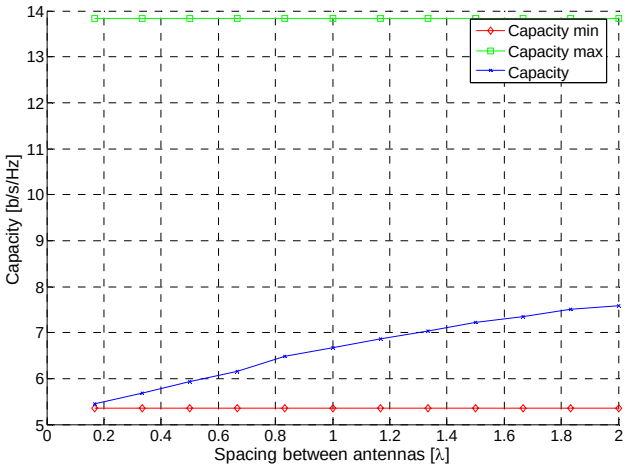

Figure G.5 – Capacity of MIMO 4×4 for different spacings for the highway scenario.

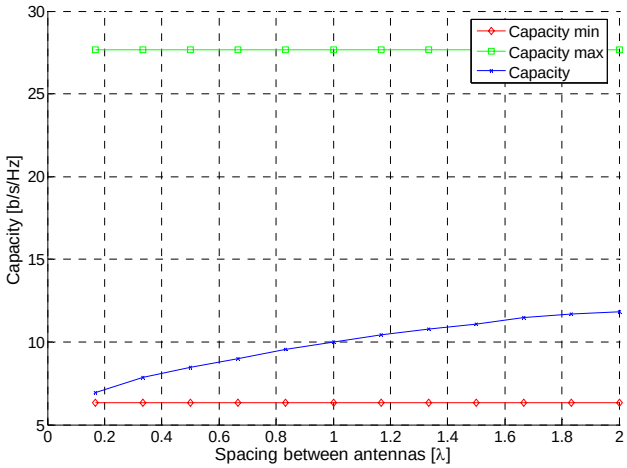

Figure G.6 – Capacity of MIMO 8×8 for different spacings for the highway scenario.

Annex H. Correlation

When considering a MIMO system, the correlation among links between the input and output sides must be analysed. A larger decorrelation enables a greater gain of capacity. Correlation between links is related with the deployment and the number of scatterers in the propagation environment. As shown in Annex E, CIRs for different scenarios have different shapes which influences the correlation in the radio channel.

The following graphs consist of correlation between all pairs of input and output antennas for different scenarios. Various separation times are compared for each scenario, as well. The separation time indicates a shift between time samples for a CIR after time filtering. Multipath components from raw CIR, related with one time sample, are summed coherently. For the present analysis, a MIMO 4×4 was chosen, so that 16 different radio links are available.

In Figure H.1, the correlation between all links for the city street scenario is presented, for a 1 ns time separation. The figure is symmetric, what was predictable, because on axes *x* and *y* the CIRs. The largest correlation is for the link that have a common end.

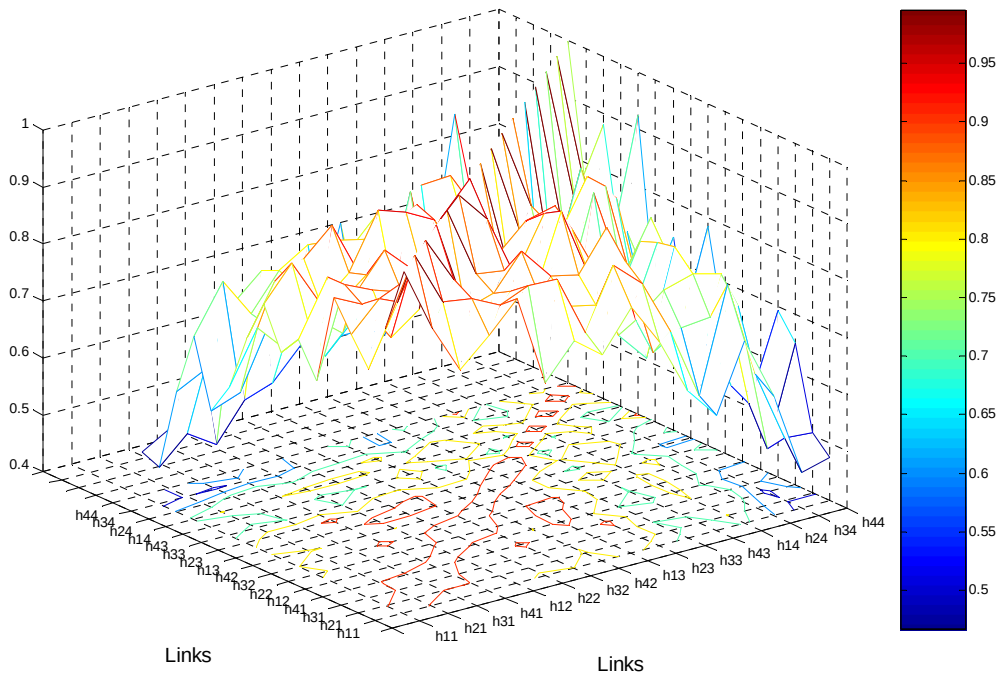

Figure H.1 – Correlation between links for the city street scenario for a 1 ns time separation.

The region with the greatest correlation is placed in the neighbourhood of the diagonal of the plane, where the autocorrelation of the links can be seen. It is obvious that the autocorrelations of the links equal 1. However, the regions with large correlation are not only near the diagonal, because some local maxima can be also observed. The location of the correlation maxima is related to the actual deployment of the clusters. The smallest correlation is between links whose ends are the most separated. The level of the correlation changes from 0.5 to 0.9, excluding the autocorrelations.

In Figure H.2, correlations for the city street scenario and for a 0.1 ns time separation are presented. Excluding the autocorrelation, the levels of correlation are significant smaller. The CIRs are presented more precisely, because the separation time is 10 times smaller. Nevertheless, the tendency from the previous graph is kept.

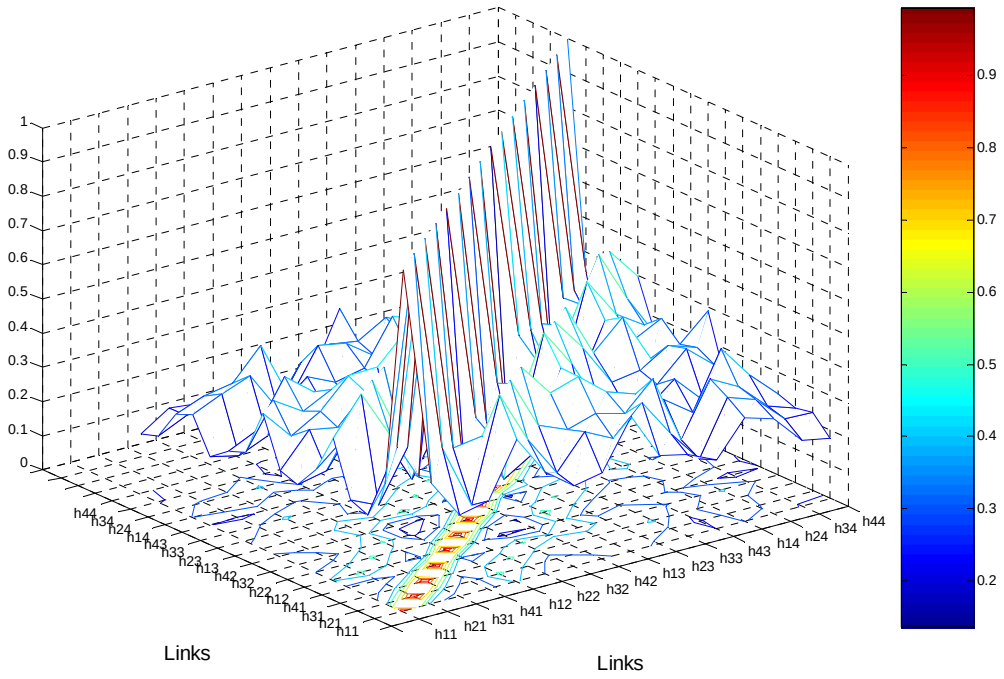

Figure H.2 – Correlation between links for the city street scenario for 0.1 ns time separation.

Correlations for the railway station scenario are shown in Figure H.3, the behaviour being similar to the one of the city street scenario. However, the regions of strong correlation placed near the diagonal of the *x*-*y* plane are greater here. The railway station scenario is the smallest one among all scenarios and has the greatest number of clusters. Clusters that have a similar distance from the transmitter imply that rays from adjacent transmit antennas are more

averaged, hence, giving more smooth influence on the shape of CIR. For the railway station scenario, this situation is more expected than for the city street scenario, because the number of clusters is significant different.

Also here, local maxima can be observed. The existence of the extremes is related with a specific deployment of clusters. The mentioned maxima are especially visible for a 0.1 ns time separation, Figure H.4.

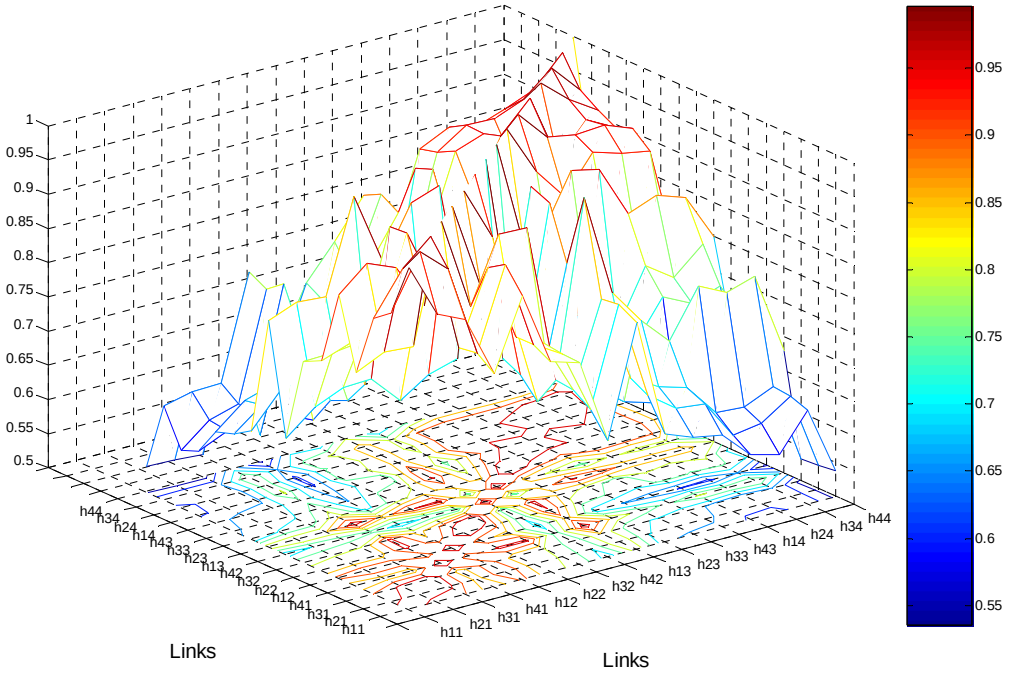

Figure H.3 – Correlation between links for the railway station scenario for a 1 ns time separation.

The profile for the highway scenario case is depicted in Figure H.5. The shape of the graph is specific for this scenario. The correlation between links leads to groups each one is related to a transmit antenna. UL is considered, so that groups are associated to antennas of the MT. The links generated by transmit antennas are strongly correlated the level of correlation reaching 0.95; the levels for all groups are almost the same. The next set of groups with a similar level of correlation is for links that have adjacent MT antennas. It is not important which combination is taken, because the level of correlation is almost the same. Receive antennas have no influence on the value of the correlation. If the distance between transmit antennas increases correlation goes down, therefore the correlation between links with farthest input antennas is the smallest for the highway scenario.

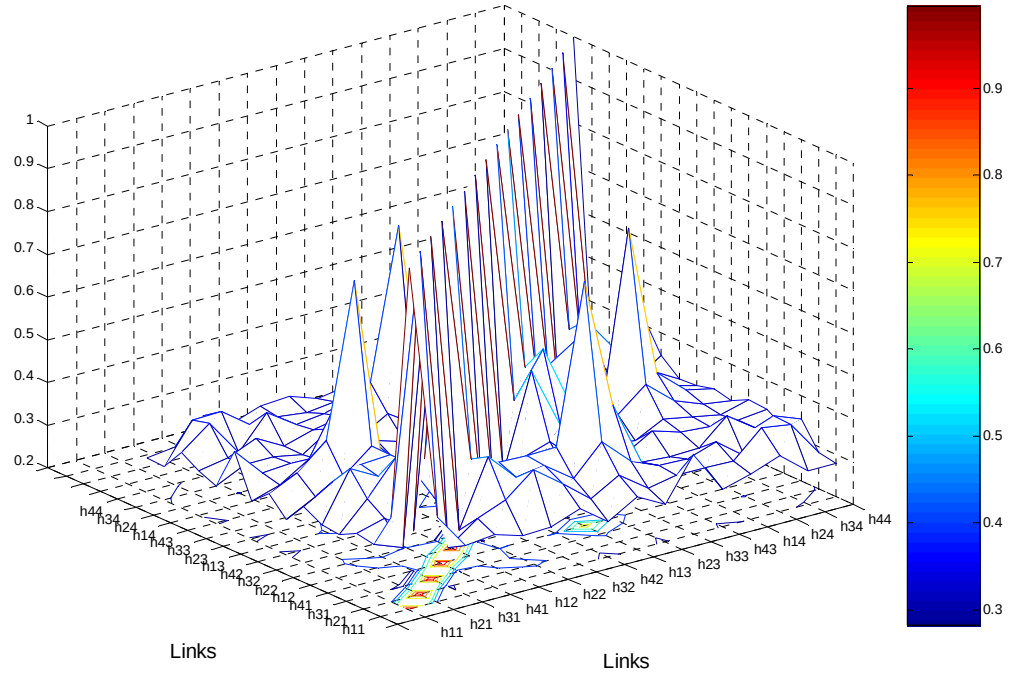

Figure H.4 – Correlation between links for the railway station scenario for a 0.1 ns time separation.

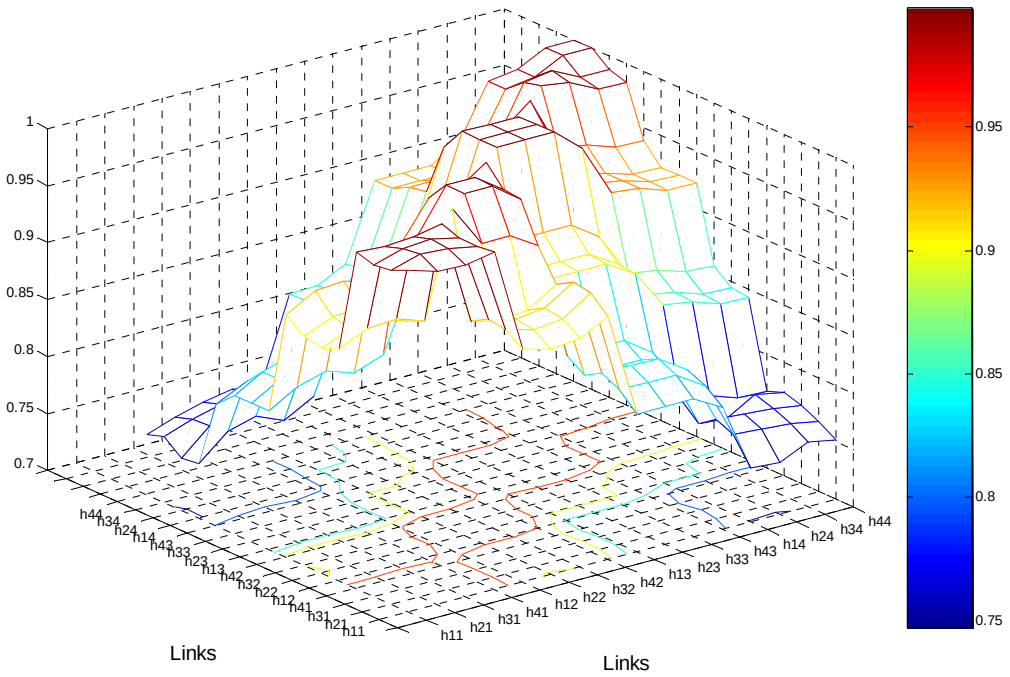

Figure H.5 – Correlation between links for the highway scenario for a 1 ns time separation.

The decrease of the time separation until 0.1 ns, as depicted in Figure H.6, influences the tendency, which is observed in the previous figure. The more separated transmit antennas do not give a smaller correlation. A greater number of samples of a filtered CIR implies that a larger number of them is zero, because impulses from different clusters are more apart. This phenomenon can be observed in figures for the highway scenario in Annex E.

The above presented figures show that the city street scenario has the smallest correlation between links between the input and output sides. However, the highway scenario is the strongest correlated. These conclusions are in agreement with the obtained values of capacity for particular scenarios. For the city street scenario, capacity is the greatest, however capacity for a highway scenario are the smallest. The railway station scenario is insignificantly more correlated than the highway one, but these two scenarios are the most similar concerning achieved levels of correlation.

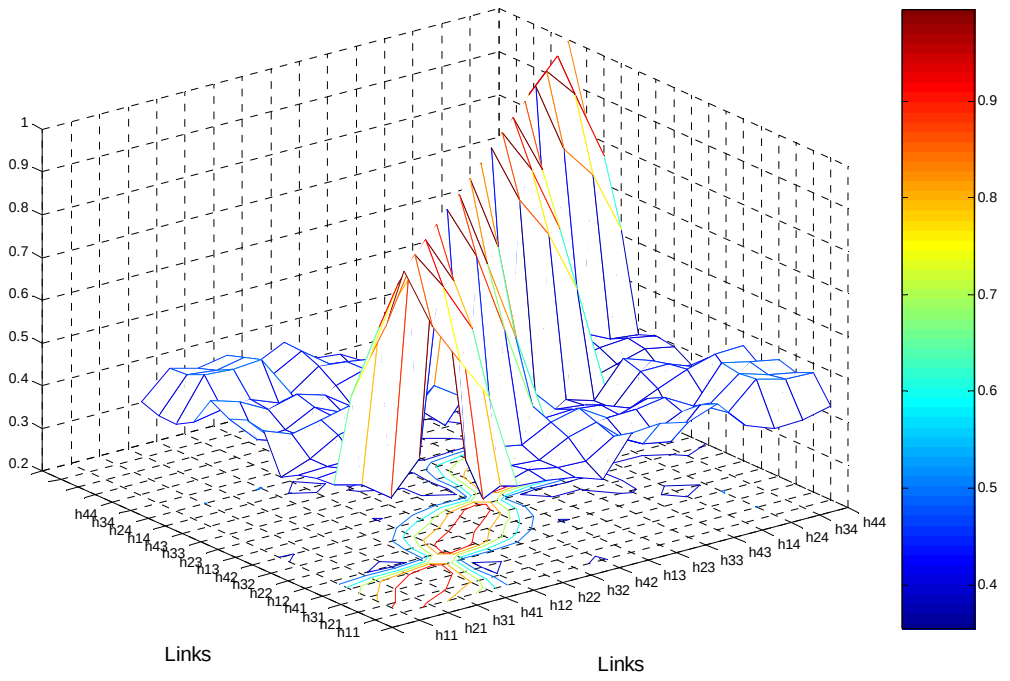

Figure H.6 – Correlation between links for the highway scenario for a 0.1 ns time separation.

Annex I. Bandwidth

This annex consists of figures with the influence of the bandwidth on the spectral capacity. In Figure I.1, the capacity for different bandwidths can be seen the bandwidth has an insignificant impact on capacity. However, the spectral capacity calculated here indicates a capacity for a unit of bandwidth. The inverse of the bandwidth defines the time separation for the filtered CIR. The process of calculation of capacity is described in Annex J.

The mode of simulation has no influence on capacity. Only for mode 3 the greatest standard deviation is obtained, which is natural, because for every run of the simulator completely new environment is generated.

A greater time separation implies that a CIR after time filtering a counts for a larger number of samples, so that all multipath components are divided into a greater number of groups. For each group of multipath components, a narrowband capacity is calculated. The average from all narrowband capacities is the final spectral capacity. This taps give always the impact on the final value of capacity.

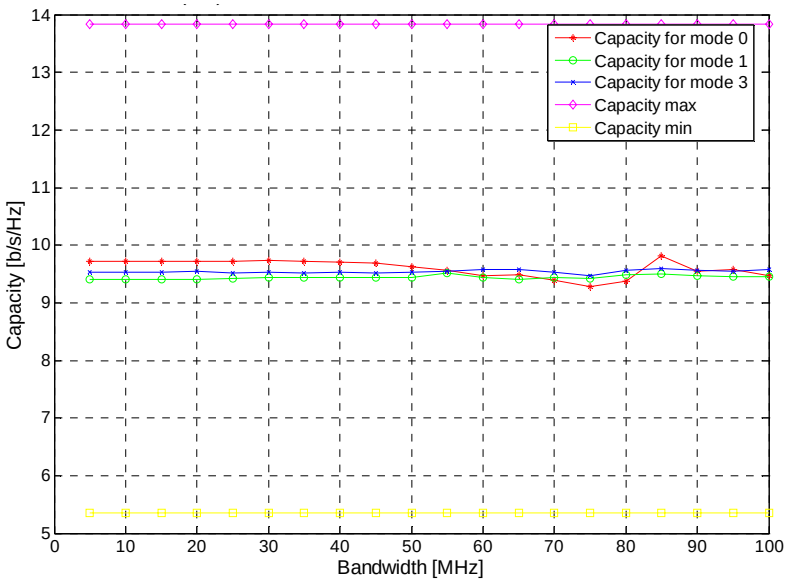

Figure I.1 – Capacity for various bandwidths for the city street scenario.

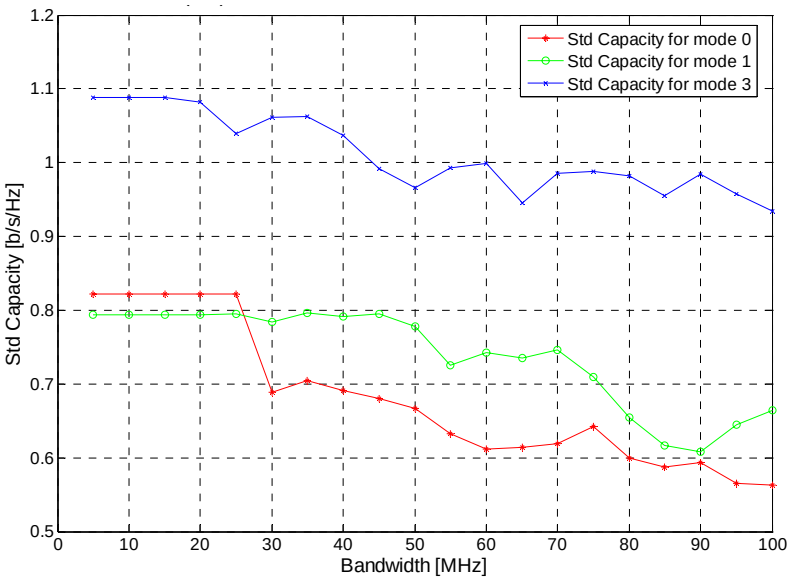

Figure I.2 – The standard deviation of capacity for various bandwidths for the city street scenario.

Annex J. Calculation of capacity

Capacity is calculated via (3.19), but, in order to use of this equation, the normalised channel transfer matrix has to be obtained. The entries of the matrix are related to the links between all pairs of input and output antennas. The number of rows is defined by the number of receive antennas, and the number of transmit antennas indicates the number of columns.

First, the CIR is filtered using a time resolution defined as the inverse of the bandwidth. For the UMTS case, the time resolution is 200 ns. The absolute values of delays of the CIR direct from the simulator are not useful, and the normalisation relative to the LoS component must be done. All multipath components are normalised by subtracting the delay of the LoS component. After that, the LoS component has a delay equal to 0, and other taps are described by the difference between the delays.

The filtered CIR consists of time slots, and the number of time slots depends on the delays in the considered scenario. For the highway scenario, only a few time slots usually exist after the time filtering, because its delays are the greatest compared to other scenarios, i.e., the city street and the railway station scenarios. So, the maximum delay of the highway scenario divided by the time resolution gives a value greater than one. Then squares of the amplitude of the taps related with particular time slot are summed in coherent way, so that the phases of the taps are respected. During the filtering all taps are moved to the centre of the time slot. A change of the delay has influence on the phase of a particular tap, but the phases of the taps are not corrected; this is not necessary, because the phases are defined by a random reflection coefficient of the scatterer. The matrix after time filtering can be 3-dimensional. Every link between transmit and receive side may be described by a vector of impulses. An example of the filtered CIR is depicted in Figure J.1.

Afterwards, the Fourier transform is calculated for each link. The transform does not change the correlation between links, but after the transformation, CIRs do not have any zero samples. Zero samples can disturb the values of capacity. After that, the CIRs in the frequency domain are normalised taking into consideration the mean values of the samples related to a particular frequency. This matrix can be used to calculate capacity.

As mentioned at the beginning, the equation gives a capacity for each frequency of the CIR after Fourier transform, being a narrowband value, an average of the narrowband capacities yields wideband capacity, and this one is presented in this work.

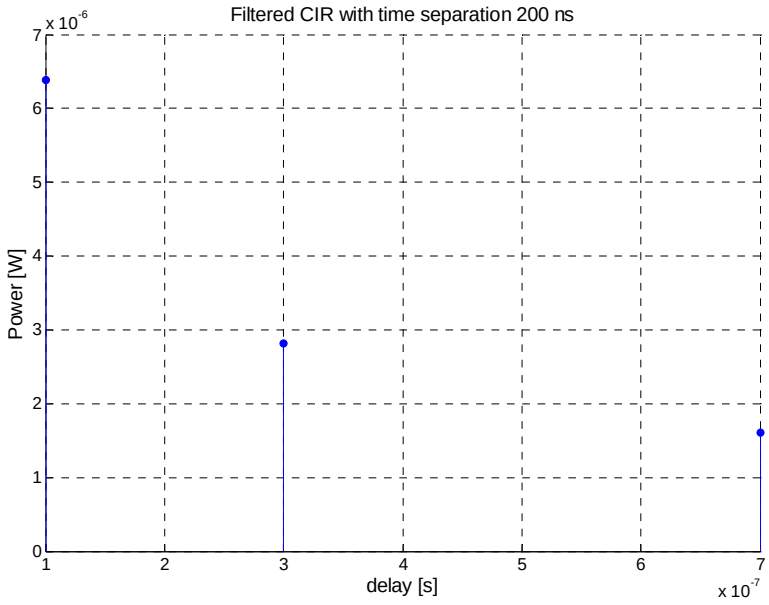

Figure J.1 – Example of filtered CIR.

References

[3GGP00] 3GGP Radio Frequency (RF) system scenarios, Technical Specification 25.942, 2000 (http://www.3gpp.org)

[Alam98] Alamouti,S.M., "A Simple Transmit Diversity Technique for Wireless Communications", *IEEE Journal on Selected Areas in Communications*, Vol. 16, No. 8, Oct 1998, pp. 1451-1458

[AMSM02] Asplund,H., Molisch,A.F., Steinbauer,M., and Mehta,N., "Clustering of scatterers in mobile radio channels - Evaluation and modeling in the COST 259 Directional Channel Model", in *Proc. ICC 2002 - IEEE Int. Conference*., New York, USA, Apr 2002

[Ande00] Andersen,J., "Array Gain and Capacity for Known Random Channels with Multiple Element Arrays at Both Ends", *IEEE Journal on selected area in communications*, Vol 18, No 11, Nov 2000, pp. 2172-2178

[CDGO05] http://www.cdg.org, Aug 2005

[DaCoT99] Damosso,E., and Correia, L.M., "Digital Mobile Radio Towards Future Generation Systems" (Final Report), COST Telecom Secretariat, European Commission, Brussels, Belgium, 1999.

[Debb03] Debbah,M., "An Information Theoretic point of view to MIMO channel modelling", Deliverable 13, IST-FLOWS Project, Froschungszentrum Telekommunikation Wien (FTW), Vienna, Austria, Sep 2003

[DGVC03] Debbah,M., Gil,J., Venes,J., Cardoso,F., Marques,G., Correia,L., "Final report on channel models", IST-2001-32125 FLOWS, FTW and IST/TUL, Lisbon, Portugal, 2003

[ErCa98] Ertel,R., Cardieri,P., "Overview of Spatial Channel Models for Antenna Array Communication Systems", Internal Report, Virginia Polytechnic Institute, 1998

[Fern04] Fernandes,P.,M., "Capacity Increase in Converging Mobile Communication Systems Through the Use of MIMO", MSc Thesis, IST/TUL, Lisbon, Portugal, 2004

[FoGa98] Foschini,G.J. and Gans,M.J., "On Limits of Wireless Communications in a Fading Environment when Using Multiple Antennas", *Wireless Personal Communication*, Vol. 6, 1998, pp. 311-335

[GeAk02] Gesbert,D., and Akhtar,J., "Breaking the barriers of Shannon Capacity: An Overview of MIMO wireless system", *Telektronikk Telenor Journal*, Vol. 98, Jan. 2002, pp. 53–64.

[GSMW05] http://www.gsmworld.com, Aug 2005.

[GSSS03] Gesbert,D., Shafi,M., Shiu,.D., Smith,P.,J., Naguib,A., "Form Theory to Practice: An Overview of MIMO Space-Time Coded Wireless Systems", *IEEE Journal on selected area in communications*, Vol 21, No 3, Apr 2003, pp. 281-302

[GVCM03] Gil,J.,Venes,J., Cardoso,F., Marques,M.G., and Correia,L.M., *IST/TUL Contribution for D13,* IST-FLOWS Project, Internal Document WP2_ISTTUL_TN_INT_066_01, IST-TUL, Lisbon, Portugal, June 2003.

[HoTo00] Holma,H., and Toskala,A., "WCDMA for UMTS – Radio Access for Third Generation Mobile Communications", John Wiley, Chichester, UK, 2000

[IEEE05] http://ieee.org, Aug 2005

[KoCi04] Kołakowski,J., Cichocki,J., "UMTS – Third generation of mobile telephony system" (in Polish), WKŁ, Warsaw, Poland, 2004.

[Kosi04] Kosiło,T.,"Mobile terrestrial radiocommunication" (in Polish), Internal Document, Warsaw University of Technology, Warsaw, Poland, 2003

[Lee73] Lee,W.C.Y., "Effects on correlation between two mobile base-station antennas", *IEEE Transactions on Communications*, Vol. COM-21, No. 11, Nov. 1973, pp. 1214-1224.

[LiRa99] Liberti,J. and Rappaport, T., "Smart Antennas for Wireless Communication: IS-95 and Third Generation CDMA Applications", Prentice Hall, Upper Saddle River, NJ, USA, 1999.

[LKTB02] Laurila,J., Kalliola,K., Toeltsch,M., and Bonek,E., "Wide-band 3-D Characterization of Mobile Radio Channels in Urban Environment", *IEEE Transactions on Antennas and propagation.*, Vol. 50, No. 2, Feb 2002, pp. 233–243.

[MaCo04] Marques,M.,G., Correia,L.M. "Adaptive antenna arrays: trends and applications", Springer-Verlag, Berlin, Germany, 2004.

[MaHu03] φMahmoud,S., Hussain, Z., O'Sheay,P., "Space-Time Geometrical-Based Channel Models: A Comparative Study", Internal Report, School of Electrical and Computer Engineering RMIT University, Melbourne, Australia, 2003

[Marq01] Marques,M.,G., "A Wideband Directional Channel Model for Micro-Cells in UMTS", MSc Thesis, IST, Lisbon, Portugal, 2001

[Math05] http://mathworld.wolfram.com, August 2005

[MoBo99] Molisch, A.F., and Bonek, E., "Efficient implementation of a geometry-based directional model for mobile radio channel", in *Proc. VTC 1999 Fall - IEEE 50th Vehicular Technology Conf*erence, Amsterdam, Holland, Sep 1999.

[MoPa92] Mouly,M., and Pautet,M., "The GSM System for Mobile Communications", M. Mouly et Marie-B. Pautet, Palaiseau, France,1992

[Orfa02] Orfanidis,J.S., "Electromagnetic Waves and Antennas", Internal Report, Rutgers University, NJ, USA, 2002 (http://www.ece.rutgers.edu/~orfanidi/ewa)

[Pras98] Prasad,R., "Universal Wireless Personal Communications. Mobile Communication Series", Artech House, London, United Kingdom, 1998

[Proa01] Proakis,J.G., "Digital Communications", Mac Graw Hill, New York, USA, 2001.

[Reis04] Reis,C., "An analytical traffic model for the UMTS radio interface", MSc Thesis, IST-TUL, Lisbon, Portugal, 2004

[SaVa87] Saleh,A.M., and Valenzuela,R.A., "A Statistical Model for Indoor Multipath Propagation", *IEEE Journal on Selected Areas in Communications*, Vol. 5, No. 2, Feb 1987, pp. 128–137

[UMTS05] http://www.umts-forum.org, Aug 2005

[UtBi05] Uthansakul,P., Białkowski,M.E., "The Effect of Mutual Coupling on The Capacity and BER Performance of A MIMO System", in proc. *9th Australian Symposium on Antennas,* Sydney, Australia, Feb 2005

[VCGC03] Venes,J., Cardoso,F., Gil,J., Correia,L.M., "Antenna Arrays for Wideband Directional Channel Models", Internal Document, IST/TUL, Lisbon, Portugal, 2003

[Zuba05] Zubala,R., "Multiuser Geometrically base channel model", MSc Thesis, Warsaw University of Technology , Warsaw, Poland, 2005